ABSTRACT

Title of dissertation: SOMATOSENSORY SIGNALING FOR FLIGHT CONTROL IN THE ECHOLOCATING BAT *EPTESICUS FUSCUS*

Mohit Chadha, Doctor of Philosophy, 2014

Dissertation directed by: Professor Cynthia F. Moss
Program in Neuroscience and Cognitive Science

Bats are the only mammals to have evolved powered flight. Their specialized hand-wings with elongated digits and a thin membrane spanning the digits not only enable flight, but give them unrivaled aerial maneuverability. Bat wing membrane is endowed with an array of microscopic hairs that are hypothesized to monitor airflow and provide sensory feedback to guide rapid motor adjustments for flight control. The goal of this thesis is to contribute to a broader understanding of the response properties of wing-associated tactile receptive fields, and the representation of aerodynamic feedback in the bat's nervous system.

Using the big brown bat, *Eptesicus fuscus*, a series of neurophysiological experiments were performed where the primary somatosensory cortical (S1) responses to tactile and

airflow stimulation of the wings were analyzed. Results demonstrate that the body surface is organized topographically across the surface of S1, with an overrepresentation of wings, head and foot. The wings have an inverted orientation compared to hand representation of terrestrial mammals, with tactile thresholds that are remarkably close to human fingertips.

Airflow stimulation of the wings was achieved by brief puffs of air generated using a portable fluid dispensing system. By changing the intensity, duration and direction, airflow sensitive receptive fields were characterized based on responses of S1 neurons. Results reveal that neuronal responses are rapidly adapting, encompassing relatively large and overlapping receptive fields with well-defined centers. S1 responses are directionally selective, with a majority preferring reversed airflow. The onset latency of evoked activity decreases as a function of airflow intensity, with no effect on response magnitude. Furthermore, when dorsal and ventral wing surfaces are stimulated simultaneously, S1 responses are either inhibited or facilitated compared to either wing surface stimulation alone. This finding suggests that outputs from the two wing surfaces are integrated in a manner that reflects the interplay of aerodynamic forces experienced by the wings.

To evaluate the central coding mechanisms of airflow sensing by bat wings, I applied an information theoretic framework to spike train data. Results indicate that the strength and direction of airflow can be encoded by the precise timing of spikes, where first post-stimulus spikes transmit bulk of the information, evidence for a latency code.

SOMATOSENSORY SIGNALING FOR FLIGHT CONTROL IN THE BIG BROWN BAT, *Eptesicus fuscus*

by

Mohit Chadha

Dissertation submitted to the faculty of the Graduate School of the
University of Maryland, College Park in partial fulfillment
of the requirements for the degree of
Doctor of Philosophy
2014

Advisory committee:

Professor Cynthia F. Moss, Chair/Advisor
Professor Catherine E. Carr
Professor Timothy K. Horiuchi
Doctor Susanne J. Sterbing-D'Angelo
Professor David D. Yager

DEDICATION

To my parents, who instilled in me a desire to pursue knowledge, and supported all my decisions. To my beloved and caring wife, for standing by me throughout this endeavor. And my loving daughter, who brings immense joy and warmth to our family.

ACKNOWLEDGEMENTS

I am very grateful to my mentor Cindy Moss for allowing me the opportunity to pursue this work in her lab. I have learned immensely under her mentorship. I am indebted to her continued guidance, support and immense patience. I thank Susanne Sterbing-D'Angelo for her creativity, and for showing me how to get things done when no solution was in sight.

I also thank Catherine Carr, for being in my dissertation committee and for always letting me access her facilities. I could always count on her when in need. I am thankful to Timothy Horuichi and David Yager for agreeing to be members of my dissertation committee, and for their contributions and suggestions regarding my research. I am also grateful to Ed Smith, for valuable discussions, troubleshooting help and his humor. I thank Pam Komarek for always keeping me posted about upcoming deadlines, meetings, reminders etc., and helping out with all NACS administrative needs.

I thank all the members of Batlab, both former and current. I especially thank Murat Aytekin for never saying no to any of my requests for help with research. I learned a lot from him. I thank Kaushik Ghose for inspiring discussions and sessions of humor. It was always fun to have him around. I am grateful to Mel and Ninad for their support, academic or not, and their friendship. I also thank Ben, Genni, Chen, Wei, and Nachum for much needed help with all things bat!

My graduate research was funded by graduate school fellowships in the first two years through NACS and the Department of Psychology. Additional funding for this research was provided by a multi-university Air Force Office of Scientific Research grant.

TABLE OF CONTENTS

LIST OF FIGURES

LIST OF TABLES

Chapter 1

Introduction

Aerial navigation by bats is made possible by an evolutionary modification of their forelimbs to support a wing membrane. The bat hand-wing consists of flexible and articulated skeletal elements with a thin, and highly adaptive skin membrane stretching across upper limbs and the body. (Swartz, Groves, et al. 1996). This specialized hand-wing endows bats the distinction of being the only mammalian group to achieve powered flight (Thewissen and Babcock 1992). Furthermore, bats are capable of remarkable aerial agility and maneuverability like hovering, perching upside down, or making sharp turns and dives (Iriarte-Díaz and Swartz 2008; Norberg 1994; Riskin, Bahlman, et al. 2009). Crucial for maintaining flight control and remaining airborne is the ability to respond to feedback about aerodynamic changes. It has been hypothesized that microscopic tactile hairs on the wings of bats can monitor airflow, thereby providing valuable feedback for the flight motor apparatus (Sterbing-D'Angelo et al. 2011; Zook 2005, 2006; Zook and Fowler 1986). But there has been relatively limited research in recognizing what aspects of airflow are sensed, or how this sensory information is represented in the bat's nervous system. The goal of this thesis is to contribute to a broader understanding of tactile sensing by bat

wings for encoding aerodynamic feedback at the level of the primary somatosensory cortex.

Addressing the question of airflow sensing by tactile hairs on bat wings requires some understanding of the aerodynamics of powered flight (especially in bats), as well as the anatomical and physiological properties of the underlying mechanosensors and sensorimotor circuits. Animal flight (bats, birds and insects) has been studied for over a century, but only recently have developments in measurement and analytical tools greatly advanced our understanding of the kinematics and aerodynamics of powered flight. In the first subsection of this chapter I will describe the basic kinematic features of flapping flight amongst insects, birds and bats, and review results of recent experiments investigating the aerodynamics of bat flight, before discussing the implications for experiments described in this dissertation.

While specific questions related to airflow sensing by bat wings are just beginning to be explored, the ability of flying animals (specifically insects) to sense airflow as a feedback mechanism for flight control has been investigated for over half a century. Research on the morphology and physiology of airflow sensors, and processing of responses by the nervous system provide valuable insights about flight control mechanisms. With the goal of learning from, and applying this knowledge to better understand airflow sensing by bat wings, I will review relevant literature in the second subsection of this chapter.

Signals about airflow at the surface of the bat wing project from peripheral receptors to the central nervous system, and are transformed through various stages of processing before reaching the primary and higher cortical regions. Which cutaneous mechanoreceptors are involved, and how is tactile information transformed and encoded the somatosensory system? While we know relatively little about the somatosensory system of bats, there exists a wealth of information about the cytoarchitectural, electrophysiological and central encoding mechanisms from primate and rodent studies. In the third and

final subsection I will review literature highlighting what is known from research on bats and other mammalian species about tactile perception, with an emphasis on the possible role of bat somatosensory system on flight control.

1.1 Kinematics and aerodynamics of flapping flight

1.1.1 Kinematics

A flying animal needs to counteract gravity and drag by generating lift and thrust forces to stay aloft. Thrust is generated by accelerating the air under the wings backwards, and lift is generated by pushing the air downwards. Whereas the magnitude of these forces can be crudely approximated using elementary physical principles, flapping flight offers tremendous challenges relative to fixed wing models, as the wings not only move forward relative to air, they also flap up and down, bend, twist and sweep forward and backward. This 'flapping translation' varies to a large degree with the species under consideration. Part of this variation relates to the disparate design characteristics of animal wings. Bats wings, for instance, are composed of a thin membrane that stretches across the forelimb bones and attaches to the side of the body, including the lower limbs. The shape of the wings is actively controlled by limb joints and wing muscles to bring about large changes in the aerodynamically active surfaces (Swartz, Iriarte-Díaz, et al. 2007). Bird wings are comparatively thicker, and are composed of arm and hand musculoskeletal elements, similar to bats. But bird wings are covered in feathers, are much stiffer compared to bat wings, with little bending during flight (Pennycuick 2008). Similarly insect wings generally show limited deformation, lacking any joints beyond their insertion in the body (Bergou et al. 2007; Combes and Daniel 2001).

The production of aerodynamic forces is a direct consequence of the trajectory the wing takes hence a substantial effort has been made in the measurement and quantitative analysis of wingbeat patterns in a wide range of animal species. Modern-day methodology for making such measurements includes the use of high-speed stereo video cameras to reconstruct motion of anatomical landmarks or artificial markers in three dimensions, of an animal flying in a wind tunnel (Gui et al. 2010; Hubel, Riskin, et al. 2010; Swartz, Iriarte-Díaz, et al. 2007; Tobalske et al. 2007). Investigations of the movements of wings and body show that flying animals rapidly alter many of the kinematic features from one stroke to the next (Sane 2003; Swartz, Iriarte-Díaz, et al. 2007; Tobalske et al. 2007; Warrick et al. 2005). The wingstroke of insects typically shows four kinematic phases: the ventral to dorsal ('upstroke') motion, dorsal to ventral ('downstroke') motion, and supination and pronation at up- and downstroke transitions (Sane 2003; Fig. 1.1). Birds show some degree of rotation, usually at the wingtip (much less than insects), with the exception of humming birds which exhibit much greater rotation about the shoulder (Warrick et al. 2005). Bats on the other hand, by virtue of their highly compliant wing membrane and a number of joints, have a large degree of freedom in actively shaping both the upstroke and downstroke including wing rotation (Swartz, Iriarte-Díaz, et al. 2007).

Although wing morphology differs greatly between the three groups of fliers (insects, birds and bats), there are certain similarities in the wing trajectories at various flight speeds. From hovering to fast forward flight, as speed increases drag forces become substantially higher, and this is reflected in the kinematic changes needed to generate greater thrust. One of the most striking changes is observed in the movement of the wing tip. Wing tip movement appears as an ellipsoid curve, and typically in bats and insects, the upstroke is anterior to that of the downstroke, which is opposite to the motion in birds (Hedenström, Johansson, and Spedding 2009; Sane 2003; Swartz, Bishop, et al. 2005; Tian et al. 2006; Fig. 1.1). The stroke plane angle is defined as the direction of the long axis of the ellipsoid path the wing takes with the horizontal. Hovering insects

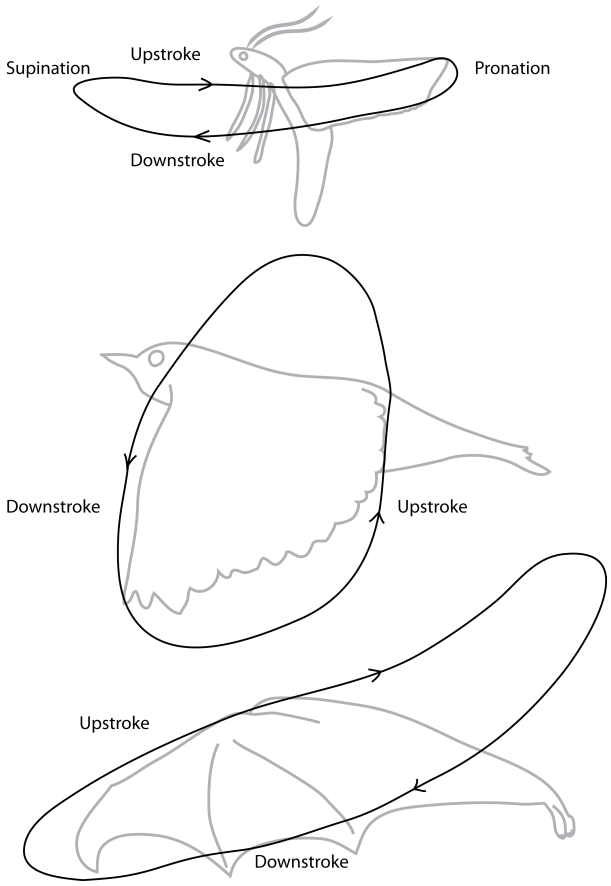

Figure 1.1: Typical wingtip trajectories. Schematic of wingtip trajectories typical of insects, birds and bats. Arrows indicate the direction wingtip takes during the wingbeat. During flapping translations, insects pronate their wings at the transition from upstroke to downstroke, and supinate at the transition from downstroke to upstroke.

exhibit a stroke plane that is either horizontal, or inclined away from the plane (Ennos 1989). When the stroke plane angle is horizontal ('normal hovering'), both halves of the wingbeat contribute equally to weight support (Willmott and Ellington 1997). This is primarily achieved by rotation of the wing along the span by almost 180°. At the end of the downstroke, normal hovering insects supinate the wings such that the ventral surface faces up, and pronate them back at the end of upstroke. This also appears to be the case in hummingbirds (unlike other small hovering birds, e.g. pied flycatcher), because of the large rotational mobility of the shoulder joint (Warrick et al. 2005). At the same time,

unlike normal hovering insects, hummingbirds with their relatively stiff wings perform asymmetrical hovering, with an active upstroke producing 25% lift force (Warrick et al. 2005).

When the wing stroke plane is inclined, as seen in hoverflies, dragon flies, small hovering birds and bats, force production is often asymmetrical, with differing kinematic mechanisms among the three groups (Hedenström, Johansson, and Spedding 2009; Sane 2003). For instance, because of their stiff wings, insects cannot flex their wings during upstroke like birds, and hence cannot make the upstroke passive. Additionally, a key difference between normal hovering and inclined plane hovering is that almost all vertical force generation occurs during downstroke in the latter (Wang 2004). Hence, if no lift production occurs during upstroke, the insect must produce twice as much force during the downstroke to support the weight of the animal. Based on these observations, it was realized early on that additional high-lift or unsteady (or time-dependent) mechanisms must be employed to stay airborne during hovering. It is now well documented that insects utilize a variety of unsteady mechanisms such as delayed stall, rotational lift and wake capture (Sane 2003). Birds and bats on the other hand show varying degrees of flexion during the upstroke with resulting changes in camber (Hedenström, Johansson, and Spedding 2009). Additionally, birds can separate their primary feathers during upstroke thus making it aerodynamically inactive (Norberg 1976a,b; Tucker 1993). Bats on the other hand lack this option due to the membranous nature of their wings, making the upstroke aerodynamically active, and generating positive thrust and weight support (Hedenström, Johansson, and Spedding 2009; Lindhe Norberg and Winter 2006; Wolf et al. 2010). In addition, having a large number of independently controlled joints allows bats to alter wing shape and camber resulting in a lifting upstroke (Hedenström, Johansson, Wolf, et al. 2007; discussed in more detail below).

During forward flight, the stroke plane angle is increased in all three classes of fliers (Fig. 1.2). Increase in forward speed is associated with increased lift production, hence a decreased need for a more horizontal movement. Depending on the speed, birds generally flex their wings to variable degrees to make the upstroke relatively passive (Hedenström, Johansson, and Spedding 2009). Bats show some degree of wing flexion during upstroke, but generally much less than birds (Lindhe Norberg and Winter 2006; Riskin, Iriarte-Díaz, et al. 2010). Insects are capable of even less flexion, and similar to the upstroke of bats, produce positive weight support by supinating the wing.

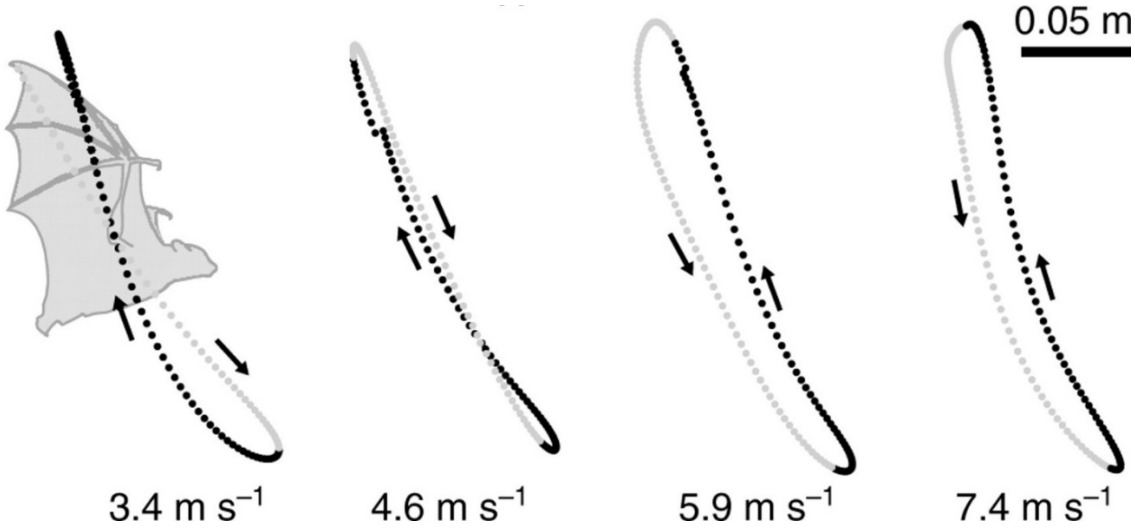

Figure 1.2: Stroke plane angle changes with flight speed. Schematic of stroke plane angle of the lesser dog-faced fruit bat, *Cynopterus brachyotis*, flying at different speeds with respect to still air. Grey traces correspond to the downstroke portion of the wingbeat. Note that stroke plane angle increases with flight speed (adapted from Iriarte-Díaz, Riskin, et al. 2011).

1.1.2 Kinematic differences across bat species

Body size, mass, and morphology of wings can be expected to have important effects on flight kinematics based on aerodynamic theory. For instance, as reviewed above, bats (as well as insects and birds) decrease their stroke plane angle as flight speed increases

from slow/hovering to cruising speeds. Bats range in size/body mass over three orders of magnitude, from $\sim$ 2 g bumblebee bat bat (*Craseonycteris thonglongyai*; Duff and Lawson 2004) to > 1 kg flying foxes (*Pteropus sp.*). Additionally, a variety of foraging habitats and wing morphology can further influence flight kinematics (Norberg and Rayner 1987). How does the wing morphology and body size influence flight kinematics specifically? This question was addressed in a recent investigation by Riskin and colleagues (2010). They compared 27 bats representing 6 pteropodid species covering a wide range of body mass (0.0278-1.152 kg). Bats were flown in a wind tunnel or a flight corridor, and wing kinematics were recorded by high speed cameras tracking markers on the wings and body. Results suggested that several kinematic variables e.g. wing stroke amplitude, stroke plane angle, wing camber, downstroke ratio and Strouhal number did not change significantly with body size. At the same time, scaling relationships for maximum wingspan, maximum wing area and wing loading differed from values reported in an earlier study by Norberg and Rayner (1987). In their analysis, Norberg and Rayner (1987) found wingspan and wing loading to scale near isometrically (scaling exponent, b = 0.350 and 0.327 respectively), and wing area to scale with positive allometry (b = 0.715). But Riskin and colleagues (2010) reported wingspan and wing area to scale with more positive allometry (b = 0.423 and 0.768 respectively), and wing loading to scale with more negative allometry (b = 0.233). The difference in these findings were most likely related to the manner in which wing measurements were acquired. Whereas Norberg and Rayner (1987) obtained the wing and body dimensions from bat specimens stretched flat on a horizontal surface, Riskin and colleagues (2010) tracked these dimensions in flight. This suggests that bats modulate their wing kinematics in flight to meet the demands of thrust and lift production, in a manner that is not predicted by body size and wing morphology alone.

1.1.3 Aerodynamics

To understand how animal flight is made possible, it becomes critical to understand how aerodynamic forces are generated and evolve by movement of the wings. As a flying animal overcomes its weight and drag to stay aloft, the forces exerted by its wings upon the surrounding air create a record of the time history of forces experienced by the animal itself by virtue of Newton's third law. The study of the wake left by an animal can thus be used to deduce the resultant forces it experiences, without needing to measure forces directly from the freely flying animal itself. The earliest studies of animal wakes relied on birds trained to fly through a cloud of helium filled soap bubbles that were illuminated by flash guns, the movement of which was captured by stereo photographs to identify and decipher vortices (Spedding, Rayner, et al. 1984). With rapid advances in technology in recent years, optical measurements of flow fields have been possible with high degree of sophistication. Digital particle image velocimetry (DPIV or PIV) is the gold standard for flow field measurements, and uses sheets of laser coupled with high speed videography to capture movement of particles or smoke suspended in the path of the flying animal. Sequential images are then used to find correlation peaks of the laser-lit particles to reconstruct flow maps describing the magnitude and direction of the surrounding air. Although recent, this technique is being applied increasingly to study insect, bird and bat flight, as well as aquatic animals.

The wake motions are generally described by distributions of vorticity, which is a measure of the direction and magnitude of the local rotation of fluid. The global wake structure then is modeled as being induced by a number of line vorticities around which the flow circulates. The strength of vortex elements is computed by integrating them to obtain circulation. Together, vorticity distributions, circulation, and local geometry are used to model and make inferences about the time history of aerodynamic forces. In recent years, such measurements have been used to study the flow around, and behind

insect and bird wings in detail (Hedenström, Rosén, et al. 2006; Johansson and Hedenström 2009; Spedding, Rosén, et al. 2003). By contrast, investigations of bat flight are in its early stages. Detailed wake structure has been studied in only three species: two relatively small nectar-feeding phyllostomid bats - *Glossophaga soricina* ($\sim$ 10 g; Alvarez et al. 1991) and *Leptonycteris curasoae* ($\sim$ 20 g; Arita and Humphrey 1988; Hedenström, Johansson, and Spedding 2009; Hedenström, Johansson, Wolf, et al. 2007; L. C. Johansson et al. 2008; Muijres et al. 2008) - and a medium-sized non-echolocating pteropid bat *Cynopterus brachyotis* (Hubel, Hristov, et al. 2009; Hubel, Riskin, et al. 2010; Tian et al. 2006). These studies are beginning to unravel the complex wake topology of bat flight, correlate wing kinematics and wake structure, and highlight differences between different species, as well as individuals of the same species.

In one of the first such studies, Hedenström and colleagues (2007) described the wake topology of *G. soricina* freely flying in a wind tunnel with speeds ranging from 1.2 to 7.5 m/s. On the basis of wake velocity and vorticity fields, they quantified the wake structure at slow (1.5 m/s), medium (4 m/s) and high (6.5 m/s) speeds. At slow speed the wings generated a strong start vortex, shed at the trailing edge of the wing at the beginning of the downstroke. With stroke progression, a trailing tip vortex was shed, along with a trailing vortex of opposite sign shed at the wing root. The transition from down- to upstroke was marked by a pitch-up motion flipping the wing upside down, and a resulting combined start/stop vortex. During upstroke the wing moved backward faster than forward flight speed and with circulation reversed, the induced flow was backward and downward, thus generating some thrust and lift. At the end of the upstroke the wing undergoes a pitch-down motion shedding a combined stop/start vortex (Hedenström, Johansson, Wolf, et al. 2007). At medium to high speeds, the wake appeared somewhat different from that of slow speed The downstroke generated a strong start vortex, but the corresponding stop vortex was weaker and diffuse. During upstroke, a weak vortex ring was seen toward the wingtip, inducing an upwash, and hence lift. At the same time,

near the root of the wing there was weak negative vorticity associated with downwash, indicative of negative lift (Hedenström, Johansson, Wolf, et al. 2007).

Based on these results, Hedenström and colleagues (2007) proposed a conceptual wake model for slow, and medium to high speed flight of *G. soricina* (Fig. 1.3). These wake models show that the aerodynamic wake signature is more complicated than indicated in previous flow visualization studies. In slow forward flight, passerines generate wakes that are described as single closed-vortex loops (Spedding, Rosén, et al. 2003), and swifts at typical cruising speed (~ 8 m/s) shed trailing wingtip vortices throughout the down- and upstroke with low amplitude cross-stream vortices shed throughout (Henningsson et al. 2008). But when considering the wake signature of *G. soricina*, it becomes clear that there are striking differences in bird and bat wakes. Bats generate two separate vortex loops, one for each wing, with upstroke producing lift except toward the end when there is negative lift production. A follow-up study using high speed (200 Hz) PIV measurements on *G. soricina*, and an additional bat species (*Leptonycteris curasoa*) confirmed the overall wake topology described here (Hedenström, Johansson, and Spedding 2009).

The results described above suggested the existence of unsteady mechanisms, especially at slow flight where the calculated lift forces were well below those required to stay airborne. Unsteady in this context means turbulent flow in the vortex loops present over the wings, and that time history is important for aerodynamic force calculations. In a subsequent study (Muijres et al. 2008) using the same bat (*G. soricina*), the instaneous flow fields around the wings were visualized while the bat was hovering to get a food reward. Results showed the presence of large leading edge vortex (LEV) attached stably to the wing during the downstroke (Fig. 1.4). When the angle of attack is high, flow usually separates at the sharp leading edge at the start of the motion forming a large vortex, and hence the name. That insects generate and use LEVs as one of the mechanisms to

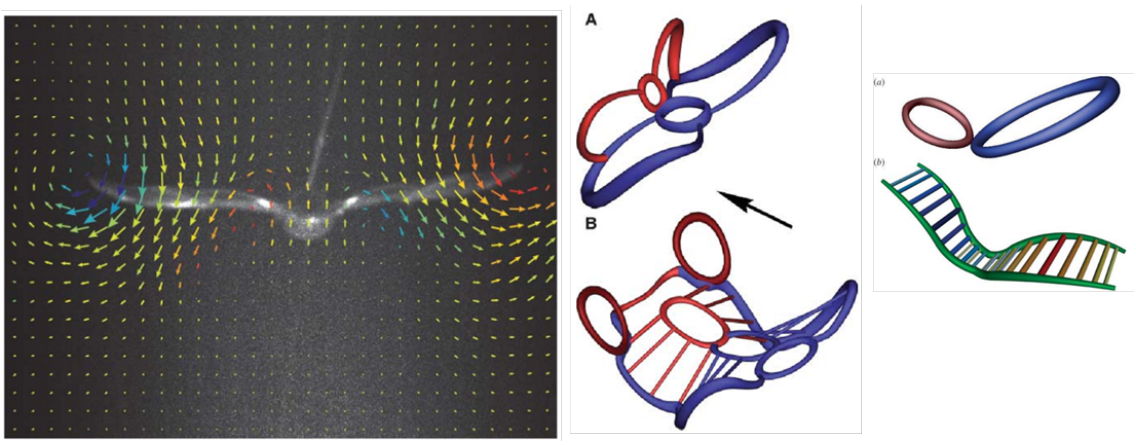

Figure 1.3: Comparing wake fields and wake models of bats and birds. On the left is shown the velocity field generated by the flight of the nectar feeding bat *G. soricina*. The image is generated by superpositioning PIV measurements of the wake field on a snapshot of the bat during mid-downstroke at 4 m/s. Note the presence of wingtip vortices and a central downwash along the wing's trailing edge. The colors and strength of the flow vectors indicate the streamwise vorticity and sign (blue, clockwise and negative; red, anticlockwise and positive). Shown in the middle are cartoons of the wake models at **(A)** slow speed (1.5 m/s) and **(B)** medium speed (4 m/s) for *G. soricina*. Colors indicate vorticies generated during the wingbeat (blue, downstroke; red, upstroke; from Hedenström, Johansson, Wolf, et al. 2007). Shown on the left is a wake model proposed for thrush nightingale (top, flight speed 7 m/s), and that for a swift (bottom, flight speed 8.4 m/s). Red and blue colors denote vorticity as described above, and green indicates the inferred trailing vortex shed at the wingtip throughout the wingbeat of the swift (adapted from Hedenström, Johansson, Wolf, et al. 2007, and Hedenström and Spedding 2008).

stay aloft was demonstrated as early as 1996 (Ellington et al. 1996). Since then it has been shown that most hovering insects generate and use LEVs for lift production. The study by Muijres and colleagues (2008) was first to unambiguously demonstrate the presence of LEVs in vertebrate flight. Not only is there a presence of LEV in a hovering bat, the flow behind the wing is found to reattach and maintain the laminar flow at the trailing edge. Additionally, estimates of circulation were found to account for up to 40% of the lift throughout the stroke.

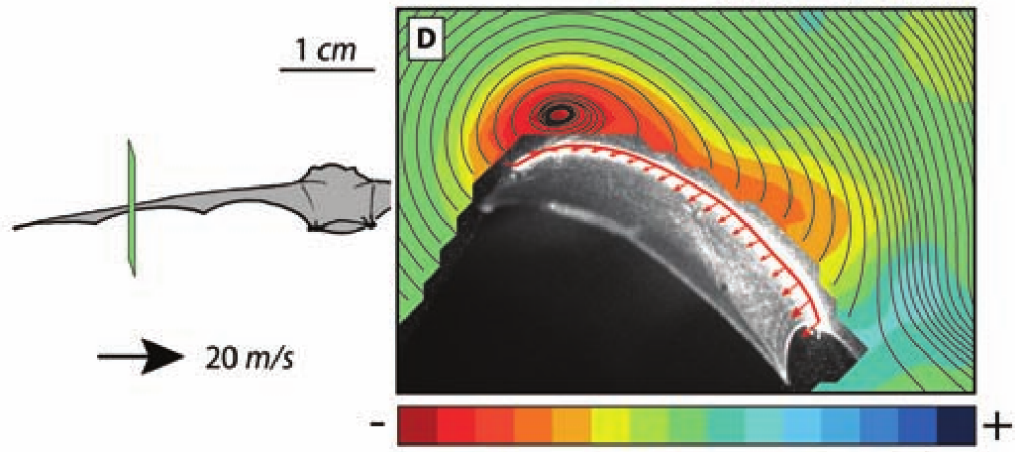

Figure 1.4: Wake-vorticity of slow flight. Wake-velocity fields generated by a slow flying (1 m/s) *G. soricina*. The flight direction is from left to right (arrow); the plane of measurement is indicated in the bat schematic (green bar) on the left. The strength of vorticity is indicated by the colorbar at the bottom (from Muijres et al. 2008).

Recently published results from a different bat species, the lesser dog-faced fruit bat *Cynopterus brachyotis* ($\sim$ 20 g; Severson 2002) combining PIV (in spanwise plane) and high speed videography for kinematics further extend the results described thus far (Hubel, Hristov, et al. 2009; Hubel, Riskin, et al. 2010; Tian et al. 2006). Kinematic and PIV data was obtained for a wide range of flight speed from 1.3 to 5.5 m/s which showed wake topology similar to that obtained from *G. soricina* and *L. curasoae* albeit with some differences, which are likely due to different bat species and experimental conditions. Over the course of a wingbeat four distinct vortices develop with circulation differing in strength, sense, correlation with wingbeat phase, and relation to wing position, for both lower and higher speed flight. The dominant structure is the trailing wingtip vortex V1 (Fig. 1.5) present during most of the wingbeat cycle, generating lift in downstroke and most of upstroke at which point it disappears. However, although the portion of the wing-beat cycle without the trailing wingtip vortex is very short, the wake structure can still be considered a vortex ring rather than a continuous vortex or ladder structure at higher speeds which has been proposed for bird flight (Henningsson et al. 2008). Simultaneous

to the appearance of wingtip vortex, a counter-rotating vortex V2 is formed closer to the body. It gains strength early in the downstroke but disappears quickly. This indicates that the left and right wings operate independently, with little or no lift generation over the body. At the end of the upstroke, a second pair of vortices V3 and V4 form at the distal wing region, with the proximal vortex V3 having the same sense as V1. This pair of vortices is similar to that described in *G. soricina* (Hedenström, Johansson, and Spedding 2009; Hedenström, Johansson, Wolf, et al. 2007; L. C. Johansson et al. 2008), suggesting the development of negative lift close to the end of upstroke.

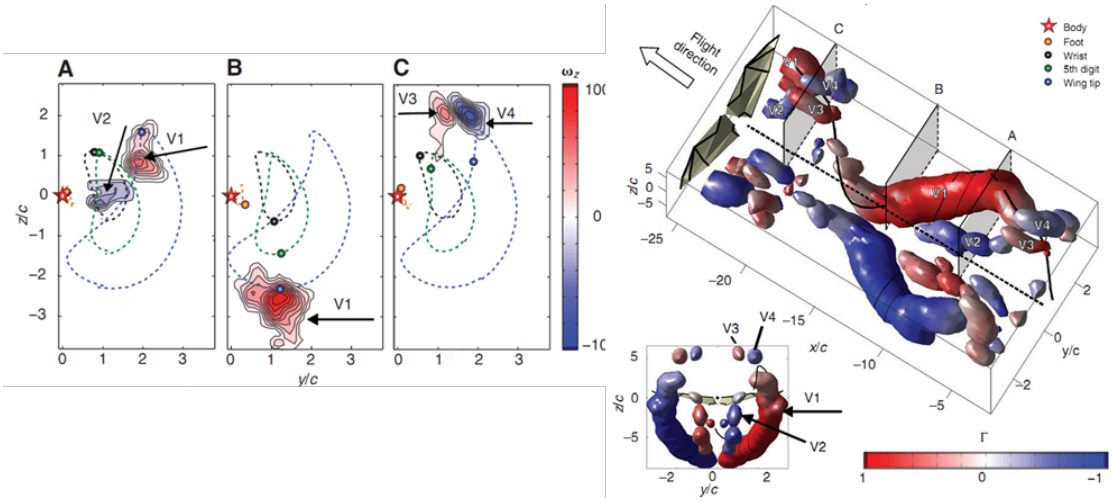

Figure 1.5: Wake velocity fields generated by *Cynopterus brachyotis*. Shown on the left are transverse views at three positions over the wingbeat cycle at 7 m/s: **(A)** upper reversal point; **(B)** lower reversal point; and **(C)** end of upstroke. Strength of the vortices is indicated by shades of the colorbar (red, counterclockwise rotation; blue, clockwise). V1-V4 indicate the four dominant vortex structures (see text). Instantaneous positions of different body parts are indicated by a star and colored dots. Shown on the right, and at the transverse plane at the bottom, is reconstruction of the wake structure over approximately one and a half wingbeat cycles. The three planes (A, B and C) as marked indicate the positions of image on the left respectively. (adapted from Hubel, Riskin, et al. 2010).

1.2 Airflow sensing by flying animals

Animal locomotion necessitates the ability to sense the surrounding substrate for the control systems to generate motor commands that minimize the difference between the measured and intended states. This feedback comes from a variety of systems that have evolved over millions of years in the animal kingdom. When considering animal flight, the generation and changes in aerodynamic forces associated with flapping kinematics, the changes in mean wind speed including the degree and nature of turbulence, and the presence of obstacles as well as prey become critically important. A large part of what we know about airflow sensing comes from studies of winged insects. It has long been recognized that insects are the most diverse group of organisms. It is estimated that there are more than 6-10 million different members in this group, constituting more than 80% of all animal diversity (Chapman 2009; May 1988). Based on the presence or absence of wings, the class Insecta is grouped in two subclasses viz. Apterygota (wingless insects) and Pterygota (winged insects). Winged insects have evolved a rich repertoire of flow sensors as well load sensors on the wings, head and body (Taylor and Krapp 2007). The morphology and physiology of insect flight sensors have been studied in remarkable detail, nevertheless, their role in flight control is not completely understood.

Compared to airflow sensing by insects, we know relatively little about how birds and bats sense airflow as a feedback mechanism to guide flight. For instance, there are only a handful of studies exploring the possible role of mechanoreceptors associated with feather follicles in bird flight control (Brown and Fedde 1993; Necker 1985), although their response characteristics have long been characterized (Necker 2000). Similarly, the presence of hair (Maxim 1912), and dense innervation of bat wing membrane has long been known (Ackert 1914; Gupta 1967; Holbrook and Odland 1978; Quay 1970; Sabussow 1910; Schöbl 1871), but it was not until much later that an association was suggested between hair receptors and airflow sensing (Zook 2005, 2006; Zook and Fowler

1986). Recent investigations from our laboratory reveal that airflow stimulation of wing hairs evokes directionally selective cortical responses, with a majority showing a preference for caudal-to-rostral direction (Fig. 1.6). Additionally, removal of wing hairs results in decreased flight maneuverability in obstacle avoidance tasks, as indicated by decreased turning angles and increased flight speed, observed in two bat species (Sterbing-D'Angelo et al. 2011).

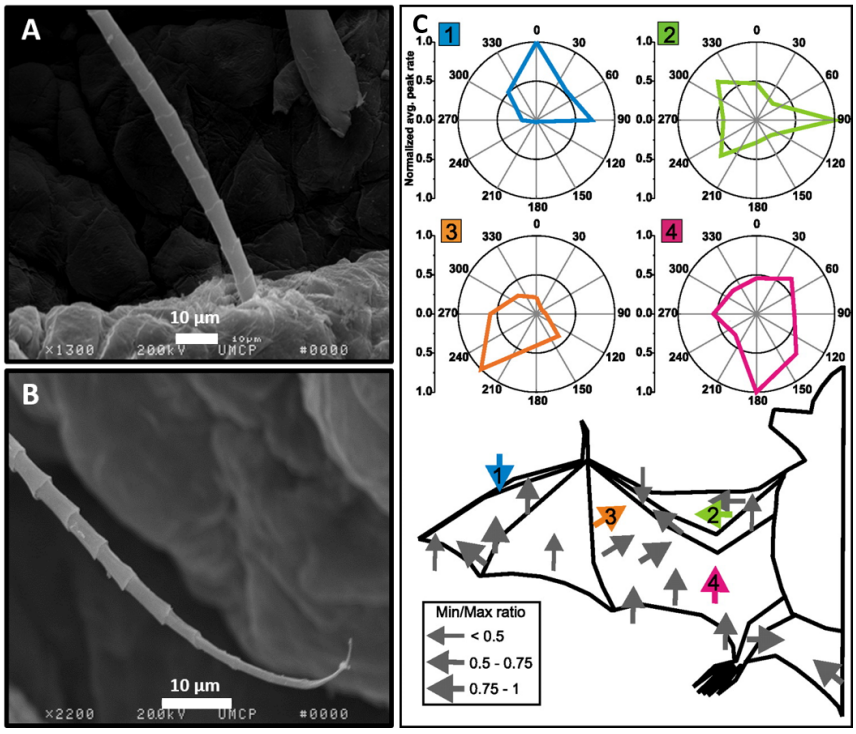

Figure 1.6: Sensory wing hair and neuronal response to directional airflow. High magnification scanning electron micrographs of sensory hair on the wings of *E. fuscus*, showing the base **(A)**, and the tip **(B)**. Images by S. J. Sterbing-D'Angelo. **(C)** Directional selectivity of multiunit S1 responses to airflow presented from 8 directions. Polar plots show averages of neuronal peak response (20 trials), normalized to the peak. Arrows in the bat schematic show locations of sampled receptive fields, color-matched to the four polar plots. Arrow direction indicates the direction of airflow that elicits the maximal response, and arrow thickness indicates the minimum-maximum ratio of the directional response strength. For example, a value of 0.5 indicates that for the non-preferred direction, the response was reduced by half compared with the preferred direction (adapted from Sterbing-D'Angelo et al. 2011).

What are these airflow sensors? What aspects of airflow are sensed? And how does this sensory input inform the motor system for optimizing flight control? In the remainder of this subsection I will address these questions by reviewing what is known about airflow sensing by flying animals, viz. insects, birds and bats.

1.2.1 Airflow sensing by winged insects

The sensory systems involved in insect flight control can be broadly grouped as optic flow sensors, airflow sensors, inertial sensors, and wing load sensors. I will focus on airflow sensors viz., antennae and trichoid sensilla, as they form the most direct form of feedback for insect flight control. The antennae and trichoid sensillae experience aerodynamic forces and moments that an insect produces, and their responses depend upon movement of the surrounding air mass.

1.2.1.1 Antennae as airflow sensors for flight control

All winged insects have a single pair of antennae. There are many roles ascribed to insect antennae, e.g. mechano-, chemo-, thermo-, and hygroreception (Schneider 1964). Their role in flight control has been demonstrated in at least 5 out of 30 designated orders that have been studied (Taylor and Krapp 2007). A number of studies have reported on the possible role of antennae in insect flight control (Gewecke 1970; Gewecke and Niehaus 1981; Heinzel and Gewecke 1987; Niehaus 1981; Niehaus and Gewecke 1978; Sane et al. 2007). One of the most direct ways to investigate the function of antennae is to amputate them. Generally, antenna removal results in a decrease in insect flight speed, and experiments where airspeed is controlled by the experimenter, e.g. with tethered insects, an increase in imposed airspeed results in decreased stroke amplitude. The observation that this effect is consistent across different orders has been used to argue for the role

of antennae in regulation of flight speed by providing peripheral feedback to the flight apparatus (Taylor and Krapp 2007).

The structure of antennae varies, but generally they are composed of two well differentiated basal segments, and a whip like flagellum made of similar elements (Schneider 1964; Fig. 1.7). There are 2-5 muscles attaching the basal most segment (scape) to the cephalic cuticle. Sensory bristles on the scape monitor the joint angle via internal mechanosensors. The second basal segment (pedicel) is held by 2-4 muscles to the scape as a hinge joint, the muscles acting as two antagonistic units. The pedicel is almost always covered by sensory bristles, and not much is known about the internal mechanosensors associated with these bristles (Taylor and Krapp 2007).

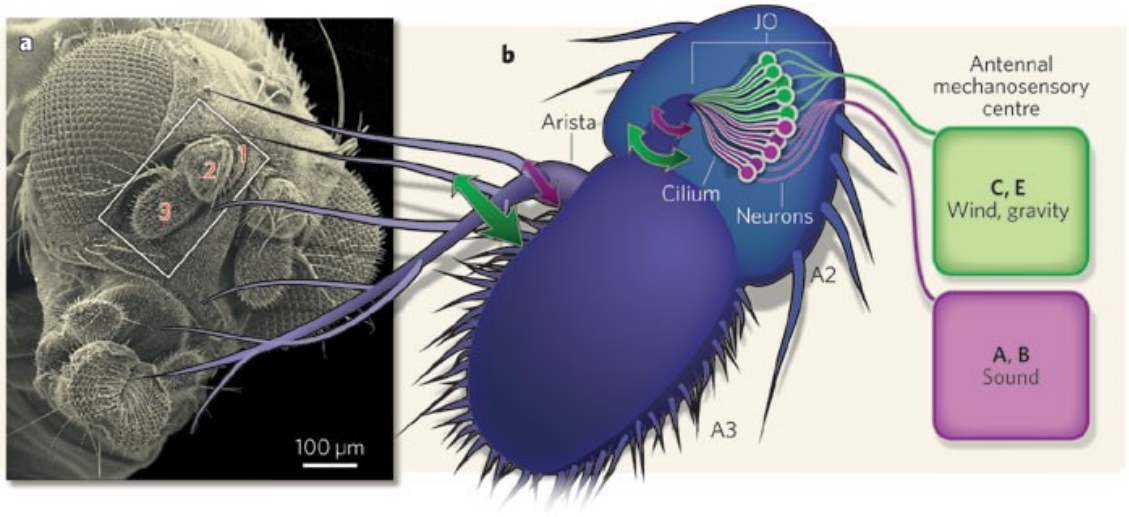

Figure 1.7: Insect antenna. Scanning electron microscope image of the head (left) and schematic of the antenna of *Drosophila melanogaster* (from Eatock 2009).

The rest of the antenna is known as flagellum and is highly variable in form, e.g. the suborder Brachycera, a major division of Diptera is characterized by a highly modified flagellum, where the first flagellar segment is enlarged as a spheroid structure from

which the remaining segments emerge laterally as fine feather-like extensions called arista (Wiegmann and Yeates 2007; Fig. 1.7). The flagellum lacks its own muscles and it articulates passively with the pedicel (Schneider 1964). The pedicel-flagellum joint is usually monitored by mechanosensors that are conserved across orders. Campaniform sensilla (flattened disc shaped mechanoreceptors sensitive to stresses in the exoskeleton) are usually present on the distal rim of the pedicel. Another feature that seems to be common is the presence of Johnston's organ, which is a stretch-sensitive receptor inserted on the pedicel-flagellar joint (Taylor and Krapp 2007).

Together, the scape muscles, the pedicellar campaniform sensilla and the Johnston's organ are thought to be involved in the antennal flight control system (Sane et al. 2007; Taylor and Krapp 2007).

A note on insect sensilla:

Sensory structures in arthropods are called sensilla. There are at least three basic types:

1. Trichoid sensilla are hair-like projections which are innervated by single or multiple neurons. These sensilla are known to be sensitive to various modalities including mechano-, chemo-, hygro- and thermoreception (their role in wind sensing is described in Subsection 1.2.1.2).

2. Campaniform sensilla arise from a dome-like swelling of the cuticle which is sensitive to mechanical deformation. Typically these are thought to perform proprioceptive functions. These sensillae are most commonly found in the membranous, flexible regions of the body, such as the leg and the wing bases.

3. Scolopophorous organs (also known as chordotonal organs) are composed of single or multiple individual sensory units called scolopidia. These are often subcuticular. Each scolopidium acts as a sensitive stretch receptor, responding to deformations

of the cuticle. In certain regions multiple scolopidia are grouped together forming specialized structures e.g. Johnston's organ (see below).

Antennal positioning reaction

A common observation in all Pterygotan species studied to date is the active protraction of antennae in preparation for flight. It is believed that this is a feedforward reaction, and functions to expose the antennae to the oncoming flow (Taylor and Krapp 2007). Moreover, when flight commences the angle of antennae is further adjusted such that it is rotated forward about the scape-pedicel joint and this is called the antennal positioning reaction, and is always effected by the scape muscles. This is a feedback response, the effect of which is a reduction of drag on the fagellum. Physiological experiments have shown that the antennal positioning reaction is unilateral, and is brought about by mechanosensors associated with the pedicel-flagellum joint, specifically the pedicellar campaniform sensilla (Gewecke 1970). It has been proposed that feedback about the position of the pedicel-flagellum joint from the pedicellar campaniform sensilla is used to control the position of the scape-pedicel joint, presumably to keep the pedicel-flagellum joint within the preferred operating range of the Johnston's organ (Taylor and Krapp 2007).

A note on Johnston's organ:

The specialized sensory organs sensitive to vibrations are subcuticular mechanoreceptors called chordotonal organs. The basic unit or building block within a chordotonal organ is called scolopidia, each of which consists of 3 cells arranged linearly: a cap cell, placed on top of a scolopale cell, which envelops the dendrite of a bipolar nerve cell. One type of chordotonal organ is called Johnston's organ, found in all adult insects studied to date. Located in the pedicel, the scolopidia attach at one end to the pedicel wall, and at the other sensory end, to the base of the third antennal segment (flagellum). Another

example of a chordotonal organ is the subgenual organ, located in the proximal tibia of each leg, and involved in sensing substrate vibrations through the legs.

Antennal oscillations

On top of the flight induced passive deflections of the pedicel-flagellum joint are small, active oscillations ($\sim 1°$ amplitude) occurring at wing beat frequency (Sane et al. 2007; Taylor and Krapp 2007). It is believed that these oscillations, brought on by thoracic vibrations, by flight induced airflow or acoustically by the flight tone, provide sufficient stimulation for the phasic response of the Johnston's organ (Sane et al. 2007). Physiological experiments with tethered insects and recordings from antennal nerves or Johnston's organs reveal two aspects about the response properties with respect to antennal stimulation. One, the compound response of antennal nerve is biphasic. Evidence suggests that this is a result of directionally sensitive individual scolopidia, and therefore fire exactly in phase or 180° out-of-phase during sinusoidal oscillations. Secondly, the phasic response of the Johnston's organ is also a function of the static airspeed. This appears to be a result of two mechanisms. One: the amplitude of antennal oscillations is a decreasing function of static airspeed, most likely due to the mechanical properties of the pedicel-flagellum joint. Hence, the afferent discharge is a decreasing function of static airspeed. Second: because the individual scolopidia are directionally sensitive, the relative amplitude of the two phases of the compound discharge depends on the mean flagellar deflection, and also airspeed. Ultimately, the Johnston's organ therefore may be providing feedback about the mean deflection of the flagellum (Sane et al. 2007; Taylor and Krapp 2007).

Together, the feedback from the antennal positioning reaction (campaniform sensilla) and antennal oscillations (Johnston's organ) serves to regulate airflow by way of sensing changes in airspeed.

1.2.1.2 Wind-sensitive hairs

Trichoid sensilla are hair-like sensory structures abundantly present in insects, at least some of which are wind sensitive (Smola 1970; Weis-Fogh 1949). The most well-known example includes the anal cerci, but these have not been implicated in flight control. The most well-studied wind-sensitive trichoid sensilla are from locusts ($\sim$ 430 trichoid sensilla located in 5 indistinctly defined fields on each side of the frons and vertex; Fig. 1.8). Description and role of trichoid sensilla on locust head capsule was first provided by Weis-Fogh (1949). Stimulation of these hairs with a jet of air in a suspended insect induced flight for as long as airflow was present. In addition, Weis-Fogh observed that airflow directed from one side, induced the locust to turn into the wind, in an apparent yaw correction maneuver. Lastly, covering the hairs with cellulose resulted in an absence of a response to airflow stimulation.

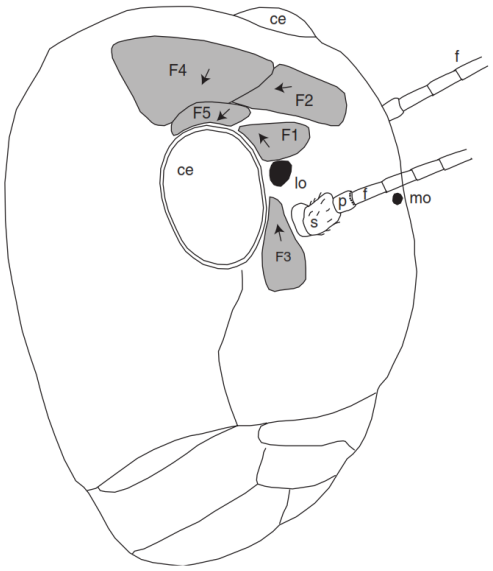

Figure 1.8: Schematic of the sensory apparatus of a locust's head. The directionally sensitive trichoid sensilla are arranged in distinct fields as determined by the average afferent discharges of hairs in each field. Arrows indicate the approximate directional sensitivity of hair fields. Note that directional sensitivity of individual hairs could vary. ce = compund eye; mo = median ocellus; lo = lateral ocellus; s = scape; p = pedicel; f = flagellum; F1-F5 = fields of wind sensitive hairs (from Taylor and Krapp 2007).

Trichoid sensilla elsewhere on the body (including the wings) in locusts and other insects have been speculated to play a role in flight control (Burrows 1996), although direct evidence is lacking (Page and Matheson 2004).

The description that follows comes from studies on locusts (*Schistocerca species*). The cephalic trichoid sensilla of locusts are curved, ranging in length from 30 to >250 µm (Smola 1970). One of the most striking feature of these sensors is their directional sensitivity. Experiments isolating different components of the system show that this directional response is a result of angular deflection of the shaft, which is a function of direction and speed of airflow, as well as mechanical and physiological properties of the system itself. In one such experiments, Camhi (1969) isolated individual trichoid sensilla and recorded extracellular afferent discharges to varying wind speed and direction. He demonstrated slowly adapting responses to airflow stimulation, with maximal firing occurring when the wind direction aligned with curvature of the hair shaft. In addition, asymmetries in the forces generated at the hair socket, and dendritic attachment contributed to the overall directional sensitivity. Knowing the directional tuning of individual sensilla, the directional properties of the entire fields have been mapped (Taylor and Krapp 2007).

Together, the selectivity to direction, and sensitivity to the speed of airflow of cephalic trichoid sensilla are thought to provide both directional and non-directional feedback (respectively) to the flight motor. It remains to be seen if the cephalic hairs are capable of sensing more than wind direction or assisting in yaw correction, e.g. angle of attack.

1.2.2 Airflow sensing by birds

As opposed to insect literature, studies on flow sensing by birds are more limited. Whereas a number of studies describe the mechanoreceptors and their response properties in general, only a handful of papers specifically address the issue of flow sensing.

Necker (2000) has summarized the mechanoreceptors in birds. There are four main types distinguished: Herbst corpuscles (HC), Merkel cell receptors, Grandry corpuscles and Ruffini endings. Similar to mammalian cutaneous mechanoreceptors, Merkel cell and Ruffini endings are slowly adapting whereas Grandry corpuscles and Herbst corpuscles are rapidly adapting. There is a wide variation in the distribution and arrangement of these receptors across the different species of birds studied.

Necker (1985) and Horster (1990) have characterized the response properties of Herbst corpuscles and suggested their role in flight control. Herbst corpuscles are the most widely distributed receptors in bird skin. These are lamellated receptors and comparable to mammalian Pacinian corpuscles, both morphologically and physiologically, e.g. relatively large size and sensitivity to vibrations between 100-1000 Hz. In the feathered skin, they are usually associated with the secondary filoplume feathers.

To address the role of wing associated mechanoreceptors in flight control, Brown and Fedde (1993) recorded activity from radial nerve of a chicken while manually moving the alular joint and feathers, or using airflow (generated by an air compressor) directed at the wings. They noted that discharge frequency correlated with elevation of covert feathers or extension of the alular joint. In addition, an increase in velocity of airflow stimulation led to increased firing rate of the secondary filoplume receptors (thought to be Herbst corpuscles). This led them to conclude that wing associated mechanoreceptors could detect possible stall at high angles of attack, as well as flight speed by the vibration frequency of secondary flight feathers.

1.2.3 Airflow sensing by bats

The wings of bats are covered by an array of microscopically small hairs that appear to arise from dome-shaped structures. The presence of these hairs has been known for over

one hundred years (Maxim 1912), but their functional role has only recently begun to be investigated (Sterbing-D'Angelo et al. 2011; Zook 2006; Zook and Fowler 1986). Hairs arising from the wing appear different from the fur or pelage hair covering most of the body of bats. Wing hairs are much shorter (10-600 µm) compared to the pelage hair which can be several mm in length, and these short wing hairs are sparsely distributed ($\sim 1\backslash mm^2$; Sterbing-D'Angelo et al. 2011). The raised domes through which the hairs arise appear similar to the touch domes of mammalian skin. In some species, e.g. in the rat, each dome is invariably associated with a large guard or tylotrich hair situated at the periphery of the dome (Nurse and Diamond 1984). In the cat, however, only 47% of the touch domes abut a guard hair (Iggo and Muir 1969), and in humans, their relationship with hairs is also inconsistent (Reinisch and Tschachler 2005).

In mammalian hairy skin, touch domes are formed by aggregates of Merkel cells, supplied each by one or more branches of myelinated sensory axons. Merkel cells were also reported in the domes and surrounding the hair follicles of bat wings (Zook and Fowler 1986). Recent collaborative efforts between our laboratory and Columbia University (Dr. Ellen A. Lumpkin, principal investigator) are shedding light on the suite of mechanoreceptors and their innervation in the wing membrane skin (Chadha et al. 2012). Findings show the presence of Merkel cells, lanceolate endings, free nerve endings and diffuse endings that resemble end-knobs described previously in bat wing skin (Ackert 1914). Additionally, these receptors are distributed differentially in the wing membrane versus skin overlying the digits. For instance, diffuse endings are sparsely distributed relative to other end-organs, but are in significantly higher density in the inter-digital membrane. By contrast, lanceolate endings and Merkel cell clusters aggregate more densely over the digital and forearm bones. Primary afferent recordings from domed-hairs of *Antrozous pallidus* (Zook 2005), and primary somatosensory cortical recordings from *Eptesicus fuscus* show highly sensitive responses to air-puffs and calibrated light touch stimuli (Sterbing-D'Angelo et al. 2011).

Together, these data demonstrate that bat wing skin is innervated by a repertoire of sensory receptors whose differential distribution suggests functionally specialized regions of the wings. Based on these findings we hypothesize that the array of tactile hairs on bat wings provide real-time airflow information in their immediate vicinity. This distributed network of airflow sensitive receptors could provide relevant information to the flight motor apparatus, to make fine-scale adjustments of wing kinematics in order to stabilize flight based on prevailing flow conditions.

1.3 The role of somatosensory system in bat flight control

At the forefront of the hypothesized ability of bats to monitor airflow is an array of microscopic hairs embedded in the wing membrane. Within the mammalian skin are many classes of afferent fibers that differ in the stimulus qualities to which they respond and in the targets and distributions of their central projections and peripheral terminations. These primary sensory neurons follow a basic body plan, where the cell bodies are grouped in consecutive pairs of ganglia adjacent to each vertebra, called the dorsal root ganglia (DRG), or at the base of the skull where they are referred to as the cranial nerve ganglia. Second-order neurons either in the spinal cord or brainstem receive converging inputs from several primary afferents, integrating and conveying activity from cutaneous stimulation to higher order neurons in the thalamus and cortex.

Cutaneous mechanoreceptors that respond to low threshold stimuli are the presumptive end-organs responsible for monitoring airflow in the vicinity of bat wings. Present throughout the mammalian hairy and glabrous skin, these receptors form the basis of the rich and complex tactile information gleaned from the environment. With respect to bat wing membrane, what receptors are potentially involved in airflow sensing? How is cutaneous sensory information processed through various stages of the central nervous

system, specifically those concerned with low threshold mechanical stimuli like airflow? What is known about the somatosensory cortical organization of bats, and how does it compare to other mammalian species? In this subsection I will review relevant literature addressing these questions.

1.3.1 Mammalian cutaneous mechanoreceptors

Cutaneous mechanoreceptors, which respond to low-threshold or non-noxious mechanical stimuli serve as the starting points for tactile perception. Much or our understanding about cutaneous mechanoreception comes from non-human primate and rodent studies. In addition to the traditional models of mechanosensory perception, there are a number of specialized systems e.g. the star-nosed mole with its 22 rays of fleshy appendages (Catania 1999), post-facial vibrissae of hyraxes (Reep et al. 2002) and naked mole rats (Crish et al. 2003). But whether one considers the standard models of somatosensory physiology, or the specialized or unique members, it becomes clear that the basic elements, i.e. the receptors, pathways, and brain regions share common features that lie within the mammalian architecture.

In bats (Chiroptera), specialized forelimbs have evolved to function as wings. The thin wing membrane with its array of microscopic hairs has been shown to possess the same repertoire of afferent fibers and end-organs that are conserved across diverse mammalian species studied. While we know relatively little about the precise role these receptors play with reference to sensing airflow, there exists a wealth of information about the cytoarchitectural, electrophysiological and central encoding mechanisms from primate and rodent studies (Fig. 1.9).

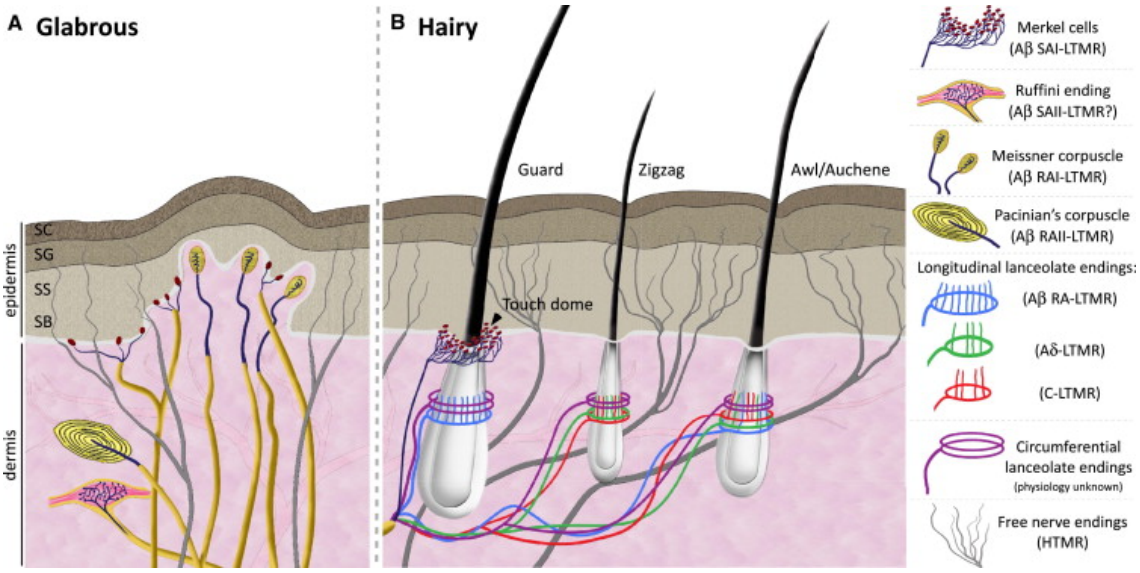

Figure 1.9: Organization of mammalian cutaneous mechanoreceptors. (A) Glabrous skin has four types of mechanoreceptors: Merkel cell-neurite complex (SA-1), Meissner corpuscles (RA), Ruffini endings (SA-2), and Pacinian corpuscles (RA). **(B)** Hairy skin has mechanoreceptors associated with the follicles (hair units), or the skin between hairs (field units). In the mouse skin (most well-studied), hair follicles fall into distinct types as shown, depending on their length, thickness and presence of kinks in the hair shaft (from Abraira and Ginty 2013).

The presence of hair on the bat wing membrane makes it non-glabrous or hairy skin. More than 90% of mammalian skin surface is covered by different types of hairs, some more dominant than others. Yet, a lot less is known about the properties of mechanoreceptors and primary afferents of hairy skin that are responsible for discriminative touch. There are a number of reasons that appear to contribute to this, e.g. local or regional differences in receptive properties across the skin surface, a large number of heterospecific specializations, and a functional role that appears diffused, e.g. thermoregulation, camouflage, protection against predators, sexual dimorphism, discriminative touch etc. At the same time, the use of rodents with their highly developed and elaborate whisker system has made tremendous contributions to our understanding of cutaneous mechanoreception.

Mechanoreceptors in the hairy skin are located in hair follicles, or in the skin between hairs. Like in glabrous skin, there are large, myelinated Aβ afferents associated with a number of receptor types. In addition, there are smaller diameter myelinated and unmyelinated (Aδ and C) fibers that may or may not occur with specific receptors. Based on the rates of adaptation to sustained mechanical stimulation, the mechanoreceptors are classified as slowly or rapidly adapting (SA or RA). SA-1 afferents innervate Merkel cells that are found in hair follicles or as aggregates in touch domes. These respond to movement, as well as static indentation of skin, and display small receptive fields with spots of high sensitivity. SA-2 afferents innervate Ruffini organs and have receptive properties similar to those in glabrous skin. They are sensitive to directional skin stretch, and are thought to contribute to hand grip (in humans) providing information about finger position (Johnson 2001; Zimmermann et al. 2009). The same applies to Pacinian corpuscles (PC units) that are found deep in the dermis, although they are much sparsely distributed compared to other receptor types.

Then there are RA units that are unique to hairy skin called hair units, innervating follicles, and field units, innervating the skin between hairs. Hair units are activated by deflection of hairs, innervate many follicles and hence have large receptive fields. Afferents belonging to hair units are of both Aβ and Aδ variety. The nerve terminals of these fibers are arranged circumferentially around the follicles and are called lanceolate or palisade endings. One variety of such receptors is called D-hair receptors, first described by Brown and Iggo (1967), were named because of their association with down hairs within the skin. These receptors are among the most sensitive receptors in the mammalian skin (Koltzenburg et al. 1997; Lewin and McMahon 1991; Lewin, Ritter, et al. 1992; Woodbury et al. 2001). Field units are Aδ fibers or C-fibers that lack the myelin sheath. These have large receptive fields as well, with zones of high sensitivity, and are generally high threshold mechano- or nociceptors, or both. But the vast majority of C-fiber afferents respond to high threshold mechanical and thermal stimuli, as well as endogenous and

exogenous chemicals (Basbaum et al. 2009), and are considered polymodal (Kruger et al. 1981).

Hair on the wings of bats are unlike common mammalian hair types (smaller and thinner). Nevertheless, the presence of Merkel cells, lanceolate endings and free nerve endings (Chadha et al. 2012; Zook 2005) in and around the domed hairs and wing skin suggests that they act to detect mechanical deflections of hairs, as well as deformation or stretching of the skin, which is expected to occur during flight. Experiments described in the proceeding chapters test this hypothesis, specifically addressing the features of airflow that are extracted and encoded by the central nervous system.

1.3.2 Subcortical and cortical organization of mammalian somatosensory system

Somatosensory information from peripheral afferents connected to skin, muscles, and joints enter the spinal cord via consecutive pairs of ganglia adjacent to each vertebra, called the dorsal root ganglia (DRG), or at the base of the skull where they are referred to as the cranial nerve ganglia. Within the spinal cord these afferents branch extensively and project to nuclei in the spinal gray matter and brainstem. Within the brainstem mechanosensory inputs terminate in the dorsal column-trigeminal nucleus complex, viz. the gracile, cuneate and spinal trigeminal nuclei. Second-order neurons from dorsal column-trigeminal nuclei cross over the midline to form the medial lemniscus pathway, before terminating in the ventroposterior complex of the contralateral thalamus (Fig. 1.10).

Somatosensory afferents mediating pain and temperature also enter the dorsal horn of the spinal cord, but terminate locally, branching extensively in the white matter forming the tract of Lissauer. Second order neurons from the dorsal horn crossover to ascend

as the anterolateral system (Kandel et al. 2000). Unlike the medial lemniscal pathway, which projects directly to thalamus, the anterolateral system has both direct and indirect connections via three ascending pathways: the spinothalamic, spinoreticular, and spinomesencephalic tract. The spinothalamic tract projects directly to the thalamus; the spinoreticular tract sends axons to the reticular formation of the medulla and pons, which then relay information to the thalamus; the spinomesencephalic tract terminates mostly in the periaqueductal gray, nucleus cuneiformis and the superior colliculus (Yezierski 1988).

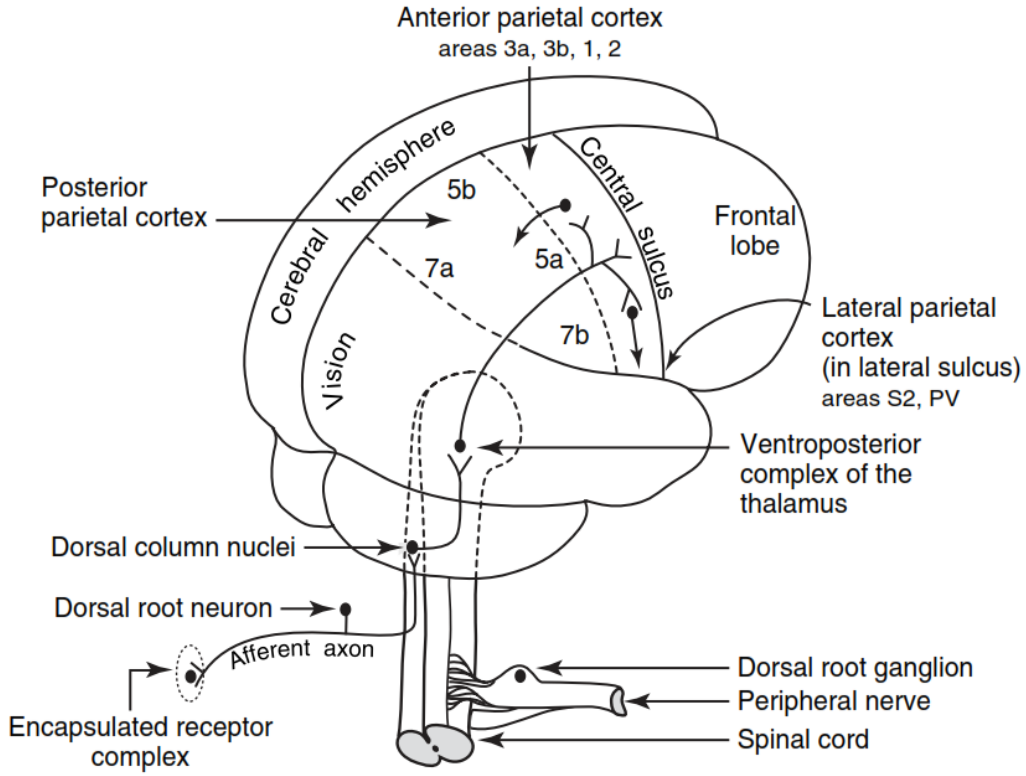

Figure 1.10: The basic components of mammalian somatosensory system. Afferents from skin, muscles and joints enter the spinal cord or brainstem and send branches to dorsal column nuclei, or the trigeminal complex. Second order neurons from here send projections to ventroposterior complex of the contralateral thalamus. Neurons from the thalamus project to S1 (or areas 3a, 3b, 1 and 2 in primates). Further projections are distributed to S2, the parietal ventral area (PV), the parietal rostral area (PR) and the ventral somatosensory area (VS) (from Kaas 2004).

The somatotopic arrangement that is characteristic of cortical areas begins to emerge in the dorsal column-trigeminal nucleus complex. The somatotopic arrangement in these nuclei extends in a rostrocaudal manner in a variety of species (Kaas 2004), such that a cross-section across all the nuclei shows a complete representation of the body. The typical mammalian representation is laid out in a mediolateral sequence from tail, foot, leg to lower body in the gracile nucleus; upper limbs and upper body in cuneate nucleus; and face representation in the spinal trigeminal nucleus. In the only bat species (the little red flying fox, *Pteropus scapulatus*) where the body surface representation in the dorsal column trigeminal nucleus complex was investigated, a different arrangement was noted (Martin 1993). Instead of the rostrocaudal arrangement, different body regions were found to be arranged in dorsolateral to ventromedial bands, such that the spatial relationships between body regions at the periphery were not maintained within this representation. This significance of this altered arrangement compared other mammals is as yet unknown.

The somatotopic arrangement that begins in the brainstem nuclei is also seen in thalamic nuclei across all mammals studied to date (Kaas 2004). Whether this is the case in bats was investigated by Manger and colleagues (Manger et al. 2001). Their results showed that representational maps in the somatosensory thalamic nuclei of the grey-headed flying fox (*Pteropus poliocephalus*) were in accordance with findings from other mammals, i.e. from medial to lateral, the representation transitions from mouth to face, forelimb, hindlimb and tail. However, the wing representation was inverted such that digits point caudally, compared to walking mammals where the digits point rostrally (Kaas 1983). This inverted wing representation has also been reported in the primary somatosensory cortex of several bats species (Calford et al. 1985; Wise et al. 1986; Zook and Fowler 1986). The somatotopic representation in the big brown bat *Eptesicus fuscus* shows similar forelimb inversion and is discussed in more detail in Chapter 2.

Somatosensory signals from thalamic nuclei are relayed to multiple interconnected somatosensory cortical regions, that project to motor cortex, other cortical areas and subcortical structures (Fig. 1.10). We now know that cortical organization in all mammals investigated reveals a shared basic plan (Krubitzer 2009). Two regions of the somatosensory cortex are common to all mammals - the primary somatosensory cortex (S1) and the secondary somatosensory cortex (S2). There are at least three other areas that appear to be present in most non-primate mammals, viz. the parietal ventral area (PV), and cortical strips along the rostral and caudal borders of S1. The parietal ventral area was described first in squirrels (Krubitzer, Sesma, et al. 1986), and subsequently in the flying fox (Krubitzer and Calford 1992), opossums (Beck et al. 1996), marmosets (Krubitzer and Kaas 1990) and monkeys (Krubitzer, Clarey, et al. 1995). The somatosensory areas lying immediately rostral and caudal to S1 have been called the rostral and caudal somatosensory areas (Beck et al. 1996). In the flying fox, the rostral field has been referred to as area 3a, because it resembles area 3a of primates in position, architecture, connections and response properties (responsive only to stimulation of deep tissues, or muscle spindle receptors). The caudal area of the flying fox has been referred to as area ½ (Krubitzer and Calford 1992) as it is in the same relative position as area 1 of primates and appears to be responsive to both cutaneous and deep receptors as area 2 of primates.

In all investigated mammals, S1 has a systematic representation of the mechanoreceptors of the skin of the contralateral body (Kaas 1983). This somatotopy in S1 usually has the tail or toe to tongue representation in a mediolateral sequence. The representations of different body parts often have a morphological counterpart in the cortex that can be visualized using appropriate histochemical techniques. The most remarkable examples exist in S1 of rats and mice, where aggregates of neurons cluster together in an orderly manner, known as barrels, each corresponding to a particular whisker. Each barrel is a target of the thalamocortical input from the medial lemniscal pathway. These structures were first discovered by Woolsey and Van der Loos (1970). Another striking instance

of cortical isomorphs in S1 is seen in the star-nosed moles, where each of the 22 fleshy appendages arising from the snout are arranged in cortical bands, easily identifiable by cytochrome oxidase staining (Catania 1999).

In a wide range of mammals S1 projects directly to S2, PV, and the rostral and caudal somatosensory areas (Beck et al. 1996) that further process information from S1. These areas also receive direct inputs from the ventral posterior thalamus. As previously mentioned, S2 appears to be a universal subdivision of the mammalian somatosensory cortex (Krubitzer, Clarey, et al. 1995; Sur, Weller, et al. 1981). S2 borders S1 laterally, with face representations adjoining. Other body parts are represented more distantly from the S1/S2 border, and the forepaw and hindpaw are represented along the rostral border of S2. The parietal ventral area (PV) was first distinguished as a mirror image representation of S2 along the rostral border of S2 in squirrels (Krubitzer, Sesma, et al. 1986), and the area has now been identified in a number of species (Beck et al. 1996). Both S2 and PV respond throughout to cutaneous stimuli. This region receives feed forward projections from S2, but also gets convergent inputs from S1, and the thalamus (ventral posterior nucleus). PV projects to the rostral and caudal parietal areas (Beck et al. 1996).

Primate somatosensory cortex is more complex and developed than all other mammalian species studied so far, i.e., a higher number of well differentiated areas, each with a complete representation of a class or classes of afferents from the contralateral somatosensory receptors, and within the primates, simian primates are more complex than prosimian species, both at the cortical and thalamic levels (Kaas 1983, 1993). The major comparative differences lie in the primary somatosensory cortices as follows. In monkeys (and humans), the anterior parietal cortex contains four mediolaterally extending regions, and each region is a distinct architectonic field, with a complete and separate representation of the body surface. These four areas of primates are traditionally called the first or primary somatosensory cortex, S1, and labeled as 3a, 3b, 1 and 2. In mon-

keys, each of the four areas receive a distinct thalamocortical input, and each contains modality specific modules. These modules are activated by either rapidly adapting, or slowly adapting cutaneous receptors, are not histologically distinct, and are most apparent in the hand regions of area 3b of macaques and owl monkeys (Sur, Wall, et al. 1984; Sur, Weller, et al. 1981). Additionally, these functionally distinct modules representing specific receptor types have not been described in S1 of most other mammals, including bats. Non primate S1 is the homologue of the single representation of area 3b (Kaas 1983). Processing of somatosensory information is highly serial from area 3b to area 1, to area 2, while area 3a relates more to motor cortex, receiving most of its projections from muscle-spindles (Kaas 1983).

1.4 Synopsis and outline of the dissertation

The evolution of powered flight in bats makes them unique amongst mammals. The hand-wings that make flight possible are hypothesized to sense airflow as a feedback mechanism for flight control through an array of tactile hairs embedded in the wings (Sterbing-D'Angelo et al. 2011; Zook 2005, 2006; Zook and Fowler 1986). While technological advancements of the past two decades are rapidly advancing our understanding of bat flight, neurophysiological investigations are still in the early stages with fundamental questions as yet unanswered. A deeper understanding of the tactile sensibility of bat wings, and representation of aerodynamic feedback by the nervous system requires a comprehensive approach, establishing connections between the kinematics and aerodynamics of bat flight, as well as the neural underpinnings of airflow sensing by the somatosensory system.

Unlike the wings of insects and birds, bat wings are highly articulated and composed of a thin and extraordinarily elastic skin. The resulting flight kinematics and aerodynam-

ics are thus much more complex than those of birds, with each wing generating its own vortex loop (Hedenström, Johansson, Wolf, et al. 2007). Moreover, the use of unsteady mechanisms, like stably attached LEVs for lift generation known to be present in hovering humming birds (Warrick et al. 2005), fast gliding swifts (Videler et al. 2004) and insects (Dickinson and Gotz 1993) have also been shown to be present in at least one bat species (Muijres et al. 2008). At the same time, separation of the LEV, e.g. at high angles of attack or making a sharp turn, can potentially result in catastrophic stall. It is still largely unknown how bats control the attached LEV. One possibility is that flow sensitive hairs on the wings can sense reversed turbulent airflow and detect separation, thereby activating rapid adjustments of the wing shape to stabilize flight. Evidence exists for the directional selectivity of cortical responses to airflow stimulation of wing hairs (Sterbing-D'Angelo et al. 2011).

The transduction of mechanical deflection of wing hairs into neuronal signals is carried out by receptors embedded at the base of hair follicles and within the wing membrane. Past studies (Zook 2005, 2006) and ongoing collaborative research (Chadha et al. 2012) reveals that a variety of tactile receptors are co-localized with hairs, including lanceolate endings, Merkel cells and free nerve endings. Lanceolate endings are known to be rapidly adapting, responding to deflections of hair. Merkel cells on the other hand are slowly adapting, responding to static indentation or stretch of the skin membrane. How these individual receptors contribute to the sensorimotor response is unknown, but their presence suggests that it is the combined output that forms the overall feedback mechanism about airflow conditions, skin stretch, and proprioception (from muscle spindles).

The importance of a sensory representation in an animal's behavioral repertoire is reflected in the amount of cortical volume devoted to that particular modality. Investigations on the organization of somatosensory cortex of several species of bats (Calford et al. 1985; Krubitzer and Calford 1992; Wise et al. 1986; Zook and Fowler 1986) have

noted a large hand-wing representation, which suggests high innervation density from peripheral tactile mechanoreceptors and the functional importance of mechanosensory input. These findings provide further support for the hypothesized role of tactile hairs of bat wings in providing sensory feedback (along with other somatosensory signals like wing membrane sretch, proprioceptive inputs, etc.) for flight control.

This thesis presents neurophysiological studies that examine the role of somatosensory signaling for flight control using the big brown bat *Eptesicus fuscus* as model animal. Chapter 2 examines the representation of somatosensory surface (especially the wings) and its organization in S1, based on tactile stimulation using von Frey hairs. Additionally, neuronal thresholds to tactile stimulation of the wings were also measured. Given the role of somatosensory feedback from wings in flight control, we hypothesize an expanded cortical representation of the wing surface, with low cortical response thresholds to tactile stimulation.

Chapter 3 addresses questions related to representation of aerodynamic feedback at the level of primary somatosensory cortex. I hypothesize that tactile receptors on bat wings measure quantities related to prevailing aerodynamic forces, informing the flight motor system for kinematic adjustments. Experiments were designed to record S1 neuronal responses, to controlled airflow stimulation of receptive fields on the wings. Parameters related to airflow, such as strength, duration, direction, and spatial location, were independently varied, to reveal the response properties of tactile receptors on bat wings.

Chapter 4 presents the analysis of how aerodynamic feedback from the wings is encoded in the responses of S1 neurons. Specifically, I apply an information theoretic framework to address the role of precise spike timing in encoding the strength, and direction of airflow. As big brown bats are relatively fast and agile fliers (flight speed 3-9 m/s,

wingbeat frequency 11-15 Hz; Kurta and Baker 1990), I hypothesize rapid signaling by spike trains to guide wing kinematics.

Lastly, Chapter 5 provides a summary and overview of the results presented, along with proposals for future experiments aimed at addressing unanswered questions about the role of somatosensory signaling for flight control in bats.

Paper title: Organization of the primary somatosensory cortex and wing representation in the Big Brown Bat *Eptesicus fuscus*

Authors: Mohit Chadha, Cynthia F. Moss and Susanne Sterbing-D'Angelo

Journal: *J Comp Physiol A* (2011) 197:89-96

Chapter 2

Organization of the Primary Somatosensory Cortex and Wing Representation in *Eptesicus fuscus*

The big brown bat is an insectivorous species that is widely distributed in North America. An aerial forager with an average weight of 16 g, a wing span of 32 cm and wing area of 166 cm^2 (Kurta and Baker 1990), *Eptesicus fuscus* has a favorable body mass to wing area ratio (i.e., low wing loading) for relatively slow flight (3-9 ms) and high maneuverability (Norberg and Rayner 1987). It is an echolocating bat that has been traditionally classified under the suborder Michrochrioptera. Relatively little is known about the somatosensory cortical organization in bats, with only two species of Microchiroptera (*Macroderma gigas* and *Antrozous pallidus*) and two species of Megachiroptera (*Pteropus poliocephalus* and *P. scapulatus*) studied to date (Calford et al. 1985; Krubitzer and Calford 1992; Wise et al. 1986; Zook and Fowler 1986). According to a new proposed phylogenetic classification based on molecular data, both *Pteropus species* and *M. gigas* belong to the same

new suborder Yinpterochiroptera, and *E. fuscus* (this study) and *A. pallidus* to the new suborder Yangochiroptera (Teeling et al. 2005). This makes *A. pallidus* the only Yangochiropteran species whose somatosensory cortex has been studied to some extent. For a more complete understanding of the organization of somatosensory cortex in Yangochiroptera, we conducted mapping studies of the somatosensory cortex of another species of this suborder, the big brown bat.

The existence of orderly representations of the sensory surface in somatosensory cortex and other brain regions has long been known. Earliest observations of correspondence between peripheral tactile stimulation and cortical excitation were reported during the late 1930s and early 1940s (Adrian 1941; Marshall et al. 1937) in cats and monkeys. Since then, tremendous progress has been made in our understanding of the development and organization of representations of sensory surfaces in cortical and subcortical structures. Studies of animals with specialized sensory systems are especially useful, as they not only provide information on how particular sensory systems operate, but they also reveal the evolutionary forces that shape brain organization and function. Noteworthy examples of the importance of somatosensory surfaces in an animal's behavioral repertoire come from reports on their cortical representations, e.g., whisker representation in mice and rat "barrel" cortex (Petersen 2007; Woolsey and Van der Loos 1970), extreme magnification of the representation of two front teeth in naked-mole rats (Catania and Remple 2002), greatly expanded representation of the "tactile fovea" in star- nosed moles (Catania and Kaas 1997), and hand and lip representation in primates (Nelson et al. 1980).

As the only mammals with true powered flight, bats combine remarkable flight capabilities including hovering, mid-air predation, and high maneuverability, with high efficiency (Winter and von Helversen 1998). The bat wing is essentially made of all the elements of a typical mammalian forelimb, with the metacarpals greatly elongated, ex-

cept for the thumb, which is not embedded in the wing membrane and is used for food handling, grooming, and climbing. The wing membrane or patagium, stretches from the side of the body to cover the entire forelimb, and the hindlimb, except the foot (Fig. 2.1). Part of the membrane lies between the shoulder and wrist, and is called propatagium. The wing section between the body and the fifth digit is called the plagiopatagium, and that between fingers 2 and 5, the dactylopatagium. The uropatagium or the interfemoral membrane (IFM) is the part of wing that stretches between the tail and the hindlimb. The wing membrane, besides being anisotropic and highly compliant (Swartz, Groves, et al. 1996), is covered by an array of tactile sensory receptors in the form of domed, microscopic hairs (Zook and Fowler 1986). It has been hypothesized that these wing receptors might provide a continuous stream of information about airflow patterns over the wing surface and help a flying bat optimize its wing shape, position and camber, in order to achieve and sustain complex flight maneuvers (Zook 2005, 2006).

By comparing the present findings with previously published reports, we can shed light on inter-species differences in cortical organization among flying and non-fling mammals, echolocating versus non-echolocating bats, and across the new taxonomical suborders of bats. Magnified cortical representations generally correspond to high innervation density and/or the behavioral importance of the sensory surface to the animal. If indeed the unique wing hairs and their associated tactile receptors (Merkel cells and others) as well as stretch receptors embedded in the membrane are important for sensing airflow around the wing membrane and the membrane shape, one might expect to find an expanded representation of the wing in the somatosensory cortex, and low tactile thresholds.

2.1 Materials and methods

2.1.1 Experimental animals

Five adult insectivorous bats (*E. fuscus*; three males and two females) weighing between 15 and 21 g were used for this study. Bats were wild-caught in Maryland and housed in a vivarium at the University of Maryland. Bats were housed under reversed 12 h light/dark conditions and given food and water *ad libitum*. All experimental procedures followed National Institute of Health guidelines and were approved by the University of Maryland Institutional Animal Care and Use Committee (IACUC).

2.1.2 Surgical preparation

At least 1 day prior to surgery the selected bat had the fur over its scalp removed with commercially available depilatory cream (e.g., Veet). On the day of the surgery, each animal was initially anesthetized with 3% Isoflurane (700 ml/min O_2) and anesthesia was maintained at 1-3% level during surgery and cortical recordings. Breathing was monitored visually and body temperature was maintained at about 37° C by placing the animal on a heating pad. Standard sterile surgical procedures were followed throughout the experiment. Once the animal was anesthetized, a midline incision exposing the skull was made and muscles of mastication deflected from the midline. A custom-made stainless steel head-post was then glued close to Bregma using cyanoacrylate glue (Loctite 4161). The bats were allowed to recover for 2-3 days before physiological recordings were initiated.

2.1.3 Electrophysiological recordings

On the day of neural recordings the bat was first anesthetized at 3% and maintained at 1-3% Isoflurane (700 ml/min O_2) during the entire session. The head-post was used to secure the head with a set screw to a vibration isolation table (Kinetic Systems). A craniotomy measuring approximately 2 mm by 2 mm was performed over the somatosensory cortical region (the dura mater was left intact) and sterile saline/silicone oil (Fluka Analytical, DC 200) was used to prevent the exposed cortex from desiccation. A low impedance ($\sim$ 1 MΩ tungsten reference electrode was inserted into a non-somatosensory region e.g., the visual cortex, of the opposite hemisphere through a 100 µm hole in the skull made with a polished needle. A high impedance recording electrode (15-20 MΩ tungsten, FHC Inc.) was used to record extracellularly from multiple units. The electrode was attached to a micromanipulator, oriented perpendicular to the cortical surface and lowered using a hydraulic microdrive (FHC Inc.). Recordings were made from multiple electrode penetrations, spaced 100-250 µm apart from depths of 50-250 µm, ensuring that electrode remained mostly within the supragranular layers of the cortex. The overall thickness of the somatosensory cortex varies from 800 to 1200 µm (Big brown bat stereotaxic brain atlas, E. Covey, University of Washington). Each recording session lasted about 4-6 h, and each animal underwent 2-6 recording sessions spread over a period of 1-4 weeks.

2.1.4 Tactile stimulation

Once the electrode was mounted and set into position, the contralateral wing was spread and taped by the tip to the recording table. Subsequently, the electrode was advanced into the cortex and the wing and body surface stimulated using a set of calibrated monofilaments (von Frey hairs, North Coast). The von Frey hairs are available in sets of 20 with

discrete, fixed weights. The hairs are calibrated in a logarithmic scale from 0.008 to 300 g (0.08-2943 mN), within a 5% standard deviation. Stimulation consisted of pressing the monofilaments at right angles against the skin until they bend and subsequently are released. Progressively thinner filaments were used to determine the neural thresholds. We applied the same method for determining the threshold as has been done in clinical studies, established by Johansson et al.(1980). Both wing surfaces were tested. Mapping was based solely on tactile stimulation with the calibrated von Frey hairs. Borders and center of receptive fields could not be determined with airpuff stimulation, because it is not spatially confined enough and the direction of force is variable. Neurons responded always to stimulation of both wing surfaces, because the wing membrane is remarkably thin (Studier 1972). However, the thresholds were sometimes lower when the ventral side was stimulated leading to the conclusion that this side was preferred. Preference of ventral or dorsal side were not mapped separately on the cortical surface, but rather random, most likely module (column) by module (column). Therefore, we did not include this information in the graphs.

2.1.5 Data collection and analysis

The neural responses were amplified using a differential amplifier (Bak Electronics, MDA-4I), band-pass filtered (500-5000 Hz, Stanford Research Systems, Model SR650), monitored on an oscilloscope and played through a speaker. Receptive fields were defined on the basis of a neural activity clearly distinguishable from baseline response as monitored on the oscilloscope and the speaker. For each electrode penetration that elicited neuronal responses to tactile stimulation, receptive fields were drawn on pictures of the bat. To document and reconstruct the recording sites, drawings of the craniotomy including the vasculature were made and electrode positions marked as noted off the digital micromanipulator (Mitutoyo) using a benchmark for reference. Receptive field data from four

bats was used to construct cortical surface maps of the body surface and wings. Neuronal threshold data were collected from five bats. At the end of the recording sessions, bats were given a lethal dose (0.05 ml) of sodium pentobarbital (390 mg/ml) via intraperitoneal injection.

2.2 Results

In the present study, a total of 221 electrode penetrations were made in five animals to define the organization of the primary somatosensory cortex (S1). Recording depths ranged from 50 to 250 µm relative to the onset of neuronal activity at the cortical surface. Hence, the recording sites were located mostly in the supragranular cortical layers II/III, a few possibly in layer IV. While the electrode was advanced into the cortex, the body surface of the bat, including the wing membrane, was stimulated using von Frey monofilaments to locate a region that elicited neural activity. Receptive fields mapped using this method of stimulation, were used to determine somatotopic organization of S1. Figure 2.1 (lower panels) outlines the findings from two animals. The overall topography that emerges from the combined results from four animals was that of a complete and ordered representation of the contralateral body surface. The most medial part of S1 represented the hind limb, with the distal parts of the foot placed rostrally. However, for most locations that represented the foot, we made no attempt to further distinguish between representation of the single toes or phalanges, because these structures are so small in the big brown bat that stimulation with von Frey hairs could not be accurately performed. The tail, including the IFM was represented lateral to the distal hindlimb. The back of the animal was represented caudomedially. The head and face of the animal were represented in the most rostrolateral area of S1. The receptive fields of the head were very small compared to other parts of the body, and often only several millimeters in diameter. Different parts of the face including the upper lip, snout with the vibrissae, the lower lip, chin, pinna

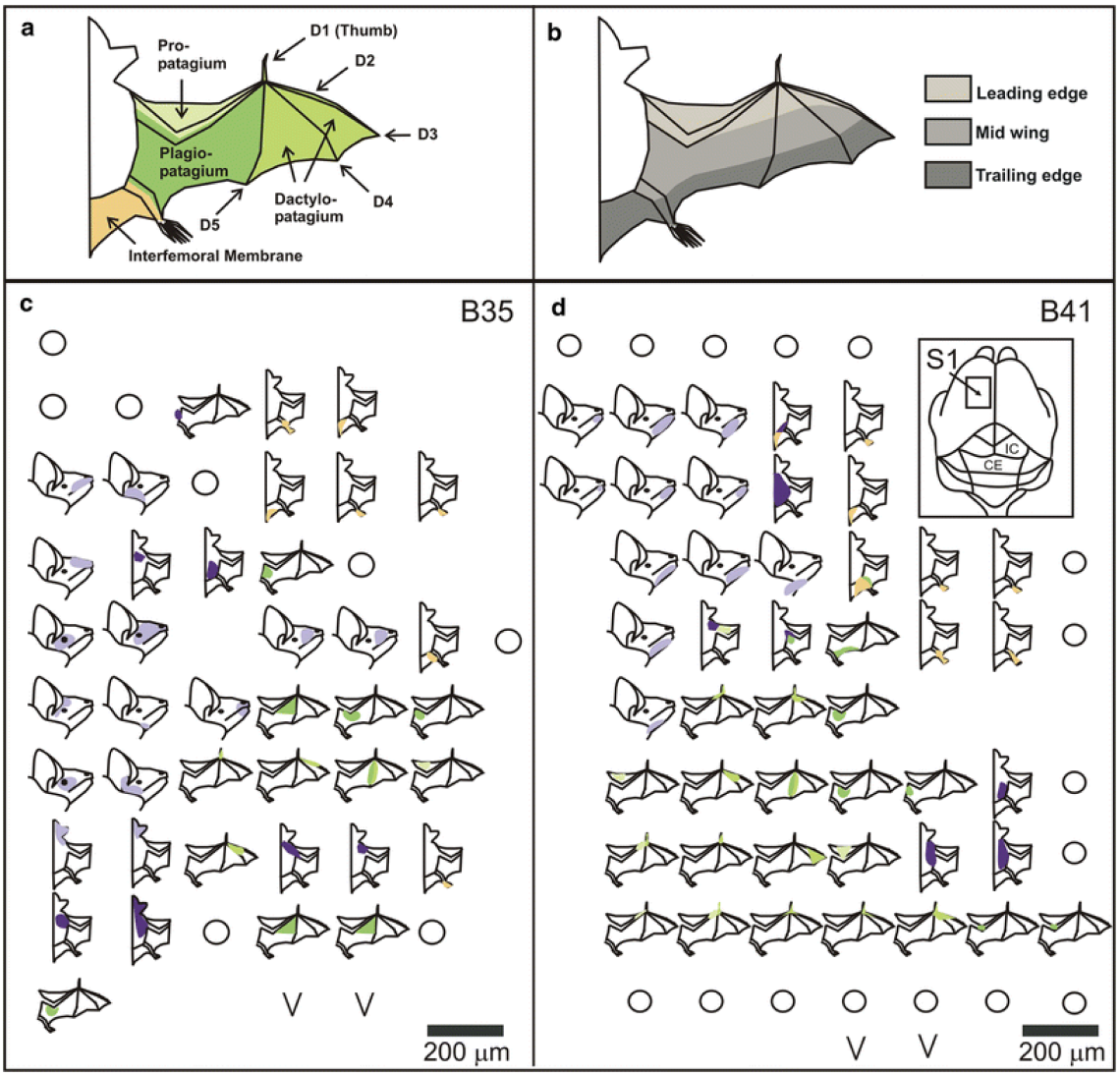

Figure 2.1: Tactile receptive fields on *Eptesicus* wings. *Top panels* The organization of the bat wing **(a)** and its functional areas **(b)**. D1-5 indicate digits 1-5 with D1 being the thumb. Results of the somatosensory cortical mapping from two bats **(c, d)**. *Colored areas* indicate receptive fields close to neuronal threshold, obtained from electrode penetrations regularly placed within a rectangular craniotomy covering S1 *(inset panel* **d**). *Open circles* indicate penetrations with no observed somatosensory activity, and V incidates regions exhibiting visual activity.

including the tragus, and the forehead had separate/non-overlapping receptive fields i.e., electrode penetrations placed only 150–250 µm apart resulted in receptive fields on distinct regions of the face.

The forelimb, along with the wing membrane, was represented centrally and caudally. The distal forelimb, including the digits and the associated membrane, were represented at the caudal border of the area. Digit 1 (D1) had small receptive fields, as compared to other regions on the body. Digits 2 and 3 (D2 and 3) had overlapping receptive fields and were situated medial to D1. Digits 4 and 5 (D4 and D5) and the associated wing membrane were located most medially in the forelimb representation. The propatagium, or the pro-wing, was represented laterally, adjacent to D1.

The representation of distal forelimb and the wing in S1 is reverse of the representation in all walking mammals, including primates, carnivores and rodents, where the digits are oriented rostrally with the palm placed caudally. Consequently, in the bat, the representations of D5 and plagiopatagium are adjacent to the representations of the flank and back instead of the hindlimb, and the representation of the thumb is close to the representations of the shoulder and pinna instead of the lower jaw in walking mammals. In most of our cases, D5 marked the border of receptive fields that were centered in the dactylopatagium, and was excluded from receptive fields that were centered in the plagiopatagium. In only a few cases and only at suprathreshold stimulus intensities, receptive fields crossed the D5 border. Results of somatosensory mapping from four animals were pooled to generate the cortical surface map as shown in figure 2.2.

Neurons in S1 were highly sensitive to tactile stimulation and responded to monofilament stimulation, light brushing of the skin with cotton-tipped applicators, blunt objects, and stimulation by air puffs. Receptive field size varied with location, with D1, foot, and the face region showing the smallest sizes compared to all other regions on the body. Receptive field size also varied with stimulation intensity, with greater monofilament weight resulting in bigger areas. Figure 2.3 shows examples of the change in receptive field size, recorded from three different S1 locations responding to stimulation of the

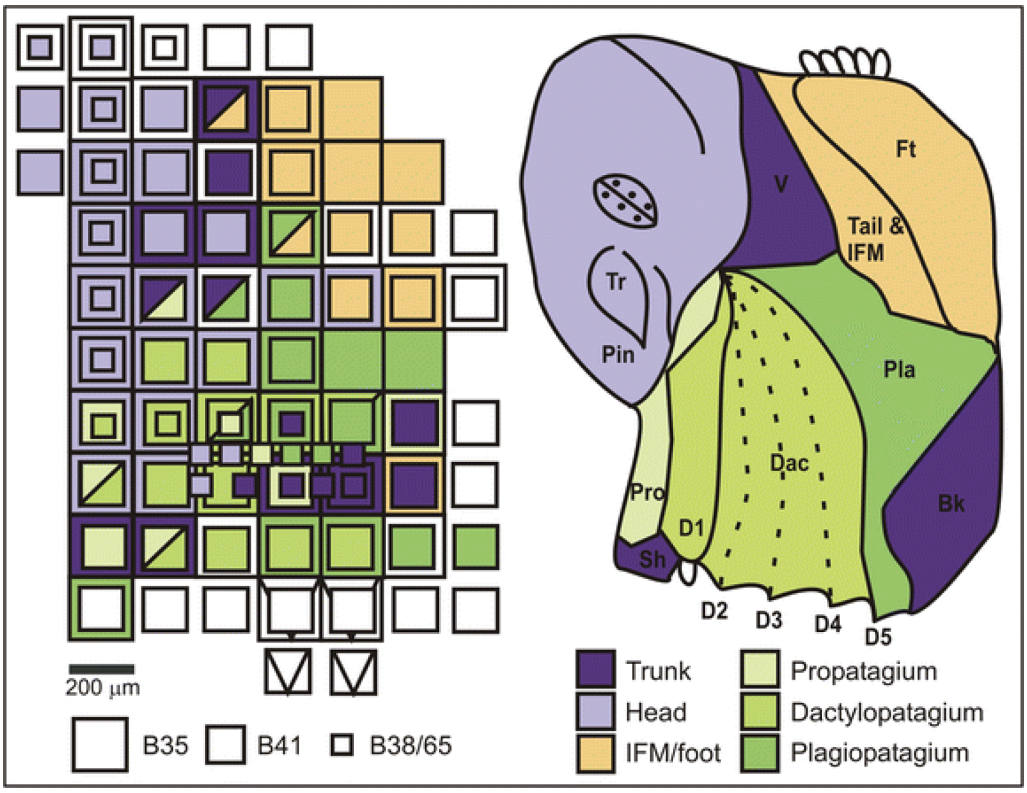

Figure 2.2: The bat homunculus. Average cortical surface map or "homunculus" obtained from pooling data from four bats. The left panel shows the matched positions of recording sites in each of the four bats. Matching was done using anatomical landmarks such as median suture, bregma, and major vessels. The color scheme matches figure 2.1. *Bk* back, *D* digit, *Dac* dactylopatagium, *Ft* foot, *IFM* interfemoral membrane, *Pin* pinna, *Pla*, plagiopatagium, *Pro* propatagium, *Sh* shoulder, *Tr* targus, *V* ventrum.

wing, including the trailing edge and wing tip, the mid-wing, and the leading edge, respectively.

Reducing stimulus intensity by choosing successively lighter monofilaments allowed us to determine the response thresholds of different parts of the wing in five animals. Figure 2.4 summarizes the results. The tactile thresholds of the plagiopatagium and the IFM were significantly higher than those of the dactylopatagium (a), with the trailing edge of the wing (including the wingtip), and most parts of the dactylopatagium including the thumb showing a response to lowest weighted monofilaments (0.02–0.04 g = 0.2–0.4

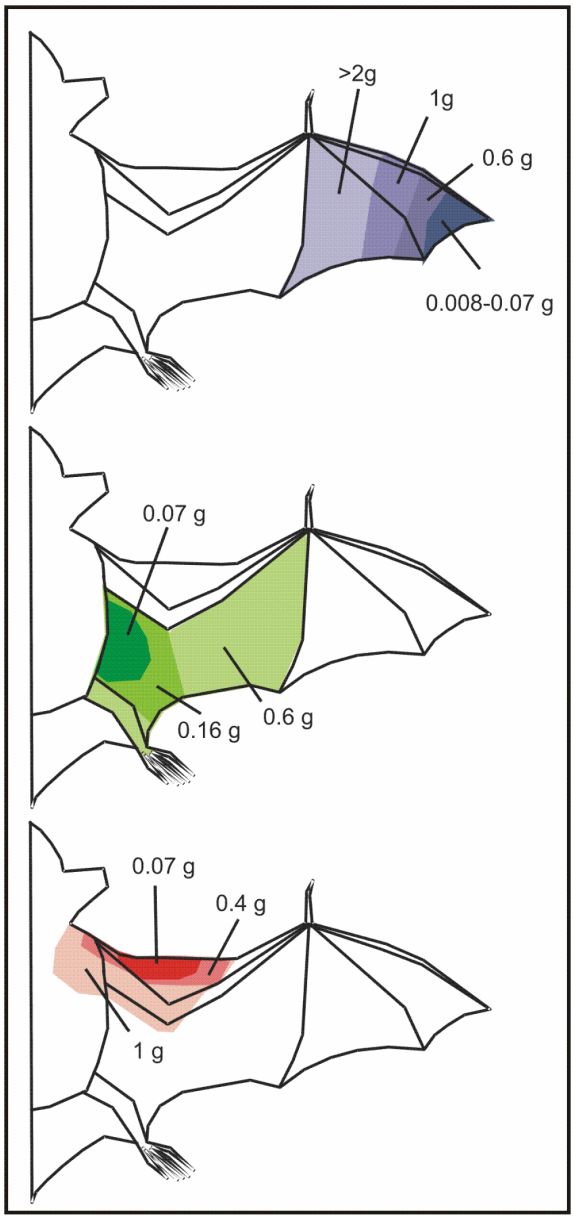

Figure 2.3: Receptive field size as a function of stimulus intensity. The size of the receptive fields increases with stimulus intensity (von Frey hairs of different filament weight). Results for three cortical locations that respond to stimulation of different parts of the wing are shown. Different colors indicate the expansion of the receptive fields under stimulation with different filament weights.

mN), as compared to other mid-wing areas, the IFM, and the propatagium (0.07–0.12 g = 0.7–1.2 mN) (b).

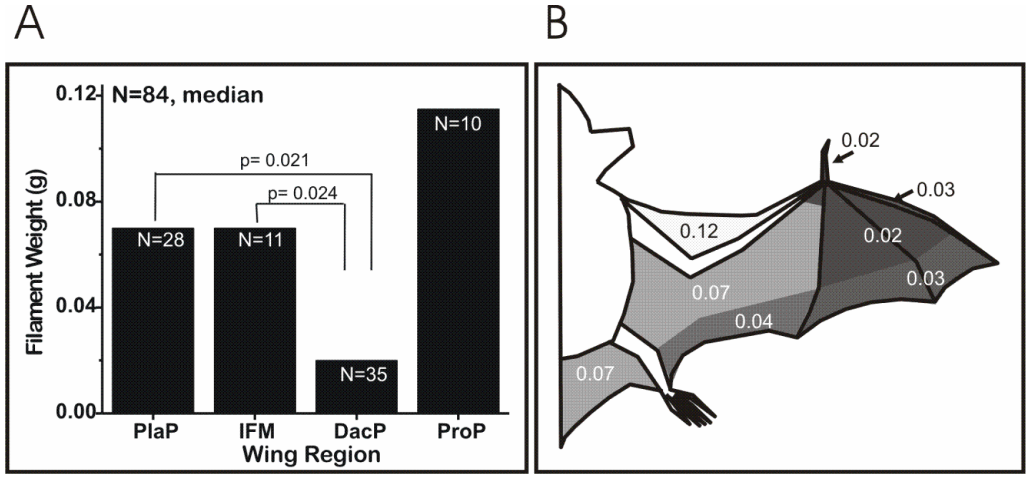

Figure 2.4: Tactile response threshold as determined using calibrated monofilaments (von Frey hairs). A data from four parts of the wing of five bats were pooled, the plagiopatagium (PlaP, see Fig. 1, N =28), the interfemoral membrane (IFM, N = 11), the dactylopatagium (DacP, N = 35), and the propatagium (ProP, N = 10). The thresholds of the dactylopatagium were significantly different from the IFM, and PlaP (Mood's Median Test p = 0.024 and 0.021, respectively). **B** Median thresholds in gram filament weight for different functional regions. The weight in g is equivalent to a ten-fold value in mN (e.g., 0.02 g equals 0.2 mN). Darker shading indicates lower thresholds. Note that, e.g., the trailing edge of the PlaP, is more sensitive than the remainder of the PlaP

2.3 Discussion

In the present study, we investigated the organization of S1 in the big brown bat, *E. fuscus*. We also characterized tactile response thresholds of different regions of the bat's wings. Our findings show a complete and orderly representation of the contralateral body surface in S1 (Figs. 2.1, 2.2), consistent with the findings from other mammalian species. However, there were features of this somatotopic map that stood out. The most noticeable aspect was the overrepresentation of the wing (including the IFM), with almost a third of S1 occupied by it. This enlarged hand and wing representation is also evident in other reports on bat somatotopic maps (Calford et al. 1985; Krubitzer and Calford 1992; Wise et al. 1986; Zook and Fowler 1986). These findings suggest that bat hand-wings have a particularly high innervation supplying the tactile mechanoreceptors. Another

possibility is that flight induced mechanosensory cortical activity is influencing the size of cortical representation of the hand-wing. In either case, it remains to be established how bats might be using this stream of sensory information during flight or other behaviors. A second feature that *Eptesicus* shares with other bat species is the disproportionate increase of D1 representation, the only free digit, which is used for food handling, climbing, and grooming.

Another feature of the somatotopy in *Eptesicus* was the reversed orientation of the distal forelimb, including the wing membrane. In other words, the bat hand-wing is represented and oriented in a manner such that the digits are directed caudally. This is in contrast to the hand representation in all walking mammals examined to date (Kaas 1983), where the digits point rostrally. First noted by Calford et al. (1985) in the gray-headed flying fox, *Pteropus policephalus*, this reversed forelimb orientation has since been reported in the other bat species examined as well (Wise et al. 1986; Zook and Fowler 1986). This finding of reversed wing representation was further explored in subcortical structures in two other studies. Martin(1993) examined the dorsal column nuclei (gracile, cuneate, and spinal trigeminal nuclei, first order synaptic stop of ascending somatosensory fibers) of *Pteropus scapulatus* (little red flying fox) and did not find any evidence of a clear topography, but instead observed the body surface representation as a series of dorsomedially to ventromedially oriented bands. In a later study, Manger et al. (2001) examined the thalamus of the gray-headed flying fox to address the locus of this reversed wing representation. Their findings revealed an inverted wing representation in the ventrobasal and posterior thalamic complexes, with the implication that ascending somatosensory fibers were getting reorganized in the medial lemniscus, between the dorsal column nuclei and the thalamus.

The significance of this inverted representation remains unknown. Calford et al. (1985) proposed that normal posturing of the bat wing, which is opposite to that of the

hand orientation in walking mammals, serves as a constraint for the observed bat cortical somatotopy. The increase of wing surface by addition of the plagiopatagium, which derives from the flank (Cretekos, Weatherbee, et al. 2005), and attaches to D5, might have been the evolutionary force for the rotation of the hand representation. The caudal representation of the distal digits might just be a byproduct of this rotation, because the dactylopatagium is a product of blocked apoptosis of the embryonal interdigital webbing (Weatherbee et al. 2006).

Despite the unusual representation of the distal forelimb and wing, the basic somatotopic representation of *E. fuscus* is similar to mammalian cortical maps (Kaas 1983). Nevertheless, when compared to the findings from flying fox (Calford et al. 1985), differences relating to the phylogeny and natural behaviors of the two bat species become evident. Compared to the fying fox (*Pteropus sp.*), a nonecholocating Yinpterochiropteran bat, *Eptesicus* has a much larger pinna representation, relating to the relatively larger pinna size and its importance in echolocation behavior. Another noticeable difference relates to the foot representation in the two species. Whereas receptive fields generally encompassed more than one digit, or the entire foot of *Eptesicus*, *Pteropus* exhibits an enlarged and well defined foot representation, with individual digits clearly discernible. Similar differences in cortical somatotopy were also highlighted by Wise et al. (1986), between their findings from the Australian ghost bat, *M. gigas*, (a Microchiropteran and Yinpterochiropteran) and the flying fox, also a Yinpterochiropteran, (Calford et al. 1985) which might be attributable to the difference in the overall size of the foot.

In addition to investigating the somatotopic organization of S1 in *E. fuscus*, we also measured the tactile response thresholds of different regions of its wings using von Frey monofilaments. Thresholds were generally low on all wing locations, matching or exceeding the average sensitivity of the human finger tip (R. S. Johansson et al. 1980).

The findings presented here raise a number of important questions with regards to the central representation of the somatosensory periphery, and its importance in the behavioral repertoire of bats. The findings of a large wing representation in S1, and extremely low thresholds for tactile sensitivity, point to the importance of the sensory feedback offered by the bat hand-wing. From a neuroethological perspective, how bats use this stream of sensory information during flight, or the tactile feedback provided while utilizing the wings and/or the tail membrane for swooping prey in mid-air, is yet unknown. It would be of great interest to unravel the underlying sensorimotor circuits, and the details of the neurohistology of the chiropteran wings. Recent experiments using quantitative flow visualization techniques have revealed that flying bats generate complex wake patterns, with inverted vortex loops that are shed near the wing tip (Hedenström, Johansson, Wolf, et al. 2007), and the presence of leading edge vortices during mid-downstroke (Muijres et al. 2008). By noting cortical thresholds to tactile stimulation intensity at different wing regions, we get indirect evidence of the importance of these regions in sensing airflow patterns to provide sensory feedback for optimal flight control. Hence, micro-air vehicles and air probes for aviation could be improved by implementing biomimetic version of the bat's wing sensor array.

Chapter 3

Response properties of airflow sensitive receptive fields on the wings of *Eptesicus fuscus*

The specialized forelimbs of bats not only make flight possible, but also give the order Chiroptera its name (literally, "hand-wing"). Bat wings are composed of a compliant and thin skin, spanning the arm and elongated digits. A number of studies have focused on bat wings with the goal of understanding how wing structure influences flight performance (e.g. Norberg and Rayner 1987; Riskin, Iriarte-Díaz, et al. 2010; Swartz 1997; Swartz, Groves, et al. 1996; Swartz and Middleton 2008). Researchers have also investigated the role of bat wings in thermoregulation (Reichard et al. 2010), wound healing rates (Faure et al. 2009; Weaver et al. 2009), ontogeny (Sears 2008; Sears et al. 2006; Weatherbee et al. 2006), and the evolution of flight (Cooper et al. 2012; Cretekos, Wang, et al. 2008; Norberg 1985). But only a few investigations have attempted to address the role of

tactile hair on bat wings in providing aerodynamic feedback for flight control (Sterbing-D'Angelo et al. 2011; Zook 2005, 2006; Zook and Fowler 1986).

The experiments described in this chapter were designed to address some fundamental questions related to airflow sensing by tactile receptors on bat wings. From the perspective of sensory feedback, I hypothesize that tactile receptors on bat wings measure quantities related to prevailing aerodynamic forces, and inform the flight motor system about the need for kinematic changes. Specifically, I investigated how information about varying airflow conditions is represented by neurons of the primary somatosensory cortex (S1). Under anesthesia, single and multiunit cortical activity was recorded in response to controlled airflow stimulation of tactile receptive fields (RF) located on the wings of big brown bats. The strength, duration, direction and spatial location of airflow were varied to ascertain the response properties of tactile receptors, and to determine what aspects of airflow are encoded. Results show that onset latency of S1 neuronal response decreased systematically as a function of airflow intensity, while the number of evoked spikes remained unaffected. In contrast, stimulus duration had no effect on the magnitude, or latency of spike trains. Individual S1 neurons encompassed relatively large tactile RFs as elicited by airflow stimuli, which was in agreement with the multiunit data obtained by von Frey stimulation (Chapter 2). These RFs were directionally selective, also in accordance with the multiunit data reported previously (Sterbing-D'Angelo et al. 2011). We found some evidence of response facilitation, i.e. simultaneous airflow stimulation of dorsal and ventral wing surface resulted in a peak response that was greater than the sum of response to either surfaces stimulated alone. Finally, I failed to observe any evidence of lateral interactions when airflow stimuli were delivered simultaneously at the center, and surrounding regions (both inside and outside the boundaries) of the RFs.

3.1 Materials and methods

3.1.1 Experimental animals

Experiments described here were performed on adult big brown bats, *Eptesicus fuscus*. Bats used in these studies were either wild-caught in Maryland, or raised in captivity at the University of Washington. Bats were housed in the vivarium located in our laboratory in the University of Maryland, under reversed 12 h light/dark conditions and given food and water ad libitum. All experimental procedures were performed under the National Institute of Health (NIH) guidelines and were approved by the University of Maryland Institutional Animal Care and Use Committee (IACUC).

3.1.2 Surgery

The experimental setup was similar to that described in the preceding chapter. In brief: 1-3 days prior to data collection, a custom made cylindrical stainless steel post (length, 20 mm; diameter, 2 mm) was affixed to the anterior skull along the midline using cyanoacrylate glue (Loctite 4161). The head-post was used to secure the bat to a vibration isolation table (Kinetic Systems Inc.) and a small craniotomy (approximately 1.5 by 1.5 mm, enlarged as needed) over the parietal cortex allowed access to the primary somatosensory cortex (Big brown bat stereotaxic brain atlas, E. Covey, University of Washington). Bats were anesthetized with 1-3% Isoflurane (flow rate, 750 cc/min O_2), body temperature maintained at 34-37° Celsius, and breathing monitored and recorded at approximately 15 minute intervals. Whereas most neural recordings were done under Isoflurane anesthesia, a small subset of data was obtained with Ketamine-Xylazine (intramuscular, standard dose of 52.4 mg/kg body weight).

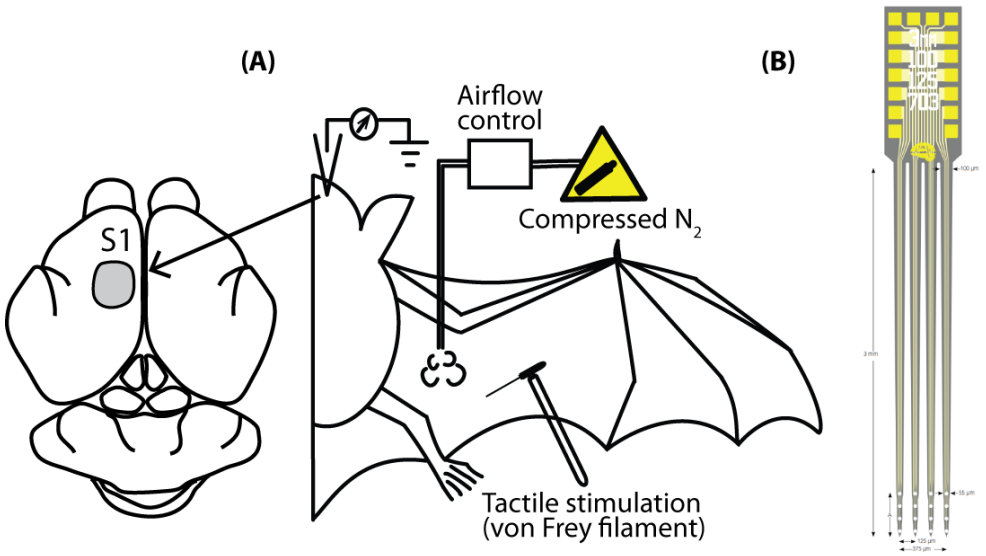

Figure 3.1: Schematic of approximate location of S1 and neurophysiology setup. (A) Under Isoflurane anesthesia, single and multiunit activity from S1 was recorded from tactile RFs on the wings of *E. fuscus*, in response to airflow and tactile stimulation. **(B)** Schematic of the linear multi-electrode probe employed in acquiring single neuron data (from Neuronexus Inc. product catalogue, 2012).

3.1.3 Electrophysiology

Multiunit recordings were acquired using tungsten microelectrodes (15-20 MΩ, FHC Inc.) referenced to a low impedance electrode (< 1 MΩ) in a non-somatosensory region of the opposite hemisphere. Single neuron recordings were acquired using a 4-pronged, 16 channel silicone probe (Neuronexus Inc.). Each prong or shank of the multi-channel electrode array is 3 mm long, with 4 recording sites linearly arranged near the tip and separated by 100 µm (impedance 1-3 MΩ; Fig. 3.1). A low impedance silver wire tucked under the scalp/muscles of mastication was used as reference. The electrode array was attached to a micromanipulator (Mitutoyo America Corporation), oriented perpendicularly to, and lowered into the cortex until all the recording sites were in the grey mater. Recording sessions lasted 4-6 hours and each animal underwent 4-12 recording sessions

spread over a period of 1-4 weeks. Conclusion of a recording session was followed by sealing the craniotomy with bone wax (W31, Ethicon Endo-Surgery Inc.), which allowed for repeated recordings from the same craniotomy over multiple days. When it was no longer possible to obtain single unit activity, the animal was euthanized with a lethal dose (0.1 ml) of sodium pentobarbital (390 mg/ml) via intraperitoneal route. Standard sterile surgical procedures were followed throughout the experiment.

3.1.4 Tactile and airflow stimulation

With the recording electrode(s) in S1, receptive fields on the wings were localized by handheld monofilament stimulation (von Frey hairs, North Coast). The von Frey filaments are available as a set to 20 stimulators, with weights in the range of 0.08-2943 mN (or 0.008-300 g) arranged on a logarithmic scale. Stimulation consisted of pressing the monofilaments at right angles against the dorsal wing membrane until they bent, and subsequently releasing them. Neuronal thresholds were determined based on the lowest weighted filaments that elicited a cortical response.

Airflow stimuli were generated using a portable fluid dispensing station (Ultra 2400, Nordson EFD) connected to a tank of compressed nitrogen gas. Stimuli were delivered using a series of flexible tubes connected to a 14 g blunt needle, placed 3 mm away at a 45° inclination relative to the wing surface. Stimuli were repeated 20-26 times at 5 s intervals. Neuronal thresholds were determined by the lowest airflow intensity that elicited a response. For all the experiments described here, airflow stimuli were 40 ms long, and delivered at or just above threshold intensity (typically 0.03-0.05 m/s), unless noted otherwise.

The speed of airflow was measured using a hot-wire anemometer (Datametrics 100VT-A). For the range of intensities used in experiments, airflow speed varied between 3.3 x

10^{-2} to 2.5 x 10^{-1} m/s (Fig. 3.2). Since the airflow probe was placed 3 mm away from the wing surface, there was a time-delay for the air column to travel this distance. This time-delay was measured by recording the output of a MEMS microphone placed 3 mm from the stimulus probe, and was estimated to be $\sim$ 30 ms. In reporting neuronal response latencies, this temporal offset was accounted for.

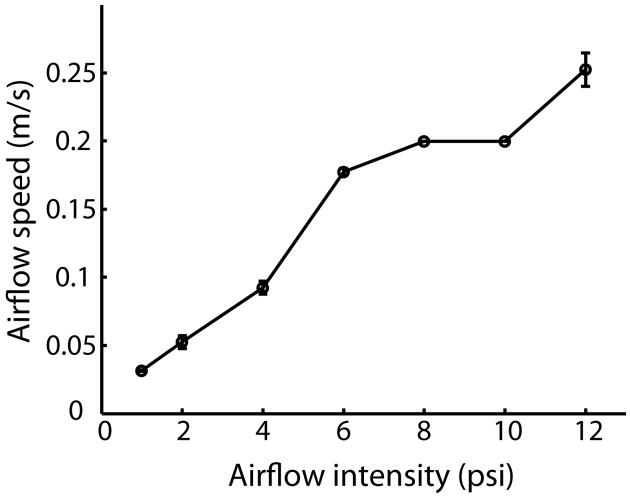

Figure 3.2: Measurement of airflow speed. The speed of airflow stimuli as meausred by a hot-wire anemometer.

3.1.5 Data acquisition

Multiunit neural signals obtained with single tungsten electrodes were sampled at 25 kHz using a data acquisition board (NI BNC-2110, National Instruments Inc.). Neural signals were differentially amplified (MDA-4I, Bak Electronics Inc.), band-pass filtered (500-5000 Hz, SR650 Series digital filter, Stanford Research Systems Inc.), and monitored via an oscilloscope and a speaker. Airflow stimulus delivery and data acquisition was simultaneously triggered via a custom made TTL pulse generator.

The 16-channel linear electrode array was connected via unity gain head-stage to a data acquisition system (Omniplex D System, Plexon Inc.). Neural signals were digitized

at 16-bit resolution, sampled at 40 kHz, amplified 200-1000X, and band-pass filtered between 500-5000 Hz. Data acquisition was initiated via a dedicated PC terminal, and a TTL pulse was used to trigger and time-stamp the onset of stimulus delivery.

3.1.6 Data analysis

Extracellular potentials acquired by tungsten microelectrodes resulted from multi-neuron clusters in all instances, but identification and isolation of spike waveforms from individual neurons was not possible due to unfavorable signal-to-noise ratio. Hence, cortical signals were rectified, averaged over trials, and low pass filtered (cut-off frequency 100 Hz, first-order Butterworth filter), to generate an "envelope" of the response (Fig. 3.3). Peak of the resulting waveform was used to quantify the strength of the response. Data was acquired and analyzed in MATLAB® computing environment (MATLAB version R2012a, The Mathworks Inc.).

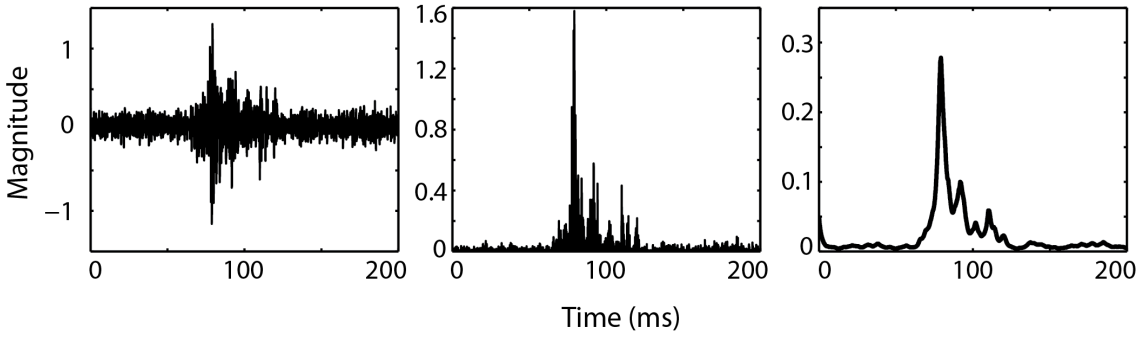

Figure 3.3: Multiunit data analysis. Extracellular potentials (left) were rectified (middle), low-pass filtered at 100 Hz (right), and averaged across trials.

Spike waveforms and timestamps of extracellularly recorded potentials acquired using multi-electrode arrays were extracted using commercially available software ("Offline Sorter", Plexon Inc.). Single unit discrimination was achieved using manual amplitude thresholding and template matching as follows. Waveforms exceeding a subjective threshold were manually selected and a template generated using least squares fitting.

The algorithm for template matching assigned a particular waveform to a template's unit if the sum of squared residuals was less than 70% of the maximum analog to digital value for that template. To further verify if the recorded waveforms belonged to single neurons, projections of the first two principal components were visualized as scatterplots for "clustering". Finally, the presence of absolute refractory period in inter-spike interval histograms was used to declassify waveforms occurring less than 1 ms apart. Further analysis on spike timestamps thus generated was done in MATLAB (version R2012a).

3.2 Results

3.2.1 Onset latency, but not spike counts vary as a function of airflow intensity

The complex airflow patterns generated by the highly compliant and articulated wings of bats vary dynamically with each stroke (Hedenström, Johansson, Wolf, et al. 2007; Hubel, Riskin, et al. 2010). It is not known however, how, or what aspects of the flow are sensed by tactile receptors on bat wings, especially in the immediate vicinity of the wing membrane. By changing the intensity of airflow stimuli applied to tactile RFs on the wings, I attempted to address the role of wing hair receptors in detecting one aspect of this flow, i.e. changes in the speed, or strength of airflow around the wing.

Specifically, I performed extracellular single neuron recordings from S1 of 10 anesthetized big brown bats to airflow stimulation of tactile receptive fields on the wings. The strength of airflow was varied over a range of 0.03-0.25 m/s keeping all other stimulus parameters constant. The duration of airflow was fixed at 40 ms. Data from 35 well-isolated single neurons is presented here (Fig. 3.4 A-B).

Table 3.1: Number of subjects and sampled neurons - airflow intensity

Bat-band number	No. of analyzed single units
OR35	5
OR22	10
OR90	2
OR69	4
OR81	1
OR6	1
OR36	4
OR18	3
W55	4
G93	1

When stimulated with air puffs, neuronal response duration varied from 1 ms to more than 50 ms, revealing both phasic and prolonged firing patterns (Fig. 3.4 C). Neural activity was also recorded in response to tactile stimulation by calibrated monofilaments (von Frey hairs) in ten airflow-sensitive sites (Fig. 3.4 D). Responses were aligned to the first post-stimulus spike to allow comparisons with response to airflow stimulation. The corresponding data sets suggest that airflow and tactile stimulation activated similar neuronal pathways. Whether this is due to the same mechanically sensitive peripheral receptors responding to either stimuli, or a result of upstream processing is unknown.

Spontaneous cortical activity was rarely observed under Isoflurane anesthesia. Individual S1 neurons fired 0-6 spikes in response to stimulation; however, 1-3 spikes per stimulus presentation were most commonly observed (Fig. 3.4 E–F).

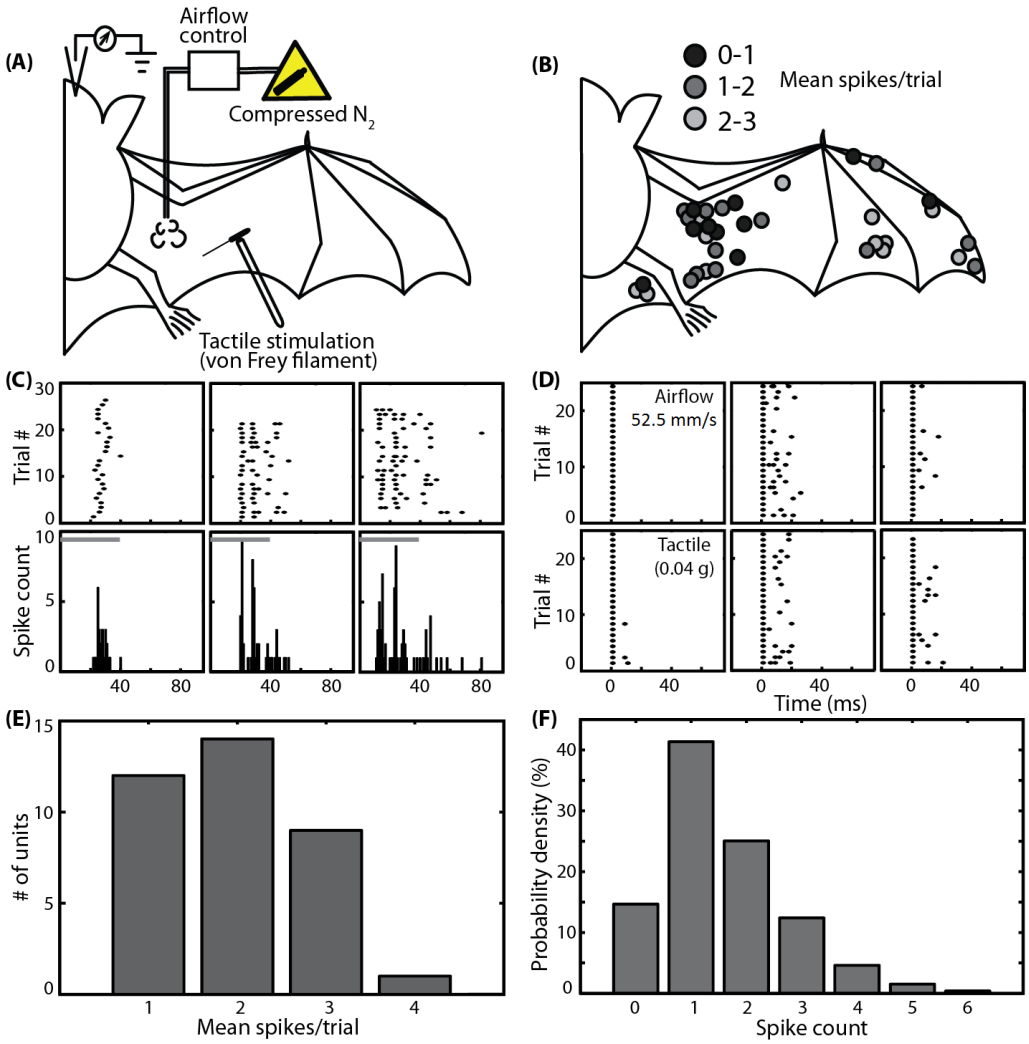

Figure 3.4: S1 neuron responses to airflow and tactile stimulation of bat wings. (A) Schematic of the neurophysiology setup. Under Isoflurane anesthesia, single neuron activity from S1 was recorded from tactile receptive fields on the wings of *E. fuscus*, by stimulation with 40 ms air puffs of varying intensity, and handheld von Frey filaments. **(B)** Receptive field locations for cortical neurons. Grayscale indicates mean number of spikes per trial. **(C)** Rasters and post-stimulus time histograms (PSTH, 1 ms bins) illustrating the responses of 3 example neurons. Grey bar in the lower panel represents airflow stimulus duration. **(D)** Raster plots illustrating responses of three neurons to airflow (upper row) and tactile stimulation (lower row). Responses were aligned to the first post-stimulus spike to compare the two stimulus conditions. **(E)** Distribution of mean spikes/trial across all neurons (n=35) and stimulus conditions. **(F)** Distribution of number of spikes emitted in response to stimulation for the population of sampled neurons (n=35) pooled across all stimuli.

Analysis of cortical responses to airflow using linear regression showed little change in spike counts as a function of stimulus intensity (R^2 range = 1.92 x 10^{-4} to 0.51, median R^2 = 0.11; slope range = -0.07 to 0.14, slope median = 0.04; Fig. 3.5 A). By contrast, onset latency decreased with airflow intensity and stabilized at higher stimulus levels, as revealed by a one parameter exponential model (R^2 range = 0.02 to 0.81, median R^2 = 0.49; decay constant range = -0.01 to -0.54, decay constant median = -0.04; Fig. 3.5 B).

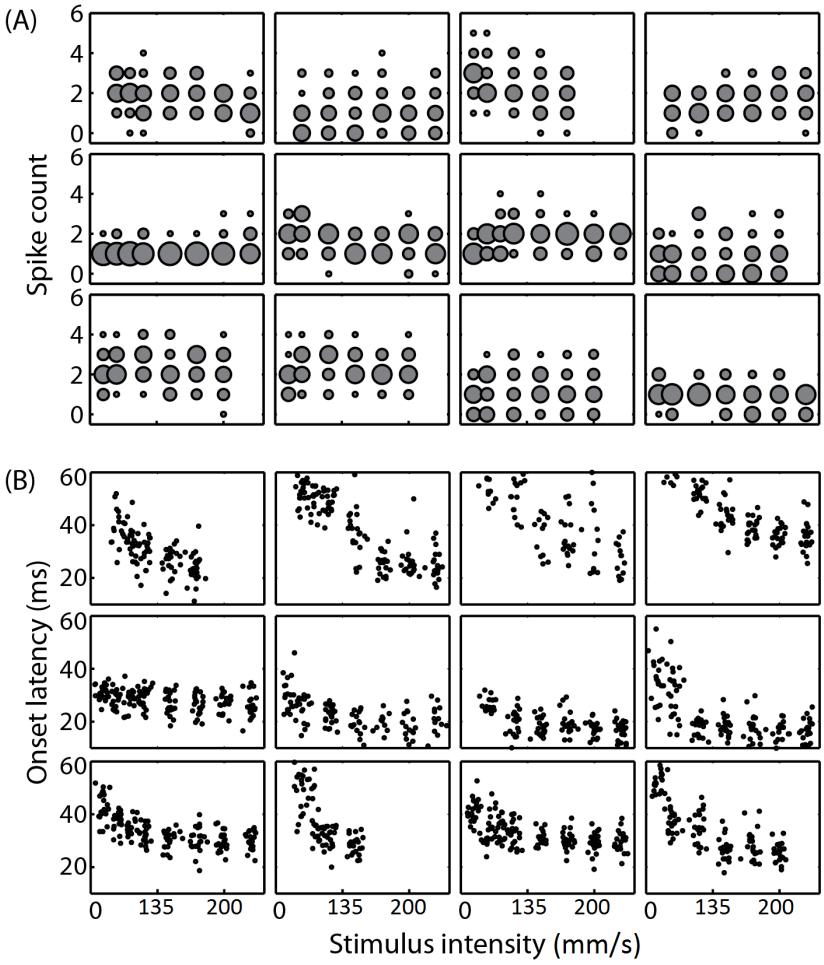

Figure 3.5: Onset latency but not spike counts vary as a function of airflow intensity. Plots of single unit responses as a function of airflow intensity from 12 representative S1 neurons. **(A)** Bubble plots of spike counts. The size of each circle represents the number of trials with corresponding number of spikes. **(B)** Scatter plots of onset latency with reference to stimulus onset. Note that points were jittered along both axes for ease of visualization.

To rule out the effect of Isoflurane on the observed responses, a small subset of neurons (n=11) were recorded under Ketamine-Xylazine anesthesia under similar conditions. While spontaneous cortical activity was rarely observed under Isoflurane, a variable amount of spontaneous firing was present with Ketamine-Xylazine. Nevertheless, stimulus evoked responses were similar across both anesthetics (Fig. 3.6).

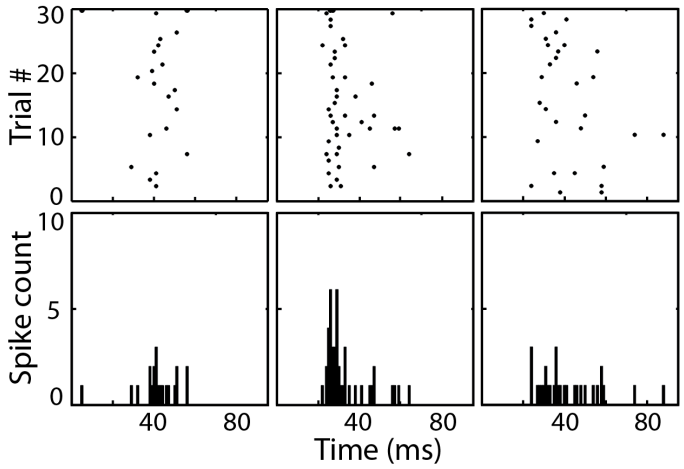

Figure 3.6: S1 responses to airflow stimulation under Ketamine-Xylazine anesthesia. Rasters and post-stimulus time histograms of three neurons in response to airflow stimulation recorded under Ketamine-Xylazine anesthesia.

3.2.2 Airflow stimulus duration does not affect spike counts, or the their timing

Big brown bats fly at speeds that range from 3-9 m/s, flapping their wings at a rate of 11-15 Hz (Kurta and Baker 1990), the two being interdependent at least at low flight speeds (Bullen and McKenzie 2002). At this rate, each stroke lasts approximately 35-45 ms. Together, flight speed and wingbeat frequency along with other kinematic parameters shape the resulting airflow patterns (Hedenström, Johansson, Wolf, et al. 2007, reviewed in Chapter 1). We wondered how sensory information about these airflow patterns is integrated and represented in S1. Specifically, does the evoked cortical activity vary as a

Table 3.2: Number of subjects and sampled neurons - airflow duration

Bat-band number	No. of analyzed single units
OR22	7
OR90	2
W55	3
G93	1

function of the duration of airflow? And does this relationship depend on the location of the RF on the wing membrane? To address these questions I recorded extracellular potentials from single S1 neurons of 4 anesthetized big brown bats in response to airflow stimuli of varying durations. Stimuli were delivered at, or just above threshold intensity (typically 0.03-0.05 m/s), while the duration was varied from 10 ms to 1 s. Data from 13 well-isolated single neurons is presented here (Fig. 3.7).

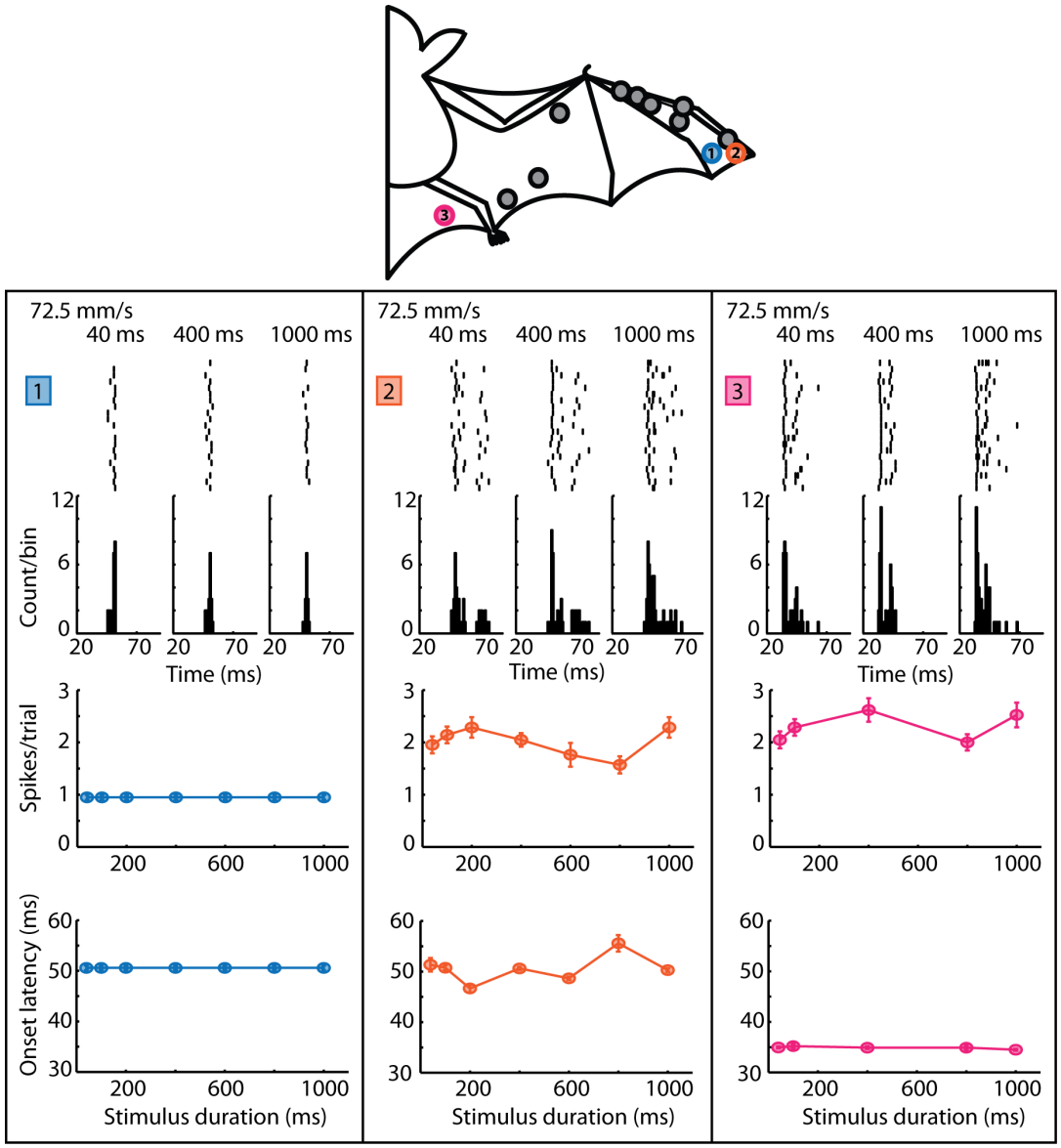

Figure 3.7: Cortical responses to varying airflow stimulus duration. On the top is a schematic of a bat with the location of sampled receptive field (circles). Below are raster plots, post-stimulus time histograms, mean spikes/trials and mean onset latencies of 3 representative neurons. Receptive field locations of these neurons are color matched to the circles in the bat schematic.

Analysis of cortical responses to varying airflow duration using linear regression showed little change in spike counts (R^2 range = 0.001 to 0.212, median R^2 = 0.04; slope range = $\sim$ 0 to 0.0013, slope median = $\sim$ 0; Fig. 3.8 A), or onset latency (R^2 range = $\sim$ 0

to 0.35, median R^2 = 0.06; slope range = −0.002 to 0.011, slope median = 0.002; Fig. 3.8 B). The same was true for the population average (Fig. 3.8 C). Note that population measures were normalized (to the maximum) as the overall firing rate and onset latencies were variable across individual neurons.

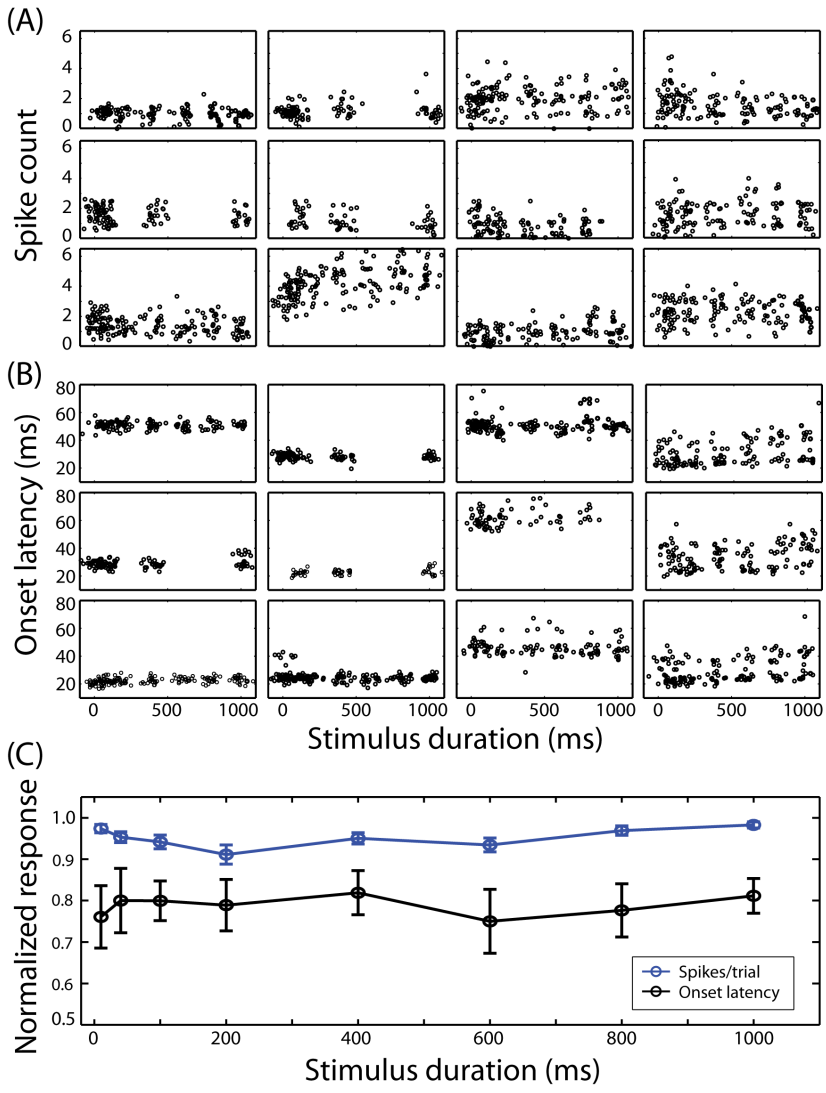

Figure 3.8: Spike count and onset latency do not vary as a function of airflow duration. Spike counts **(A)** and onset latencies **(B)** of 12 representative neurons are shown as sub-plots, with each dot representing spikes emitted in response to near threshold airflow stimulation. Data points are jittered along both the x- and y-axes for ease of visualization. **(C)** Normalized population-averaged spike counts and onset latencies (n = 13) as a function of near threshold airflow stimulus duration.

3.2.3 Airflow stimuli reveal large receptive fields on the wings

Tactile stimulation of the wing membrane with hand-held von Frey filaments shows variable but relatively large-sized RFs (Chapter 2 and Fig. 3.9). The size of these tactile RFs varies from punctate on the thumb to large on wing membranes, and this might reflect multiunit responses, innervation of multiple hair follicles by single afferents, or cortical integration from many sensory neurons. Here, I investigated the spatial extent of tactile RFs as measured by sensitivity to handheld tactile and airflow stimulation, while recording extracellularly from single S1 neurons. The aim of this investigation was twofold: (1) to measure the size of airflow sensitive tactile RFs, and (2) to compare with results obtained from handheld von Frey filament stimulation.

Single neuron responses to airflow stimulation (n=8, 2 bats) were recorded at near threshold intensity (0.03-0.07 m/s), while moving the stimulus probe away from the RF center in 5 mm steps along the rostrocaudal and mediolateral dimensions of the wings. Stimulus duration was fixed at 40 ms. Boundaries of a RF were defined as the location on the wing membrane where the response fell below 50% of the peak firing (as measured at RF center). When stimulated by von Frey hairs, the evoked spiking activity to lowest weighted filament was used to determine RF boundaries. Spike waveforms (n=9) were monitored audio-visually, and RFs were hand-drawn on sketches of a bat.

Table 3.3: Number of subjects and sampled neurons - receptive field size

Bat-band number	No. of analyzed single units
OR69	4
OR35	4

Results revealed the presence of relatively large RFs, with size dependent on the method of stimulation (Fig. 3.9). Generally, RFs obtained by von Frey filament stimulation were larger compared to those elicited by airflow. This could due to different subsets

of afferents being excited, and/or the method of determining the boundaries. Nevertheless, these results are in agreement with the previously reported findings (Chapter 2).

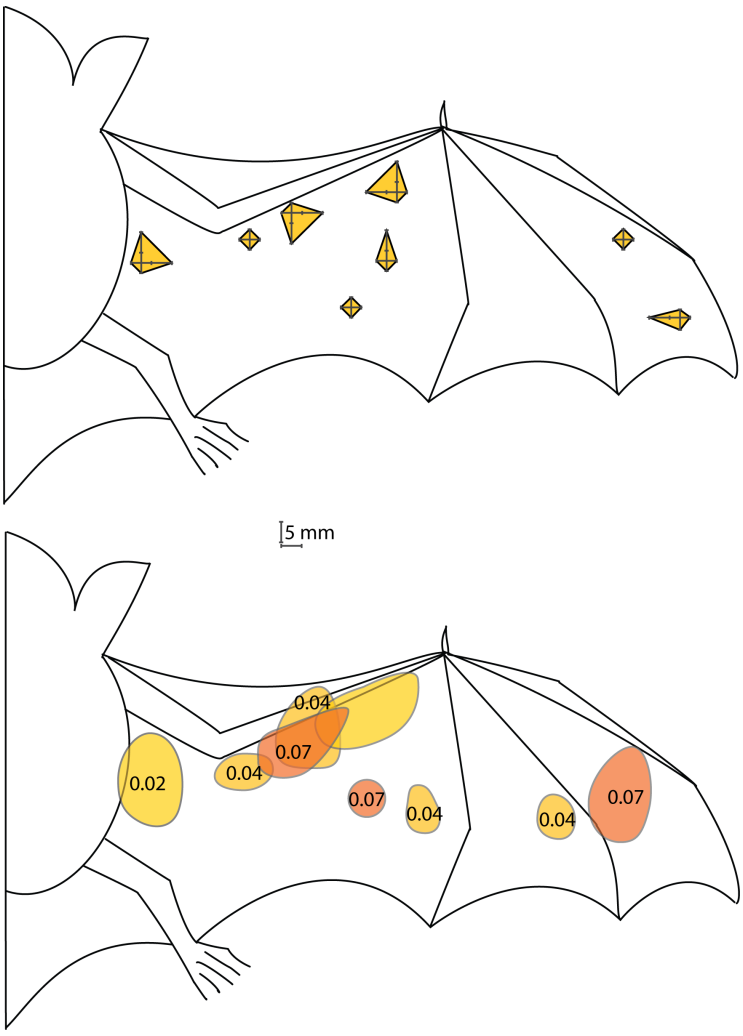

Figure 3.9: Receptive fields of S1 neurons elicited by tactile and airflow stimulation of the wing. Bat schematics showing RFs determined by airflow (top) and von Frey stimulation (bottom), drawn approximately to scale. Numbers indicate the lowest weight of von Frey filament in grams that evoked a response

3.2.4 S1 neurons show directional sensitivity to airflow stimulation of the wing membrane

In a previous study, we reported that multiunit neuronal activity in S1 shows evidence of directional selectivity to airflow stimulation of tactile RFs on the wings of *E. fuscus* (Sterbing-D'Angelo et al. 2011). I extended this investigation to examine single neuron responses in a similar experimental setup, but employing 4 directions in 90° steps as opposed to 8 directions used previously. Stimulus duration was fixed at 40 ms, delivered at, or just above threshold intensity (typically 0.03-0.05 m/s).

3.2.4.1 Directional tuning elicited by spike counts

Extracellular spike waveforms of 22 well-isolated single S1 neurons from 4 bats were acquired in response to airflow stimuli delivered from 4 directions (90° steps, rostrocaudal and mediolateral axes). Response to stimulation (mean spikes/trial) for the preferred direction was compared to the remaining stimulus directions by one-way analysis of variance (ANOVA) and Bonferroni's post-hoc test. In agreement with the previously reported findings, all of the neurons sampled showed directional selectivity (Fig. 3.10; direction of arrows in the bat schematic), with a majority strongly selective for a single direction (i.e., significantly higher firing compared to all remaining stimulus directions; 14/22, or 64% of the units). Furthermore, a majority (15/22 or 68%) of neurons were tuned to reversed airflow direction.

Table 3.4: Number of subjects and sampled neurons - airflow direction

Bat-band number	No. of analyzed single units
OR36	1
OR69	14
W81	1
G35	6

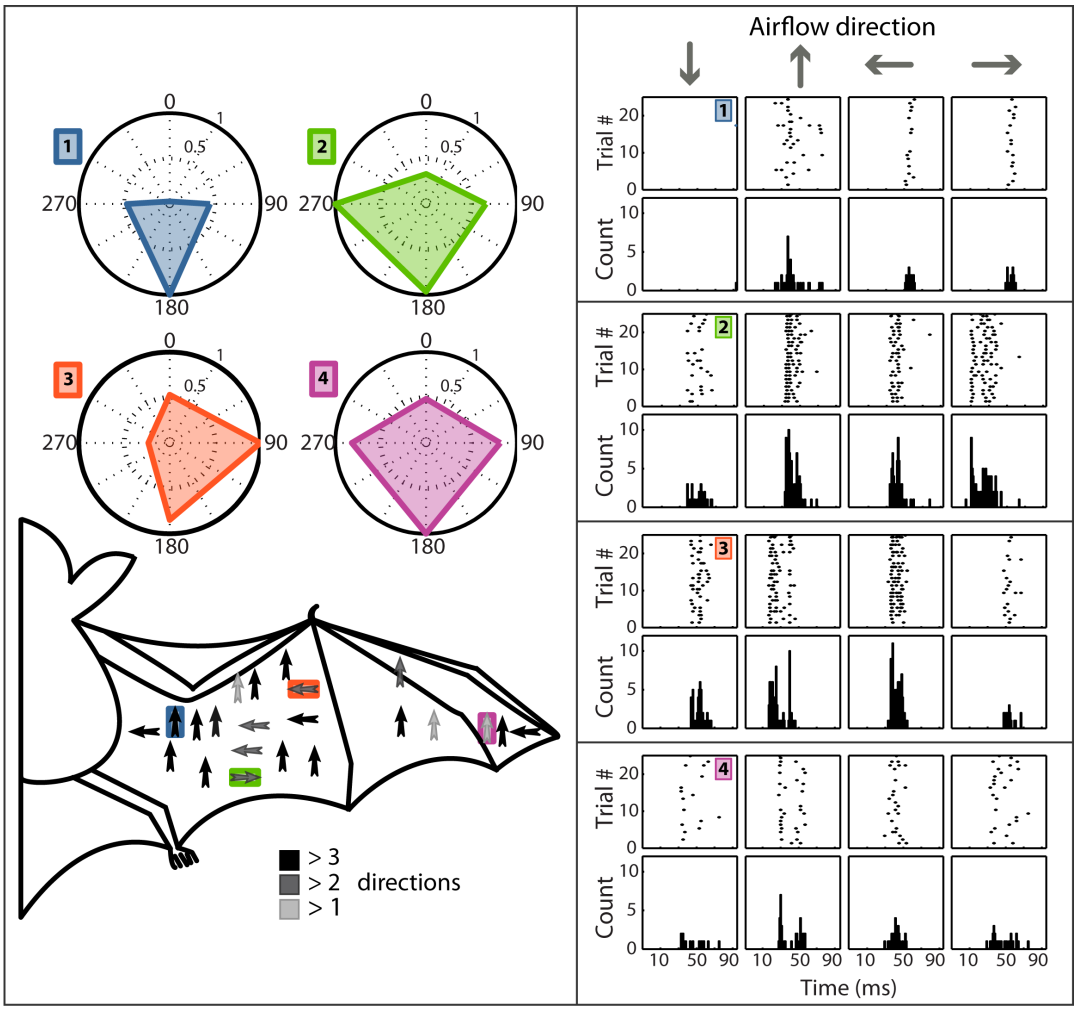

Figure 3.10: Directional selectivity of S1 neurons to airflow stimulation. Rasters, post-stimulus time histograms and polar plots showing response of four representative neurons (spike counts normalized to the maximum) to near threshold airflow stimuli delivered from four directions. Receptive field locations of these units are color matched to arrows in the bat schematic. The preferred direction (see text) is denoted by arrows in the bat schematic, with arrow shades indicating the strength of selectivity, i.e. black, dark gray, and light gray correspond to significantly higher firing compared to remaining 3, 2 or 1 directions respectively.

3.2.4.2 Response onset latency varies as a function of airflow direction

The number of spikes elicited in response to airflow stimulation varies as a function of airflow direction as seen in the preceding section. The "tuning curves" thus generated provide an estimate of directional selectivity exhibited by S1 neurons. How is the timing, specifically the latency of response affected by stimulus direction? Response latency could potentially represent a stimulus feature, and addresses the larger issue of the role of spike timing as an encoding mechanism (discussed in Chapter 4).

For the population of sampled neurons, response latency varied as a function of airflow direction, and not surprisingly, stimulus direction with the highest firing rate (the "preferred direction") also showed the lowest response latency (Fig. 3.11).

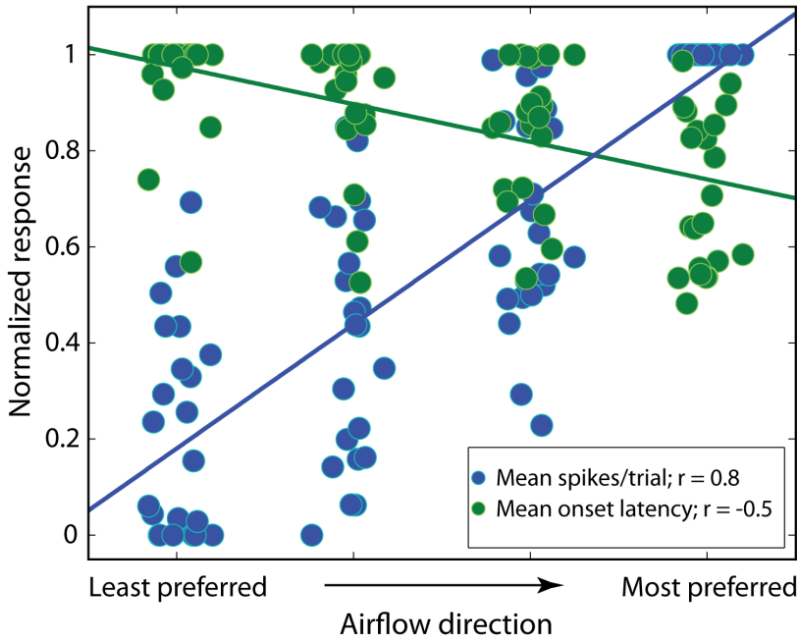

Figure 3.11: S1 responses o directional airflow. Scatter plot of mean normalized spike counts and onset latencies across all trials and neurons.

3.2.5 Simultaneous dorsal and ventral wing membrane stimulation by airflow reveals nolinear interactions

The specialized wing membrane of bats with its array of microscopic hairs on both the dorsal and ventral surfaces is an unusually thin, two-sided tissue consisting of epidermal layers sandwiching a thin dermis. Nerve trunks and blood vessels extend through the dermis along with an extensive network of collagen-elastin bands (Crowley and Hall 1994). Primary afferents innervating hairs from both the dorsal and ventral surfaces (piloneural complexes) traverse along the dermis, forming intradermal axonal bundles (Crowley and Hall 1994; Czech et al. 2008). Airflow and tactile stimulation on either surface of a localized RF results in cortical responses that are similar (Fig. 3.12, and Section 2.1.4). At the same time, during flight the dorsal and ventral wing surfaces experience somewhat different aerodynamic forces (Hedenström, Johansson, Wolf, et al. 2007; Hubel, Riskin, et al. 2010). Could the sensory output from the two surfaces of the wing interact in a manner that provides an indication of the differences in airflow? We tried to address this question in a simple experimental setup by simultaneously stimulating both wing surfaces using airflow, and compared the results to either wing surface stimulated alone. Ten RF sites (multiunit) from 3 bats were sampled using single tungsten microelectrodes (Fig. 3.12). With the center of receptive field localized on the wing membrane, 40 ms air puffs were delivered with intensities raning from 0.03-0.25. Cortical responses were recorded with the stimulus delivered on the dorsal, ventral, or both wing surfaces simultaneously. When both wing surfaces were stimulated simultaneously, airflow intensity was adjusted such that only half the airflow was delivered on either wing surfaces.

Table 3.5: Number of subjects and sampled neurons - dorsal+ventral sitmulation

Bat-band number	No. of analyzed single units
BK51	2
W25	7
W43	1

To quantify and compare cortical responses to simultaneous wing surface stimulation with either surface stimulated alone, I defined a response index (**RI**) as:

[Simultaneous response – (Dorsal + Ventral response)] / (Dorsal + Ventral response)

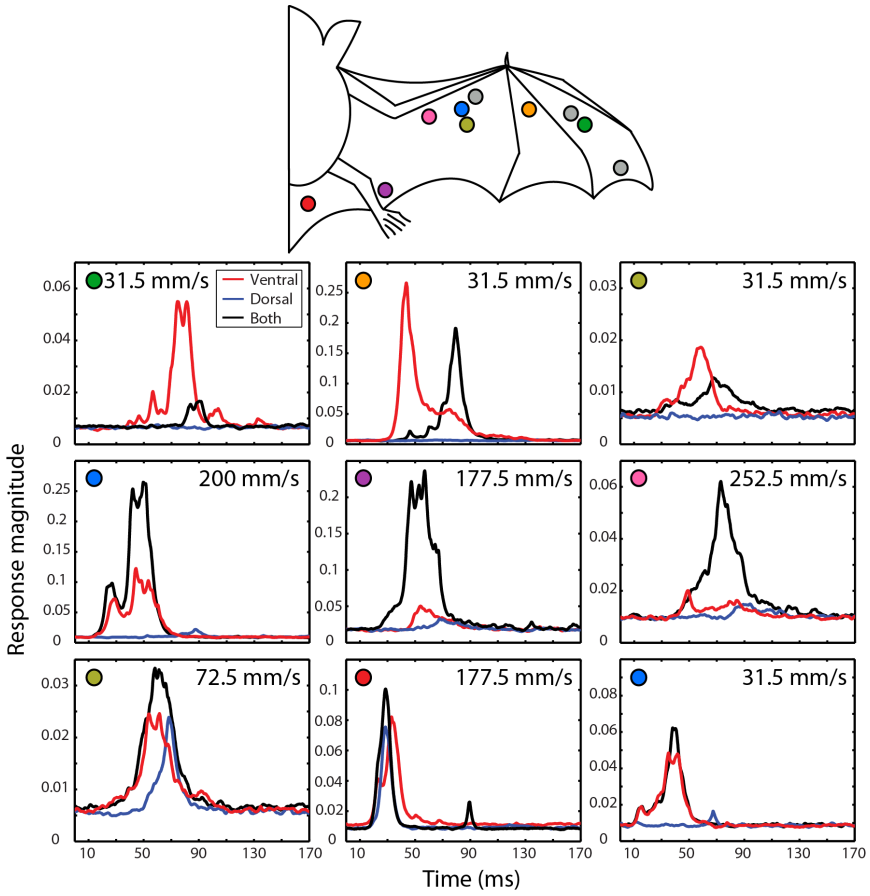

Figure 3.12: Cortical responses to airflow stimulation of both or either wing surfaces. Schematic of a bat showing the sampled RF locations. Airflow stimuli were delivered on the dorsal, ventral or both wing surfaces simultaneously. Averaged rectified multiunit responses showing the range of observed responses in the panels below. Colored dots in the panels correspond to RF locations in the bat schematic.

For the population of sampled RF locations across all trials, RI values ranged from -0.73 to 1.8, showing both "facilitation" (RI > 0) to "inhibition" (RI < 0; Fig. 3.13), with a positive skew in the distribution. Although RI values were not correlated with RF locations, these findings suggest that cortical responses to airflow stimulation from dorsal and ventral wing surfaces are integrated in a way that reflects the interplay of aerodynamic forces experienced by both wing surface simultaneously. The level at which these responses are integrated, whether at the periphery or further downstream is not known.

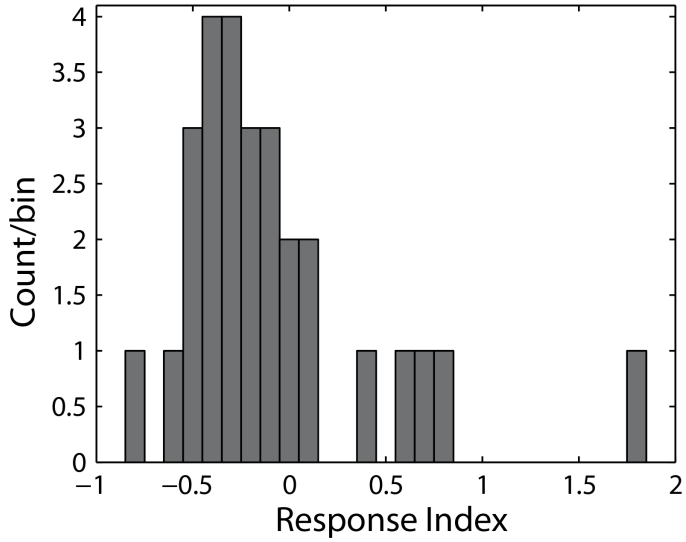

Figure 3.13: Distribution of Response Index values. Histogram of Response Index values across all trials and stimulus conditions (mean $\pm$ std. dev = -0.03 ± 0.53; median = -0.18; sample skewness = 1.79).

3.2.6 Airflow sensitive receptive fields on bat wings do not show lateral interactions

The phenomenon of lateral inhibition is well-known and a widespread feature of the nervous system, first described in the somatosensory system more than 50 years ago (Mountcastle and Powell 1959). In general, lateral inhibition can be observed when the activity of an excitatory neuron at the center of a receptive field is seen to be inhibited or

suppressed by excitation of nearby neurons. It is widely believed that this phenomenon serves to increase spatial resolution. Could this be a feature of airflow sensitive receptive fields on the bat wing membrane? We tried to address this question by directing airflow stimuli simultaneously at the center and surrounding areas of the receptive field, both within and outside its boundaries. The stimulus probe at the center of the receptive field was fixed in position, while a second probe was systematically moved in 5 mm steps, in either one or both the rostrocaudal and mediolateral directions. Airflow stimuli delivered by the movable probe were in the same and/or opposite direction to the fixed probe. All stimulus parameters other than the location of second probe were kept constant throughout the experiment (Fig. 3.14). Data from 12 single units from 4 bats was analyzed.

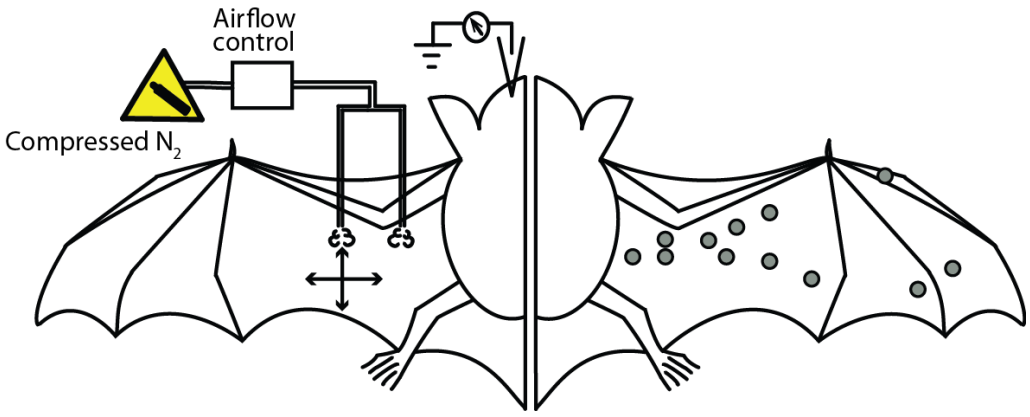

Figure 3.14: Experimental setup for eliciting lateral interactions. Schematic of a bat showing the experimental setup. Airflow was split to stimulate the center and surrounding regions of a RF. Intensity of airflow ranged from 0.03-0.09 m/s. The probe at the center of a RF was fixed in location while the second probe was moved in 5 mm steps along the rostrocaudal and mediolateral dimensions as denoted by double-headed arrows. Sampled RF locations are shown on the right as circles (n=12).

For any sampled neuron, the baseline spike count and onset latency was defined as the response to 40 ms long, near suprathreshold airflow stimulus (0.03-0.09 m/s) delivered at the center of the RF in the preferred direction. Response magnitude, and onset latency of the same neuron was then measured after introducing the second stimulus as

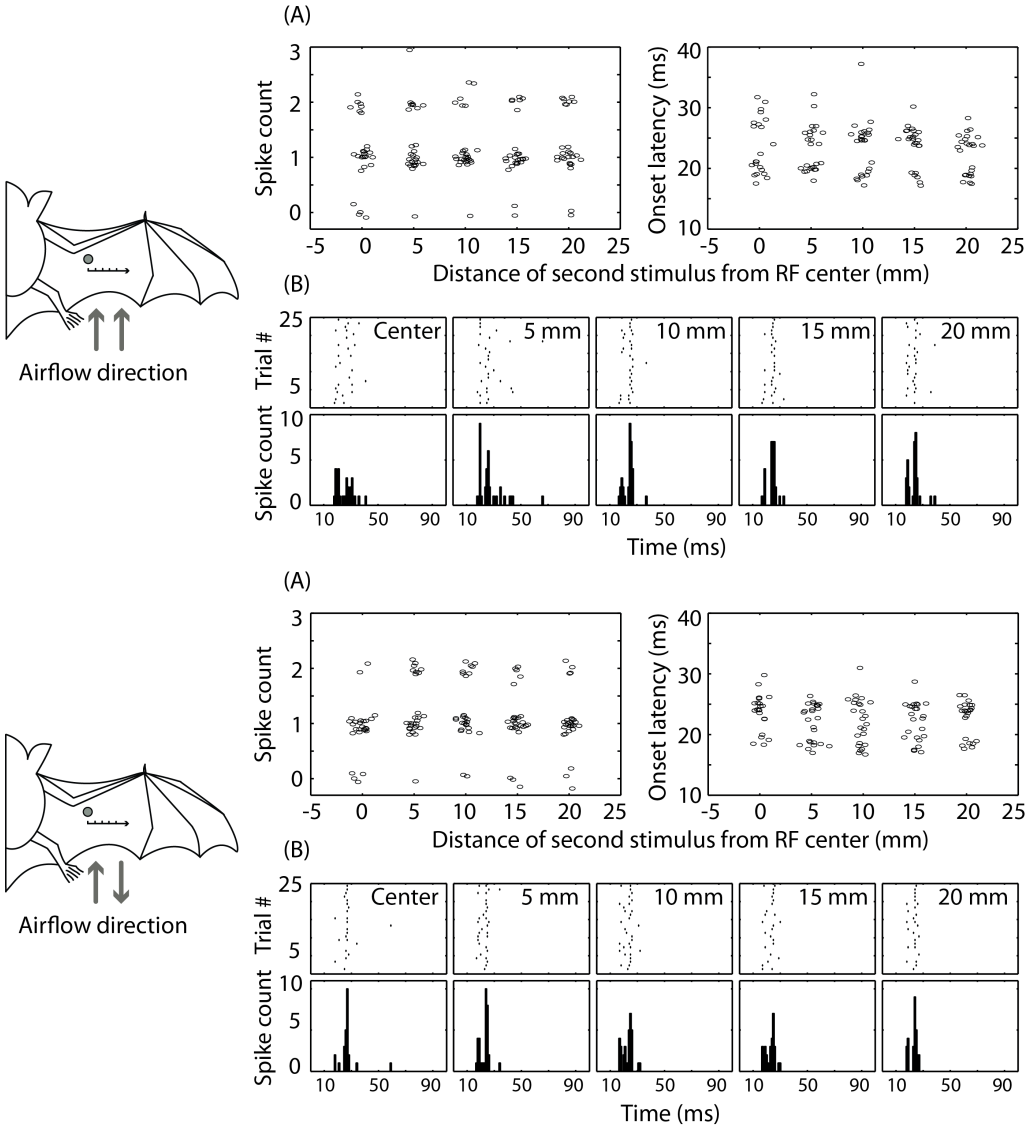

Figure 3.15: Cortical responses to simultaneous airflow stimulation inside and outside receptive fields. Schematic of a bat showing the RF location of a representative neuron, as the second probe is moved in the medial-to-lateral direction (shown by the horizontal arrow). Airflow direction is denoted by arrows below the schematic. **(A)** Scatter plots showing spike counts and onset latencies, with dots representing responses across trials and distance of the second stimulus probe from RF center. Data points are jittered along both the x- and y-axes for ease of visualization. **(B)** Rasters and post-stimulus time histograms showing responses as a function of the position of second stimulus probe.

it was stepped away from the RF center. Analysis of cortical responses to simultaneous airflow stimulation within and outside the RFs (using linear regression) showed little change in spike counts (R^2 range = 0 to 0.297, median R^2 = 0.195.; slope range = -0.075 to 0.012, slope median = 0.004; Fig. 3.15 A), or onset latency (R^2 range = $\sim$ 0 to 0.008, median R^2 = 0.046; slope range = $\sim$ 0 to 0.03, slope median = 0.001; Fig. 3.15 B).

3.3 Discussion

With over two dozen joints and a thin elastic membrane, bat wings are unlike those seen in birds and insects. As a result of the highly articulated design, bat wings generate some of the most complex aerodynamic trails by a flying vertebrate (Hedenström, Johansson, Wolf, et al. 2007). Multiple vortices of varying strengths and rotations are shed during different phases of the wingbeat cycle (Hedenström, Johansson, Wolf, et al. 2007; Hubel, Riskin, et al. 2010, also reviewed in Chapter 1). In past studies it has been hypothesized that microscopic hairs on the wings of bats play a role in sensing flight induced aerodynamic changes, thereby providing sensory feedback for guiding flight control (Sterbing-D'Angelo et al. 2011; Zook 2005, 2006; Zook and Fowler 1986). Controlled airflow stimulation of the wing membrane reveals relatively large RFs with rapidly adapting responses that do not vary with the length of airflow stimulation. Delineation of tactile RFs using von Frey hairs produced similar results (Chapter 2). While some differences in the size of receptive fields as measured at primary sensory cortical levels have been attributed to specific cortical layers (Armstrong-James and Fox 1987; Chapin 1986; Chapin and Lin 1984; Moore and Nelson 1998; Zhu and Connors 1999), others have shown that inhibition also plays a role (Hicks and Dykes 1983). While it is not known if layer-specific cortical inputs, local inhibitory circuits, subcortical processing, or a combination of these factors is responsible for shaping the outputs we observe, the data presented here suggests that unlike terrestrial species that use their hands (or other specializations) for tactile explo-

ration, e.g. primates with their large hands and fine tactile acuity, the wings of big brown bats are adapted to signal fast, and highly sensitive responses to mechanical disturbances over relatively large areas of the wing membrane. Although large RFs have traditionally been equated to broad tuning curves, recent reports are challenging the notion that broad tuning curves are necessarily less discriminative than sharp tuning curves (Brown and Bäcker 2006; Foffani, Chapin, et al. 2008; Pouget et al. 1999; Zhang and Sejnowski 1999).

With a relatively small size (weighing approximately 12-24 gm), and moderate aspect ratio wings (Norberg and Rayner 1987; aspect ratio is the length of wingspan squared divided by the surface area of wing), big brown bats are classified as low Reynolds number fliers ($\sim$ 103). Reynolds number is a dimensionless quantity in fluid mechanics, defined as the ratio of inertial to viscous forces, which determines the nature of generated flow patterns. In terms of aerial navigation, this implies that the smallest disturbances in ambient airflow conditions can have a big impact on flight stability. The ability to detect small perturbations in the flow field can thus potentially play a significant role in informing the flight motor apparatus with respect to flight control. My data demonstrates that wing tactile RFs can signal not only the direction, but also the strength of airflow in their immediate vicinity. The directional selectivity of S1 neurons aligns with the previously reported multiunit data (Sterbing-D'Angelo et al. 2011), showing a preference for reversed airflow. Together with information about the speed of airflow, this could potentially be a mechanism for stall detection, as turbulent, reversed airflow conditions arise when the laminar boundary layer flow is disrupted, for instance, at high angles of attack, such that exceeding the "critical" angle of attack results in serious stall conditions with sudden loss of altitude. Further evidence in support of this hypothesis is provided by bat flight experiments, where depilation of wing hairs along the trailing edge resulted in a significant increase of flight speed (Sterbing-D'Angelo et al. 2011). Increasing flight speed is one way to prevent stall at high angles of attack, and in the absence of sensory feedback this could serve as a way to avoid just that.

While detection of fluctuations in the boundary layer provides potentially valuable feedback for flight control, monitoring airflow along the dorsal and ventral wing surfaces could be equally important. This is because the upper and lower wing surfaces experience varying aerodynamic forces during flight. My findings show that when both wing surfaces are stimulated simultaneously, responses vary from being inhibited to being facilitated, compared to either wing surface stimulation alone. This non-linear integration of outputs from the two wing surfaces could signal the differential airflow patterns at the two wing surfaces.

Tactile RFs on the wings of *E. fuscus*, as elicited by airflow and tactile stimulation were often found to overlap. Generally, lateral inhibition, a widespread phenomenon in the nervous system across all modalities, serves to enhance spatial contrast in this situation. But the use of airflow stimulation in the center and surrounding regions of wing RFs did not show evidence of lateral interactions. This could be a result of airflow stimulus exciting a relatively large spatial area of the wing. Additionally Simons and Carvell (1989) showed that lateral inhibition in the barrel cortex of rats peaks at approximately 10-20 ms after stimulation of the surrounding or non-principal whisker. The use of simultaneous center-surround stimulation paradigm in the experiments described above could also account for not observing lateral inhibition. The use of less spatially distributed stimulus (e.g. use of a finer needle and smaller distance between the stimulus probe and wing membrane), along with introduction of temporal offset between center-surround stimulation could help address this issue.

The findings presented thus far suggest that airflow sensitive tactile receptive fields are highly sensitive to detect and measure small changes in airflow. Monitoring the strength and direction of the boundary layer, along with differential signaling from the dorsal and ventral wing surfaces, could potentially serve as valuable aerodynamic feed-

back for the flight motor apparatus. In the following chapter I address how this information is encoded at the level of S1 by applying an information theoretic framework.

Chapter 4

The role of spike timing in encoding airflow by bat wings

The role of precise spike timing in the representation of sensory information deals with the fundamental problem of neural coding in the field of neuroscience. For instance, results presented thus far indicate that tactile RFs on the wings of *E. fuscus* transmit information about the speed and direction of airflow, by modulations of firing rate and/or temporal onset at the primary somatosensory cortical level. From the perspective of aerodynamic feedback however, it is not known how modulations in spike counts, or their timing represent this information. This issue is addressed here by applying entropy based measures to quantify, and compare information transmission by spike counts and spike timing to changes in the direction and strength of airflow stimuli.

Specifically, extracellular single neuron recordings were performed from S1 of anesthetized big brown bats to airflow stimulation of tactile RFs on the wings. The direction and strength of airflow was varied independently, while keeping all other stimulus parameters constant. By applying information theory (Shannon 1948), the amount of in-

formation transmitted by spike counts and precise timing of responses was quantified. Results show that on average, varying the intensity of stimulation transmits 75% more information by spike timing compared to the number of evoked spikes. When applying directional stimulation, spike timing conveys 51% additional information compared to spike counts. Furthermore, bulk of this information was contained in the latency of the first spike (a latency code), and estimated to be as much as 57.5%, and 84% of the total spike timing information for airflow intensity, and direction, respectively. Collectively, these results point to the significance of precise spike timing in rapidly signaling aerodynamic fluctuations of the flow field in the vicinity of bat wings.

4.1 Methods

4.1.1 Experimental setup

Data for the findings reported here was obtained in experiments described previously (Chapter 3). Briefly, extracellular single unit potentials were obtained from S1 of 10 anesthetized big brown bats (*E. fuscus*). Spike waveforms were extracted using commercially available software (Offline Sorter, Plexon Inc.) with further analysis on spike timestamps done in MATLAB (version R2012a, The Mathworks Inc.). Stimulation consisted of 21-26 presentations of 40 ms long air puffs delivered at 5 s intervals. The intensity of airflow was varied from 0.03-0.25 m/s. Directional stimulation consisted of near threshold intensity airflow delivered along the rostrocaudal and mediolateral dimensions (4 directions, 90° steps). Stimuli were delivered using a 14 g blunt-tipped needle, located at a distance of 3 mm and 45° inclination relative to the wing membrane. Data from 35 well-isolated single neurons was used in analyzing the effect of airflow intensity, and 22 units for directionality.

4.1.2 Application of information theory to spike train data

The application of information theory provides one of the many ways which helps address the question of sensory encoding by the nervous system. Following is a brief description of the basic principles and application of information theory for quantification of sensory encoding of airflow stimuli by the bat wings.

Information theory was introduced by Shannon (1948) as a mathematical theory to describe transmission of information over a noisy channel of communication. Since then it has found wide applications across a large number of disciplines including biological systems. Information theory is fundamentally based on probability theory. When applied to sensory systems, the main question that is addressed is the maximal reduction of uncertainty about which stimulus s occurred by observing the neural response r on a single trial. This is quantified by Mutual Information (MI). It is defined as follows:

$$\mathrm{I(S;R)} = \mathrm{H(R)} - \mathrm{H(R \mid S)}$$

where S is the set of possible stimuli $\{s\}$ and R is the set of possible responses $\{r\}$. The first term H(R) is called the response entropy, and it quantifies the overall variability of the response. It is defined as:

$$\mathrm{H(R)} = -\sum \mathrm{P(r)} \log_2 \mathrm{P(r)}$$

where P(r) is the probability of observing response r to any stimulus. The second term is also called noise entropy and it quantifies the variability in the response specifically due to trial-to-trial differences in the response to repeated presentations of the same stimulus. It is defined as:

$$\mathrm{H(R \mid S)} = -\sum \mathrm{P(s)} \sum \mathrm{P(r \mid s)} \log_2 \mathrm{P(r \mid s)}$$

Where P(r | s) is the probability of observing a response conditioned on the presence of stimulus *s*, and P(s) is the probability of stimulus *s* being presented.

Mutual information is measured in bits because of representation of probabilities in $\log_2$ terms in the expression: 1 bit of information corresponds to a reduction of uncertainty by a factor of 2.

One of the key advantages of using entropy based measures, specifically mutual information, is that it does not make any assumptions about the nature of the stimulus being encoded by a neuron (or a population of neurons). A second advantage is that it quantifies the reduction in uncertainty about the stimulus given the observation of a single response. This is important because it does not require the response be averaged over repeated presentations, or over a population of neurons. These and other advantages of using mutual information have been reviewed extensively (Borst and Theunissen 1999; Rieke et al. 1997; Victor 2006).

The application of information theory therefore requires the estimation of probability distributions over the state space of the system. This is typically achieved by repeated presentations of the stimulus and recording the response over a defined time window. Since the probabilities in calculation of mutual information are estimated from a limited number of trials, the statistical errors lead to a systematic bias in both the response and noise entropy (Panzeri, Senatore, et al. 2007). Specifically, since H(R) depends on only P(r), which is sampled across all trials to all stimuli, the bias is much smaller than that of H(R | S), which depends on P(r | s). This results in an overall upward bias of mutual information estimates. The past 15 years or so have seen the development of a number of bias correction measures based on physiological and simulated data (reviewed in Panzeri, Senatore, et al. 2007). To compensate for the bias in mutual information estimates presented here, a quadratic bias correction procedure was applied (Strong et al. 1998).

To quantify how much information about the stimulus is gained by either scheme, mutual information was quantified as either "spike count" information or "spike timing" information as described next. The simplest neural code transmitting information about the stimulus is a rate code, where modulations in firing frequency over a certain time window carry knowledge about the stimulus. To quantify information gained by the probability of spiking, the total number of spikes emitted in response to stimulation by a neuron were counted in a 50 ms post-stimulus time window, and mutual information estimated directly from the stimulus-conditional response probabilities.

To test if the mutual information estimated for spike counts for a particular neuron was statistically significant, it was compared to a null distribution created as follows. The spike count responses were shuffled across trials by allocating them randomly (using a discrete random distribution), with the effect that any stimulus-response correlation was destroyed, while keeping the spike counts preserved. The process was repeated 1000 times to create a distribution of mutual information values and 95% confidence interval about the mean was estimated by bootstrapping 1000 times. Spike count mutual information values exceeding the upper bound of the confidence limit were considered significant.

To assess if the timing of spikes emitted in response to stimulation was informative, the 50 ms post-stimulus response window was discretized into different bin sizes (from 2 to 25 ms), with 0 denoting the absence of spikes in a time-bin, and 1 representing the presence of at least 1 spike. The result is a representation of the response as a binary string, or a 2-25 letter "word". Similar to spike count coding, mutual information was directly calculated from the estimated probability distributions (Strong et al. 1998).

To evaluate the contribution of the first spike (latency code) in the mutual information estimate for spike timing, the latency on a given trial was defined as the first discretized time-bin that contained 1 or more spikes. Trials with no response could take any value.

To test if the mutual information conveyed by onset latency of a neuron was more than expected by chance, the time-bin containing the spike was randomly assigned (using a discrete uniform distribution) to any of the 25 time-bins of the discretized response. The procedure was repeated 1000 times to create a null distribution from which 95% confidence intervals were estimated by bootstrapping 1000 times. If the mutual information for latency exceeded the upper bound then the neuron was considered to be involved in latency coding.

4.2 Results

4.2.1 S1 neurons respond with sub-Poisson variability

In the previous chapter it was reported that onset latency but not the number of evoked spikes appear to vary as a function of airflow intensity (Section 3.2.1). If the onset latency of individual spikes is informative about a stimulus, how "reliable" is the latency cue for discriminating airflow intensity? Reliability of responses can be quantified in terms of the trial-to-trial variability of spike counts, as well as their temporal precision. Observations on the stochastic nature of spike trains have led to modeling spikes as events of an inhomogeneous Poisson process (Mazurek and Shadlen 2002; Shadlen and Newsome 1998, 2001; Softky and Koch 1993; Tolhurst et al. 1983). The interpretation of this irregularity has led to the view that this reflects stochastic "noise", and hence to obtain an estimate of instantaneous firing rate one needs to average the response of a neuron over a certain time window, or pool the responses of a population of neurons. A corollary to this interpretation is that precise timing of individual spikes conveys little information. A statistic commonly used to model the variability in spike trains is Fano factor, defined as the ratio of empirical variance and mean spike counts across trials. For a perfectly stochastic process this ratio is 1. To test if observations in spiking variability follow a

Poisson distribution, the computed Fano factor for the population of sampled neurons across all trials where stimulus intensity was varied, was tested against a gamma distribution (Eden and Kramer 2010). Results indicate that a majority of responses (163/200 = 74%, $p < 0.05$) are sub-Poisson, indicative of more reliable spiking (Fig. 4.1).

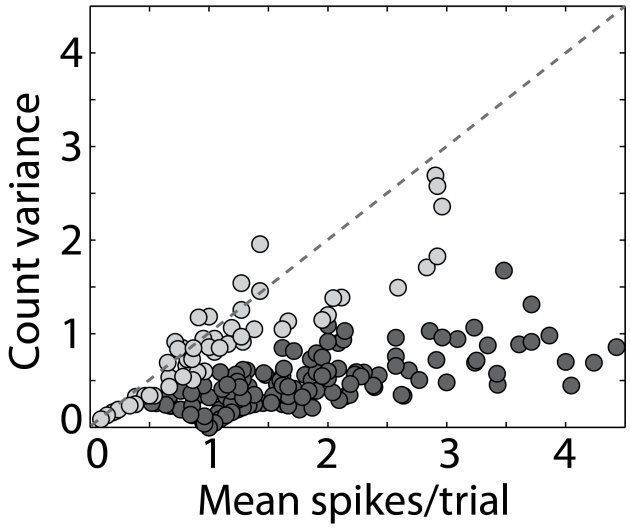

Figure 4.1: S1 neurons respond with sub-Poisson variability. Variance of spike counts across the population of sampled neurons as a function of mean spikes per trial. Filled circles are significantly less than 1 (i.e. sub-Poisson; $p < 0.05$, gamma distribution, shape parameter (n-1)/2 and scale parameter 2/(n-1); n=sample size).

Reliability in the spike trains was also reflected in small temporal dispersion of response onsets, for which the population average was low (average absolute deviation about mean=2.93 ms, average absolute deviation about median=2.69 ms; Fig. 4.2). As shown in the following section, this relatively low jitter in the response onset is a major factor enabling encoding of information about the stimulus by first spike latencies.

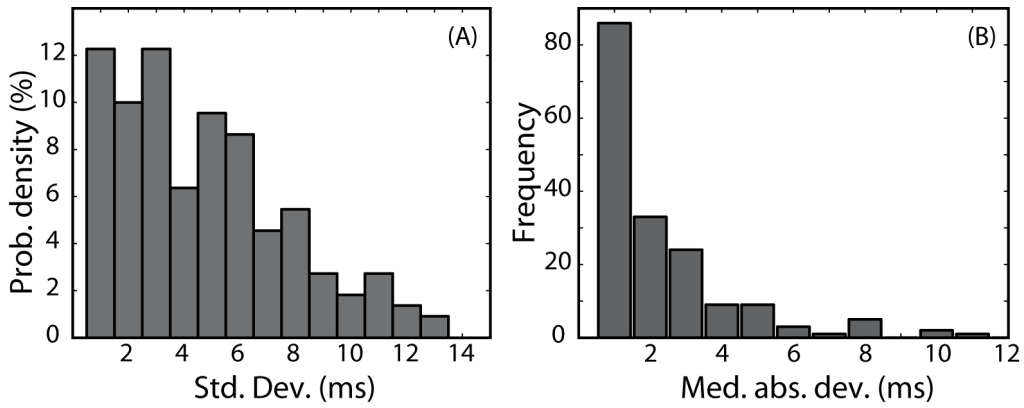

Figure 4.2: S1 neurons respond with low jitter. Frequency distribution of the onset jitter, plotted as **(A)** standard deviation and **(B)** median absolute deviation across all units and stimulus conditions (bin size, 1ms).

4.2.2 Comparing information transmission by spike counts versus spike timing

To compute how informative either of these measures is about the stimulus, information theoretic measures were applied to spike trains emitted in response to varying airflow direction, and intensity (mutual information; Shannon 1948). The application of information theoretic framework for quantification of sensory information provides a metric for discrimination of stimuli on single trial basis. There were two principal questions that were addressed: (1) What is the timescale for information encoding? In other words, how much information is transmitted by the total number of evoked spikes ("spike count code") compared to their timing ("spike timing code")? (2) What is the contribution of first spike latency in the information available from spike timing? First, to test if the calculated mutual information for individual neurons by either coding schemes was more than expected by chance, it was compared to the upper bound of 95% confidence interval of a null distribution (see Methods). When the direction of airflow was varied, all the sampled neurons (n=22) contributed significant information by spike counts, compared to 91% (20/22) of the cells that transmitted significant information by the precise timing

of evoked spikes. The numbers were comparable when the intensity of airflow was varied: 32 out of 35 (or 91%) neurons contributed significant information by spike counts, and 100% of the sampled cells by spike timing.

What is the degree of precision underlying spike timing encoding for airflow stimuli? To address this question, the resolution at which spike times were binned was varied, and average information across stimuli computed. Results show that precision is highest at the 10 ms bin resolution (Fig. 4.3). This temporal precision can also be appreciated qualitatively, in the good alignment of spikes across trials and sharp peaks in the peri-stimulus time histograms (Figs. 3.4 and 3.10). For information to be encoded at a high temporal precision, across-stimulus latency differences should be higher than the trial-to-trial variability in the first spike times (see Figs. 3.5 and 4.2).

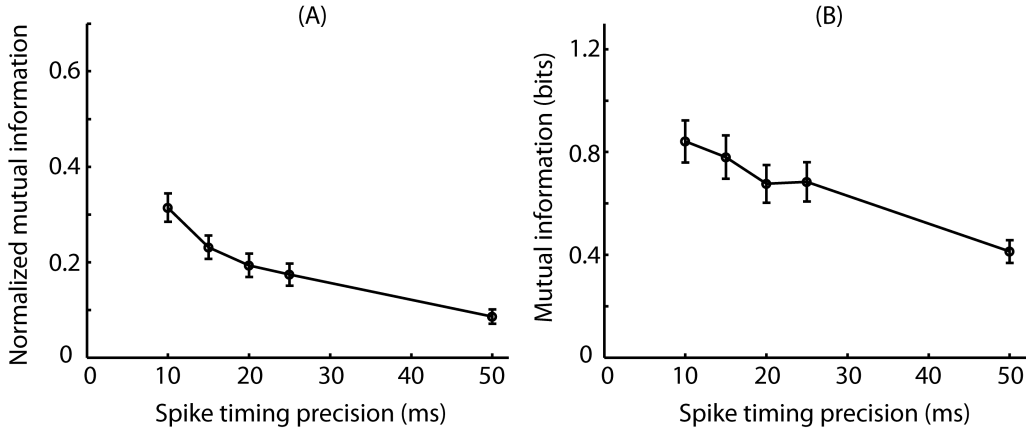

Figure 4.3: Spike timing precision. Variation of mutual information as a function of time-bin size, for airflow intensity **(A)** and direction **(B)**, computed for the sampled cells across all stimuli. Vertical bars denote standard error. Note that mutual information estimates for airflow intensity were normalized to maximum possible values as stimulus levels were variable across the sampled neurons.

The issue of bias as mentioned in Section 4.1.2, becomes a significant constraint on the reliable estimation of mutual information when the sampling is limited, and the number of possible responses large (e.g. the length of the response "words"). Analytical approximations for measuring the bias have been calculated (Golomb et al. 1997; Panzeri and

Treves 1996), according to which, information estimated is reliable provided the ratio of number of trials to number of possible responses is ≥ 1. At the same time, bias also depends on the reliability of the response, such that more reliable the neural response, fewer the observed responses to a stimulus, and thus lesser the bias (Panzeri, Senatore, et al. 2007). Responses of S1 neurons reported here were highly reliable (Figs. 4.1 and 4.2) and hence the bias problem is less severe compared to analyzing unreliable neurons (Arabzadeh et al. 2005; Panzeri, Senatore, et al. 2007). Nevertheless, the presence of a systematic bias in estimation of mutual information for discretized responses makes it unreliable with limited sampling, and a large number of possible responses. Therefore, the mutual information estimates presented here were restricted to responses binned at 10 ms, although values for up to 2 ms bins were computed.

Next, mutual information conveyed by individual cells was estimated, either by spike count or spike timing codes, to directional airflow stimulation, delivered at near threshold intensity ($\sim$ 0.03-0.05 m/s). All but 1 neuron conveyed more information by spike timing compared to spike counts (Fig. 4.4 A). On average, units conveyed 0.41 ± 0.21 bits (mean $\pm$ SD) by spike count and 0.84 ± 0.38 bits by spike timing. The spike timing code was significantly more informative, transmitting 51% additional information ($p < 0.05$, Wilcoxon sign rank test, Fig. 4.4 B).

Finally, the contribution of onset latency in the total information available by the timing of spikes was evaluated. To test if the estimated mutual information using the first spike was significantly higher than expected by chance, it was compared to the upper bound of the 95% confidence interval of a shuffled distribution as described earlier (see Methods). All the sampled neurons transmitted significantly more information than chance, on average 0.71 ± 0.36 bits, which was 84.5% of the total spike timing information. Results were comparable when stimulus intensity was varied. Every neuron of the sampled population conveyed significantly more information by spike timing compared

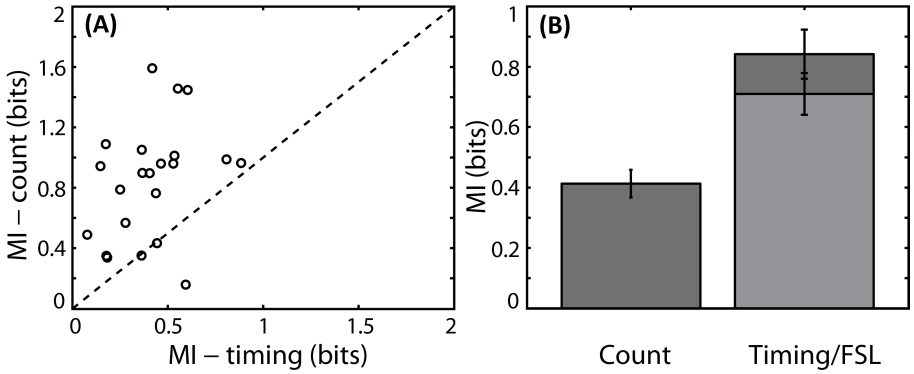

Figure 4.4: Spike timing carries significantly more information than spike counts about airflow direction. **(A)** Scatter plot comparing mutual information (MI) estimates for spike count and spike timing. Each circle represents a single neuron. **(B)** Average MI across all trials and stimulus conditions for the two candidate codes. The light gray shade indicates contribution of first spike latency (FSL) to the total mutual information estimate for spike timing. Vertical lines on the bars denote standard error.

to spike counts (Fig. 4.5 A). On average, spike timing conveyed 75% more information than spike counts, which was significantly higher than 8% of the total information available by spike counts ($p < 0.05$, Wilcoxon sign rank test, Fig. 4.5 B). For the spike timing code, 57.5% of this information was due to the first spike alone.

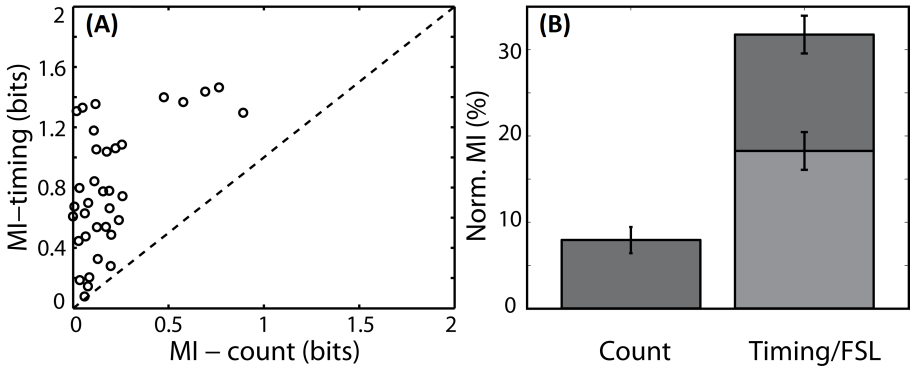

Figure 4.5: Spike timing is more informative that spike counts about the intensity of airflow. **(A)** Scatter plot comparing Mutual Information (MI) for spike count and spike timing. Each circle represents a single neuron. **(B)** Average MI normalized to the maximum possible MI for spike counts, spike timing and first spike latency. The light grey shade indicates contribution of first spike latency to the total MI estimated for spike timing. Vertical lines on the bars represent standard error.

4.3 Discussion

The aim of the present investigation was to understand the nature of the neural code with respect to airflow sensing by bat wings. Information theoretic framework was applied to evaluate the timescales of information transmission by primary somatosensory cortical neurons. Results show that precise timing of evoked spikes – in particular the latency of first post-stimulus spike – encodes significantly more information than spike counts, about the direction and strength of airflow in the vicinity of bat wings. Systematic bias due to finite sampling limits the consideration of temporal precision to values greater than 10 ms, although higher precision (up to 2 ms) is likely given the highly reliable responses (Figs. 4.1 and 4.2).

It has long been recognized that the bandwidth of information transmission, at least theoretically, increases tremendously when considering temporal patterns of spikes emitted by single neurons, or coordinated temporal activity across a population, under the assumption that timing of individual spikes is reliable at short timescales (MacKay and McCulloch 1952). The precision of spike timing in 1-10 ms time scales have been observed across different sensory systems in diverse species (Bair and Koch 1996; Borst and Theunissen 1999; Buracas et al. 1998; Butts et al. 2007; de Ruyter van Steveninck et al. 1997; deCharms and Merzenich 1996; Foffani, Morales-Botello, et al. 2009; Gawne et al. 1996; Heil 1997; Johansson and Birznieks 2004; Kara et al. 2000; Meister and Berry 1999; Panzeri, Petersen, et al. 2001; Rieke et al. 1997). Although spike timing precision generally decreases from the periphery to the central nervous system, many cortical areas exhibit precision on the order of 10 ms or less in response to both static and dynamic stimulation (Arabzadeh et al. 2005; Bair and Koch 1996; Kayser et al. 2010). However, these findings raise the question of how, and if downstream neural systems decode these high fidelity signals. For instance, while the experimenter is fully aware, and in control of the precise onset of the stimulus, the subject has no knowledge of it, and there is no explicit refer-

ence available for decoding the temporally precise spikes. This issue is specifically left unaddressed by information theoretic measures, where only the information available is revealed, but how or whether it is used by the next stage of processing is unresolved.

This issue of reference signal has been tackled in some recently published reports, both theoretically (Delorme 2003; Pawlas et al. 2010; Thorpe et al. 2001), as well as experimentally (Chase and Young 2007; Johansson and Birznieks 2004; Storchi et al. 2012). One such proposal, as shown experimentally, is relative spike timing i.e., if the recorded spike times as measured relative to population onset time can deliver as much or more information when referenced to stimulus onset, then an explicitly coded stimulus onset is not needed (Chase and Young 2007; Foffani, Chapin, et al. 2008). A similar but slightly different approach where the stimulus onset is not coded explicitly involves measures such as rank order coding (Gollisch and Meister 2008; Johansson and Birznieks 2004). Here for example, the stimulus attribute under investigation could be accurately decoded from the rank order of relative latencies within a population, which is robust even under "noisy" conditions.

Evidence for yet another way to overcome the reference problem comes from active sensory systems, e.g., the exploratory whisking behavior in rodents (Fee et al. 1997), or saccadic eye movements in primates (Ahissar and Arieli 2001; Martinez-Conde et al. 2000). Here, more often than not, sensory stimuli are acquired by association with motor commands. These leading motor signals could potentially relay an efference copy, thereby providing a temporal reference for the incoming spike trains. I speculate that a similar system exists in bats, where the onset of each powered wing stroke could feed in to the sensorimotor loop, serving the role of a precisely timed relative reference for airflow invoked sensory signals. The sparsely firing responses of S1 neurons, and a wing stroke lasting 35-45 ms provide support to this hypothesis.

In the recent past we provided evidence that airflow induced primary somatosensory activity arises from an array of microscopic hairs on the wings of *E. fuscus* (Sterbing-D'Angelo et al. 2011). The dimensions of these hairs make them ideally suited to detect changes of the flow field in the immediate vicinity of the wing membrane (Dickinson 2010). In fluid mechanics, this region of (fluid) flow near the surface is referred to as boundary layer. Viscous forces dominate here, resulting in fluid velocity that changes from zero at the surface to free stream value as one moves further away. For a low Reynolds number flier like the big brown bat, boundary layer is characterized by laminar flow. But turbulence and separation of the boundary layer from the wing surface can occur, for instance, at high angles of attack or when making a sharp turn, features not uncommon in the highly maneuverable flight of *E. fuscus*. For any flying animal, the effects of boundary layer disruption are highly undesirable e.g. increased drag, reduced lift, and stall. The presence of hair sensors on the wing membrane, with their ability to detect flow velocity can potentially provide critical information of an impending loss of controllability.

Any measurement of changes in the boundary layer flow (either direction or speed), and the resulting flight motor adjustments, need to be rapidly orchestrated to avoid undesirable consequences. This is because big brown bats are agile fliers with speeds of 3-9 m/s, and a wing beat rate of 11-15 Hz (Kurta and Baker 1990). The sparse but reliable nature of S1 responses to airflow stimulation of the wing, and the high information content of the first spike suggest fast signaling to guide kinematics, such as changes in angle of attack and camber.

Chapter 5

Conclusions and Future Directions

Long before echolocation was discovered, it was believed that bats were able to navigate in darkness through tactile feedback from their wings (Maxim 1912). The results presented in this thesis provide empirical evidence demonstrating the role of somatosensory system in providing sensory feedback for flight control in the big brown bat, *Eptesicus fuscus*.

Bats have been used extensively as model animals for studying echolocation and their role in orientation during flight. At the same time, very little research has been conducted on any aspect of the somatosensory system or its role in sensing aerodynamic changes, crucial for aerial navigation (Sterbing-D'Angelo et al. 2011). In Chapter 2, I presented the first investigation on the organization of primary somatosensory cortex in *E. fuscus*, especially with respect to the wing representation. The results show a slight variation of the typical mammalian topographic representation, with an overrepresented and inverted wing as compared to forelimb representation in terrestrial mammals. We also measured cortical response thresholds to tactile stimulation, and found remarkable tactile sensi-

tivity along regions of the wing membrane, comparable to human fingertips. Together, these findings point to the importance of tactile sensory feedback arising from wings.

Next, we investigated the role of microscopic hairs on the wing membrane as the main source of tactile feedback needed for flight control. A series of experiments were performed with the goal of revealing the fundamental properties of tactile receptive fields on the wing membrane, as detailed in Chapter 3. In the past we have shown that depilation of the wing hairs results in abolition of cortical responses to airflow, but not to tactile stimulation using hand-held monofilaments (Sterbing-D'Angelo et al. 2011). At the same time, airflow and monofilament stimulation activates similar neuronal pathways as shown by strikingly similar responses of S1 neurons to both stimuli. It remains to be seen if this is due to same mechanically sensitive peripheral receptors responding to either stimuli, or a result of upstream processing.

We found relatively large tactile receptive fields on the wing membrane, a shared feature for both monofilament and airflow stimulation. Generally the size of a RF has an inverse relation with the ability of a sensory surface to resolve spatial details of a stimulus (Kandel et al. 2000). At the same time, it has been shown (theoretically) that for two dimensional features, the accuracy of coding is insensitive to tuning width (Zhang and Sejnowski 1999). In addition, we failed to see any evidence of surround suppression in areas of the wing membrane outside of RF boundaries. This could be due to the fact that lateral inhibition (in the barrel cortex of rats) has been reported to peak at approximately 10-20 ms after stimulation of surrounding regions (i.e. non-principal whiskers; Simons and Carvell 1989), whereas we utilized a simultaneous stimulation paradigm of the center and surround. Collectively, the presence of large and overlapping but highly sensitive tactile RFs on the wings suggests that detection, rather than localization plays a more important role in airflow sensing.

What are the stimulus attributes encoded by tactile RFs on the wings? In the remainder of Chapter 3 and Chapter 4 I presented results of studies where I systematically varied the duration, direction or the intensity of airflow stimuli, and analyzed its effect on the magnitude and timing of cortical responses. My data shows that the duration of airflow stimulus, whether 10 ms or 1 s long, does not influence spiking activity of S1 neurons, both in terms of spike counts or their timing. Additionally, the activity of these neurons is, and remains rapidly adapting, regardless of the direction, intensity, or mode of stimulation (monofilament versus airflow). To rule out the effect of Isoflurane anesthesia in shaping the cortical output, I acquired single neuron activity using Ketamine-Xylazine, which showed similar responses to airflow stimulation.

When the direction of airflow stimulus is varied, S1 neurons respond selectively, with a preference for a particular direction that depends on the RF location. This directional selectivity is reflected both in the firing rate, as well as onset latency e.g., the preferred direction is usually the one with the highest firing rate and lowest onset latency. But the amount of information transmission is significantly higher by the timing of spikes (mostly by the first spike latency) compared with spike counts. On the other hand, the strength of airflow stimuli is encoded by the timing of spikes, and not by spike counts. But here again, a majority of information transmission occurs by the first spike latency. It is worth noting here that for information about a stimulus to be encoded by the timing of spikes, the precision or temporal reliability has to exceed the trial-to-trial variability, generally regarded as noise.

Bringing it all together

Bats are the only mammals capable of powered flight, and they achieve it with impressive maneuverability. Past research has provided some evidence that microscopic hairs arising from the wing membrane play a role in sensing airflow thereby providing feedback for optimizing flight control (Sterbing-D'Angelo et al. 2011; Zook 2006; Zook

and Fowler 1986). The findings presented here provide a deeper understanding of how aerodynamic feedback is represented at the level of the primary somatosensory cortex. Results show that bat wings can not only sense airflow, but inform about the strength and direction of airflow patterns in their vicinity.

The conundrum of low Reynolds number fliers from a standard aerodynamic perspective relates to the improbability of achieving aerial navigation based on their small size, and at least in bats, a wing that undergoes active shape changes throughout a stroke. But recent advances in studying the kinematics and aerodynamics of bat flight indicate an active control of flow (Busse 2011). The first such report by Muijres and colleagues convincingly demonstrated the presence of a stably attached leading edge vortex (LEV) in slow flying Pallas's long-tongued bat, *Glossophaga soricina* (Muijres et al. 2008). The authors estimated that the LEV accounted for about 40% of the lift. The presence of LEV has long been known to be a contributor to lift generation in insects, and suspected to be present in bats, but this was the first time that it was experimentally established. But it is still unknown, if and how bats control the attached LEV in relation to wing kinematics like camber, angle of attack and orientation of the leading edge.

A second issue relating to lift generation is known as boundary layer separation, or flow separation. This potentially catastrophic and highly undesirable phenomenon can occur, for instance, at high angles of attack or when making a sharp turn. It is marked by turbulent, even reversed airflow conditions on the wing surface (or any airfoil for that matter), and results in stall unless rapidly corrected. This problem is especially acute at low Reynolds numbers (typical of bats), and hence, the presence of hair sensors on the wing membrane, with their ability to detect flow velocity can potentially provide critical information of an impending loss of controllability.

My data shows that tactile receptive fields on the wings of bats are a valuable source of information about aerodynamic changes arising from complex kinematics of powered

flight. This feedback arises from an array of microscopic hairs on the wing surface, which not only provides information about flow direction, but also its strength. This information reaches the primary somatosensory cortical level from relatively large and overlapping, but highly sensitive tactile receptive fields, as precisely timed spikes and changes in the firing rate. Of particular importance is the speed with which information transmission occurs, because of the demands of aerial navigation.

Future directions

The results presented in this thesis raise a number of important questions worthy of future pursuits. Following is a proposal for future experiments that would help us further our understanding of bat flight from a neuroethological perspective.

Comparison with other species

The diversity of bats as a group (order Chiroptera), with over 1200 species is only exceeded by rodents. Whereas the existence of hairs and their arrangement on bat wings has been described for a handful of species, it is not known if airflow sensing by wing hair receptors is a shared feature even across model species employed most commonly for laboratory studies. For instance, there is a wide range in the size, weights, foraging habits and wing aspect ratios within the group, and this translates directly into flight capabilities. The big brown bat, and the similarly sized short-tailed fruit bat *Carollia perspicallata*, with their low aspect ratio wings and relatively slow flight are capable of remarkable aerial agility and maneuverability (Sterbing-D'Angelo et al. 2011), as opposed to a bigger species like the Egyptian fruit bat *Rousettus aegyptiacus* weighing over 10 times as much (160 g), with a wing span of about 2 feet, which are capable of much higher flight speeds (10-16 m/s) but not as maneuverable. Whether somatosensory specializations specifically for sensing aerodynamic changes exist, and are utilized by other members of the group is unknown.

Identity and organization of peripheral tactile receptors

In spite of being one of the most remarkable features of bats, we know very little about the fundamental questions about the arrangement and identity of tactile receptors associated with their wings. It would not be a stretch to assume that bats are no different from other mammalian species, where the basic template of end-organs and associated pathways are preserved, but modified to suit their respective needs. Nevertheless, knowing precisely what these receptors are, how they are arranged, and what specializations (if any) exist, is primordial in interpreting the functional significance of any neurophysiological recordings acquired at any level of the somatosensory system. Recent collaborative efforts between our laboratory and Columbia University (Dr. Ellen A. Lumpkin, principal investigator) aimed at addressing these issues are shedding light on the subject. Findings show the presence of Merkel cells, lanceolate endings, free nerve endings and diffuse endings that resemble end-knobs described previously in bat wing skin (Ackert 1914). Additionally, these receptors are distributed differentially in the wing membrane versus skin overlying the digits. For instance, diffuse endings are sparsely distributed relative to other end-organs, but are in significantly higher density in the inter-digital membrane. By contrast, lanceolate endings and Merkel cell clusters aggregate more densely over the digital and forearm bones. Together, these data demonstrate that bat wing skin is innervated by a unique repertoire of sensory receptors whose differential distribution suggest functionally specialized wing domains.

Dynamic stimulation

The results presented in this thesis make use of a simple yet effective and well controlled stimulus paradigm of generating puffs of air for stimulating the bat wing membrane. Even with this setup, there are unanswered questions about the nature of the stimulus itself, e.g., what are the characteristics of the turbulence associated with the flow? Once released, how does the column of air evolve in space? Upon contact with the wing

surface, how much wing area is impacted, and what is its profile? Answers to these questions are important in understanding the tactile receptive fields from a functional context. A static stimulus with controlled variation of one parameter at a time in discrete steps is needed as a very first step in understanding the interplay between a sensory structure and the stimulus attribute under question. The results presented here typify this. But naturally occurring stimuli are rarely static or discrete. Observations based on controlled yet dynamic stimuli would potentially add a new dimension in understanding sensory processing by the airflow sensitive hairs on bat wings.

Processing of sensory inputs at subcortical levels

One of the earliest discoveries in the field of somatosensory research was the observation that the profile of outputs associated with peripheral afferents not only depended on the nature of the stimulus used, but also with the source, or specific afferent fiber situated under the recording electrode. For instance, it is now well established that there are distinct peripheral receptor types along with their associated afferent fibers in the mammalian somatosensory system, which respond to specific features of the stimulus or submodality, with patterns of spike trains that are highly specific to the class of respective afferent type (reviewd in Chapter 1). This knowledge has been extensively exploited when performing peripheral recordings, not only to identify the underlying receptor/afferent class with great accuracy, but also to understand in great detail how specific stimulus features get encoded starting at the periphery. This has been fundamental to our understanding of haptic perception.

Experiments performed during the course of this study employed cortical recordings, specifically from the primary somatosensory cortex of *E. fuscus*, while stimulating at the periphery (the wing membrane). How incoming signals are processed at each successive stage, from the peripheral afferents, to brainstem nuclei, and the thalamus is not known.

Probing these areas would help us better understand how information about relevant stimuli is shaped at each these areas, with reference to their functional significance.

Mechanics of the receiver

The array of microscopic hairs on bat wings lie at the forefront of converting mechanical disturbances into voltage changes in the associated transducer elements. It is easy to see the profound effect mechanical properties of these hairs potentially have in shaping physiological outputs. A well-known example are the "fields" of cephalic trichoid sensilla of locusts, tiny hairs on the cephalic capsule that are highly sensitive to the direction of airflow, and are believed to be crucial in providing feedback directly to the flight motor (Camhi 1969). It is also well established, that the directional properties arise because of the mechanical properties of the hair shafts, and their insertion in the cephalic cuticle. Is a similar feature responsible for the directional selectivity of bat wing hairs, as reported in Chapter 3? A closer examination of the orientation, mechanical properties and flow associated effects would help answer this important piece of the puzzle.

Behavior

Any data based on physiological and/or anatomical measures alone would be of low significance in the absence of definitive behavioral evidence. Previous experiments (Sterbing-D'Angelo et al. 2011; Zook 2006), and ongoing behavioral investigations provide support for the main hypothesis that bat wing hairs are involved in sensing aerodynamic flow for the purpose of flight control. Observations on changes in flight behavior after depilation of wing hairs are easy to appreciate. At the same time, designing an optimum experiment is a challenging endeavor. For instance, the contribution of sensory feedback emanating from wing hairs in relation to simultaneous sensory inputs by other modalities is not known. Without a reference, designing an experiment that aims to disambiguate the role of wing hairs in flight control is an endeavor that requires testing the

bounds of what is behaviorally possible, and what is measurable. However challenging, without these studies any claim based on physiological data alone would not carry substantial weight.

Capturing the complexity of a natural setting

Aerodynamic forces in the vicinity of bat wings during flight change constantly, rapidly and in a highly complex manner. The experimental paradigm employed in the studies described here is a vastly simplified scenario, which is needed to achieve precise control on parameters affecting the outputs. The value of any such experiment cannot be emphasized more as stated above, but the ability to interpret the results, as applied to a natural behavioral state is limited. A natural extension then, is to either employ stimuli that mimic or come close to what is experienced, or have the subject involved in a behavioral task that achieves something similar. Recent successful attempts at neural telemetry from freely flying bats are a major step toward the latter. With a full repertoire of flight behavior under controlled conditions, and the resulting fluctuations in aerodynamic forces, studies of this nature can vastly expand our understanding of these nascent investigations.

Bibliography

Abraira, V. E. and Ginty, D. D. (2013). The sensory neurons of touch. *Neuron* 79.4, pp. 618–639.

Ackert, J. E. (1914). The innervation of the integument of Chiroptera. *J Morphol* 25.2, pp. 301–343.

Adrian, E. D. (1941). Afferent discharges to the cerebral cortex from peripheral sense organs. *J Physiol* 100.2, pp. 159–191.

Ahissar, E. and Arieli, A. (2001). Figuring space by time. *Neuron* 32.2, pp. 185–201.

Alvarez, J., Willig, M. R., Jones Jr., J. K., and Webster, W. D. (1991). Glossophaga soricina. *Mammalian Species*, pp. 1–7.

Arabzadeh, E., Zorzin, E., and Diamond, M. E. (2005). Neuronal encoding of texture in the whisker sensory pathway. *PLoS Biol* 3.1, e17.

Arita, H. T. and Humphrey, S. R. (1988). *Revisión taxonómica de los murciélagos magueyeros del género Leptonycteris (Chiroptera: Phyllostomidae)*. Instituto de Ecología.

Armstrong-James, M. and Fox, K. (1987). Spatiotemporal convergence and divergence in the rat S1 "barrel" cortex. *J Comp Neurol* 263.2, pp. 265–281.

Bair, W. and Koch, C. (1996). Temporal precision of spike trains in extrastriate cortex of the behaving macaque monkey. *Neural Comput* 8.6, pp. 1185–1202.

Basbaum, A. I., Bautista, D. M., Scherrer, G., and Julius, D. (2009). Cellular and molecular mechanisms of pain. *Cell* 139.2, pp. 267–284.

Beck, P. D., Pospichal, M. W., and Kaas, J. H. (1996). Topography, architecture, and connections of somatosensory cortex in opossums: evidence for five somatosensory areas. *J Comp Neurol* 366.1, pp. 109–133.

Bergou, A. J., Xu, S., and Wang, Z. (2007). Passive wing pitch reversal in insect flight. *Journal of Fluid Mechanics* 591, pp. 321–337.

Borst, A. and Theunissen, F. E. (1999). Information theory and neural coding. *Nat Neurosci* 2.11, pp. 947–957.

Brown, A. G. and Iggo, A. (1967). A quantitative study of cutaneous receptors and afferent fibres in the cat and rabbit. *J Physiol* 193.3, pp. 707–733.

Brown, R. E. and Fedde, M. R. (1993). Airflow sensors in the avian wing. *Journal of experimental biology* 179.1, pp. 13–30.

Brown, W. M. and Bäcker, A. (2006). Optimal neuronal tuning for finite stimulus spaces. *Neural Comput* 18.7, pp. 1511–1526.

Bullen, R. D. and McKenzie, N. L. (2002). Scaling bat wingbeat frequency and amplitude. *J Exp Biol* 205.Pt 17, pp. 2615–2626.

Buracas, G. T., Zador, A. M., DeWeese, M. R., and Albright, T. D. (1998). Efficient discrimination of temporal patterns by motion-sensitive neurons in primate visual cortex. *Neuron* 20.5, pp. 959–969.

Burrows, M. (1996). *The Neurobiology of an Insect Brain*. Oxford University Press. ISBN: 0198523440.

Busse, R. von (2011). *The Trinity of Energy Conversion: Kinematics, Aerodynamics and Energetics of the Lesser Long-nosed Bat (Leptonycteris Yerbabuenae)*. Shaker.

Butts, D. A., Weng, C., Jin, J., Yeh, C.-I., Lesica, N. A., Alonso, J., and Stanley, G. B. (2007). Temporal precision in the neural code and the timescales of natural vision. *Nature* 449.7158, pp. 92–95.

Calford, M. B., Graydon, M. L., Huerta, M. F., Kaas, J. H., and Pettigrew, J. D. (1985). A variant of the mammalian somatotopic map in a bat. *Nature* 313.6002, pp. 477–479.

Camhi, J. M. (1969). Locust wind receptors. I. Transducer mechanics and sensory response. *J Exp Biol* 50.2, pp. 335–348.

Catania, K. C. (1999). A nose that looks like a hand and acts like an eye: the unusual mechanosensory system of the star-nosed mole. *J Comp Physiol A* 185.4, pp. 367–372.

Catania, K. C. and Kaas, J. H. (1997). Somatosensory fovea in the star-nosed mole: behavioral use of the star in relation to innervation patterns and cortical representation. *J Comp Neurol* 387.2, pp. 215–233.

Catania, K. C. and Remple, M. S. (2002). Somatosensory cortex dominated by the representation of teeth in the naked mole-rat brain. *Proc Natl Acad Sci U S A* 99.8, pp. 5692–5697.

Chadha, M., Marshall, K. L., Sterbing-D'Angelo, S. J., Lumpkin, E. A., and Moss, C. F. (2012). Tactile sensing along the wing of the echolocating bat, *Eptesicus fuscus*. *Soc Neurosci Abstr*. Vol. 523. 03.

Chapin, J. K. (1986). Laminar differences in sizes, shapes, and response profiles of cutaneous receptive fields in the rat SI cortex. *Exp Brain Res* 62.3, pp. 549–559.

Chapin, J. K. and Lin, C. S. (1984). Mapping the body representation in the SI cortex of anesthetized and awake rats. *J Comp Neurol* 229.2, pp. 199–213.

Chapman, A. D. (2009). Insecta. *Numbers of Living Species in Australia and the World*. Australian Govt., Dept. of the Environment, Water, Heritage, and the Arts.

Chase, S. M. and Young, E. D. (2007). First-spike latency information in single neurons increases when referenced to population onset. *Proc Natl Acad Sci U S A* 104.12, pp. 5175–5180.

Combes, S. A. and Daniel, T. L. (2001). Shape, flapping and flexion: wing and fin design for forward flight. *J Exp Biol* 204.Pt 12, pp. 2073–2085.

Cooper, L. N., Cretekos, C. J., and Sears, K. E. (2012). The evolution and development of mammalian flight. *Wiley Interdiscip Rev Dev Biol* 1.5, pp. 773–779.

Cretekos, C. J., Wang, Y., Green, E. D., Martin, J. F., Rasweiler, J. J., and Behringer, R. R. (2008). Regulatory divergence modifies limb length between mammals. *Genes Dev* 22.2, pp. 141–151.

Cretekos, C. J., Weatherbee, S. D., Chen, C.-H., Badwaik, N. K., Niswander, L., Behringer, R. R., and Rasweiler 4th, J. J. (2005). Embryonic staging system for the short-tailed fruit

bat, Carollia perspicillata, a model organism for the mammalian order Chiroptera, based upon timed pregnancies in captive-bred animals. *Dev Dyn* 233.3, pp. 721–738.

Crish, S. D., Rice, F. L., Park, T. J., and Comer, C. M. (2003). Somatosensory organization and behavior in naked mole-rats I: vibrissa-like body hairs comprise a sensory array that mediates orientation to tactile stimuli. *Brain Behav Evol* 62.3, pp. 141–151.

Crowley, G. V. and Hall, L. S. (1994). Histological observations on the wing of the grey-headed flying-fox (Pteropus-poliocephalus)(Chiroptera, Pteropodidae). *Australian journal of zoology* 42.2, pp. 215–231.

Czech, N. U., Klauer, G., Dehnhardt, G., and Siemers, B. M. (2008). Fringe for foraging? Histology of the bristle-like hairs on the tail membrane of the gleaning bat, Myotis nattereri. *Acta Chiropterologica* 10.2, pp. 303–311.

de Ruyter van Steveninck, R. R., Lewen, G. D., Strong, S. P., Koberle, R., and Bialek, W. (1997). Reproducibility and variability in neural spike trains. *Science* 275.5307, pp. 1805–1808.

deCharms, R. C. and Merzenich, M. M. (1996). Primary cortical representation of sounds by the coordination of action-potential timing. *Nature* 381.6583, pp. 610–613.

Delorme, A. (2003). Early cortical orientation selectivity: how fast inhibition decodes the order of spike latencies. *J Comput Neurosci* 15.3, pp. 357–365.

Dickinson, B. T. (2010). Hair receptor sensitivity to changes in laminar boundary layer shape. *Bioinspiration & biomimetics* 5.1, p. 016002.

Dickinson, M. H. and Gotz, K. G. (1993). Unsteady aerodynamic performance of model wings at low Reynolds numbers. *Journal of Experimental Biology* 174.1, pp. 45–64.

Duff, A. and Lawson, A. (2004). *Mammals of the world: A checklist*. Yale University Press.

Eatock, R. A. (2009). Neuroscience: Up, down, flying around. *Nature* 458.7235, pp. 156–157.

Eden, U. T. and Kramer, M. A. (2010). Drawing inferences from Fano factor calculations. *J Neurosci Methods* 190.1, pp. 149–152.

Ellington, C. P., Berg, C. van den, Willmott, A. P., and Thomas, A. L. R. (1996). Leading-edge vortices in insect flight. *Nature* 384.6610, pp. 626–630.

Ennos, A. R. (1989). The kinematics and aerodynamics of the free flight of some Diptera. *Journal of Experimental Biology* 142.1, pp. 49–85.

Faure, P. A., Re, D. E., and Clare, E. L. (2009). Wound healing in the flight membranes of big brown bats. *Journal of Mammalogy* 90.5, pp. 1148–1156.

Fee, M. S., Mitra, P. P., and Kleinfeld, D. (1997). Central versus peripheral determinants of patterned spike activity in rat vibrissa cortex during whisking. *J Neurophysiol* 78.2, pp. 1144–1149.

Foffani, G., Chapin, J. K., and Moxon, K. A. (2008). Computational role of large receptive fields in the primary somatosensory cortex. *J Neurophysiol* 100.1, pp. 268–280.

Foffani, G., Morales-Botello, M. L., and Aguilar, J. (2009). Spike timing, spike count, and temporal information for the discrimination of tactile stimuli in the rat ventrobasal complex. *J Neurosci* 29.18, pp. 5964–5973.

Gawne, T. J., Kjaer, T. W., and Richmond, B. J. (1996). Latency: another potential code for feature binding in striate cortex. *J Neurophysiol* 76.2, pp. 1356–1360.

Gewecke, M. (1970). Antennae: another wind-sensitive receptor in locusts. *Nature* 225.5239, pp. 1263–1264.

Gewecke, M. and Niehaus, M. (1981). Flight and flight control by the antennae in the Small Tortoiseshell (Aglais urticae L., Lepidoptera). *Journal of comparative physiology* 145.2, pp. 249–256. ISSN: 0340-7594.

Gollisch, T. and Meister, M. (2008). Rapid neural coding in the retina with relative spike latencies. *Science* 319.5866, pp. 1108–1111.

Golomb, D., Hertz, J., Panzeri, S., Treves, A., and Richmond, B. (1997). How well can we estimate the information carried in neuronal responses from limited samples? *Neural Comput* 9.3, pp. 649–665.

Gui, L., Fink, T., Cao, Z., Sun, D., Seiner, J. M., and Streett, D. A. (2010). Fire ant alate wing motion data and numerical reconstruction. *J Insect Sci* 10, p. 19.

Gupta, B. B. (1967). The histology and musculature of plagiopatagium in bats. *Mammalia* 31.2, pp. 313–321.

Hedenström, A., Johansson, L. C., and Spedding, G. R. (2009). Bird or bat: comparing airframe design and flight performance. *Bioinspir Biomim* 4.1, p. 015001.

Hedenström, A., Johansson, L. C., Wolf, M., von Busse, R., Winter, Y., and Spedding, G. R. (2007). Bat flight generates complex aerodynamic tracks. *Science* 316.5826, pp. 894–897.

Hedenström, A., Rosén, M., and Spedding, G. R. (2006). Vortex wakes generated by robins Erithacus rubecula during free flight in a wind tunnel. *J R Soc Interface* 3.7, pp. 263–276.

Hedenström, A. and Spedding, G. (2008). Beyond robins: aerodynamic analyses of animal flight. *J R Soc Interface* 5.23, pp. 595–601.

Heil, P. (1997). Auditory cortical onset responses revisited. I. First-spike timing. *J Neurophysiol* 77.5, pp. 2616–2641.

Heinzel, H. G. and Gewecke, M. (1987). Aerodynamic and mechanical properties of the antennae as air-current sense organs inLocusta migratoria. *Journal of Comparative Physiology A* 161.5, pp. 671–680. ISSN: 0340-7594.

Henningsson, P., Spedding, G. R., and Hedenström, A. (2008). Vortex wake and flight kinematics of a swift in cruising flight in a wind tunnel. *J Exp Biol* 211.Pt 5, pp. 717–730.

Hicks, T. P. and Dykes, R. W. (1983). Receptive field size for certain neurons in primary somatosensory cortex is determined by GABA-mediated intracortical inhibition. *Brain Res* 274.1, pp. 160–164.

Holbrook, K. A. and Odland, G. F. (1978). A collagen and elastic network in the wing of the bat. *J Anat* 126.Pt 1, p. 21.

Hörster, W. (1990). Histological and electrophysiological investigations on the vibration-sensitive receptors (Herbst corpuscles) in the wing of the pigeon (*Columba livia*). *Journal of Comparative Physiology A* 166.5, pp. 663–673.

Hubel, T. Y., Hristov, N. I., Swartz, S. M., and Breuer, K. S. (2009). Time-resolved wake structure and kinematics of bat flight. *Experiments in fluids* 46.5, pp. 933–943.

Hubel, T. Y., Riskin, D. K., Swartz, S. M., and Breuer, K. S. (2010). Wake structure and wing kinematics: the flight of the lesser dog-faced fruit bat, Cynopterus brachyotis. *J Exp Biol* 213.Pt 20, pp. 3427–3440.

Iggo, A. and Muir, A. R. (1969). The structure and function of a slowly adapting touch corpuscle in hairy skin. *J Physiol* 200.3, pp. 763–796.

Iriarte-Díaz, J., Riskin, D. K., Willis, D. J., Breuer, K. S., and Swartz, S. M. (2011). Whole-body kinematics of a fruit bat reveal the influence of wing inertia on body accelerations. *J Exp Biol* 214.Pt 9, pp. 1546–1553.

Iriarte-Díaz, J. and Swartz, S. M. (2008). Kinematics of slow turn maneuvering in the fruit bat Cynopterus brachyotis. *J Exp Biol* 211.Pt 21, pp. 3478–3489.

Johansson, L. C. and Hedenström, A. (2009). The vortex wake of blackcaps (Sylvia atricapilla L.) measured using high-speed digital particle image velocimetry (DPIV). *J Exp Biol* 212.Pt 20, pp. 3365–3376.

Johansson, L. C., Wolf, M., von Busse, R., Winter Y.and Spedding, G. R., and Hedenström, A. (2008). The near and far wake of Pallas' long tongued bat (Glossophaga soricina). *J Exp Biol* 211.Pt 18, pp. 2909–2918.

Johansson, R. S. and Birznieks, I. (2004). First spikes in ensembles of human tactile afferents code complex spatial fingertip events. *Nat Neurosci* 7.2, pp. 170–177.

Johansson, R. S., Vallbo, A. B., and Westling, G. (1980). Thresholds of mechanosensitive afferents in the human hand as measured with von Frey hairs. *Brain research* 184.2, pp. 343–351.

Johnson, K. O. (2001). The roles and functions of cutaneous mechanoreceptors. *Curr Opin Neurobiol* 11.4, pp. 455–461.

Kaas, J. H. (1983). What, if anything, is SI? Organization of first somatosensory area of cortex. *Physiol Rev* 63.1, pp. 206–231.

Kaas, J. H. (1993). The functional organization of somatosensory cortex in primates. *Ann Anat* 175.6, pp. 509–518.

Kaas, J. H. (2004). Somatosensory System. *The Human Nervous System*. Ed. by G. Paxinos and J. K. Mai. Elsevier Academic Press, pp. 1059–1092.

Kandel, E. R., Schwartz, J. H., and Jessell, T. M. (2000). *Principles of Neural Science*. McGraw-Hill Medical. ISBN: 0838577016.

Kara, P., Reinagel, P., and Reid, R. C. (2000). Low response variability in simultaneously recorded retinal, thalamic, and cortical neurons. *Neuron* 27.3, pp. 635–646.

Kayser, C., Logothetis, N. K., and Panzeri, S. (2010). Millisecond encoding precision of auditory cortex neurons. *Proc Natl Acad Sci U S A* 107.39, pp. 16976–16981.

Koltzenburg, M., Stucky, C. L., and Lewin, G. R. (1997). Receptive properties of mouse sensory neurons innervating hairy skin. *J Neurophysiol* 78.4, pp. 1841–1850.

Krubitzer, L. A. and Calford, M. B. (1992). Five topographically organized fields in the somatosensory cortex of the flying fox: microelectrode maps, myeloarchitecture, and cortical modules. *J Comp Neurol* 317.1, pp. 1–30.

Krubitzer, L. A., Clarey, J., Tweedale, R., Elston, G., and Calford, M. (1995). A redefinition of somatosensory areas in the lateral sulcus of macaque monkeys. *J Neurosci* 15.5 Pt 2, pp. 3821–3839.

Krubitzer, L. A. and Kaas, J. H. (1990). The organization and connections of somatosensory cortex in marmosets. *J Neurosci* 10.3, pp. 952–974.

Krubitzer, L. A., Sesma, M. A., and Kaas, J. H. (1986). Microelectrode maps, myeloarchitecture, and cortical connections of three somatotopically organized representations of the body surface in the parietal cortex of squirrels. *J Comp Neurol* 250.4, pp. 403–430.

Krubitzer, L. (2009). In search of a unifying theory of complex brain evolution. *Ann N Y Acad Sci* 1156, pp. 44–67.

Kruger, L., Perl, E. R., and Sedivec, M. J. (1981). Fine structure of myelinated mechanical nociceptor endings in cat hairy skin. *J Comp Neurol* 198.1, pp. 137–154.

Kurta, A. and Baker, R. H. (1990). Eptesicus fuscus. *Mammalian species* 356, pp. 1–10.

Lewin, G. R. and McMahon, S. B. (1991). Physiological properties of primary sensory neurons appropriately and inappropriately innervating skin in the adult rat. *J Neurophysiol* 66.4, pp. 1205–1217.

Lewin, G. R., Ritter, A. M., and Mendell, L. M. (1992). On the role of nerve growth factor in the development of myelinated nociceptors. *J Neurosci* 12.5, pp. 1896–1905.

Lindhe Norberg, U. M. and Winter, Y. (2006). Wing beat kinematics of a nectar-feeding bat, Glossophaga soricina, flying at different flight speeds and Strouhal numbers. *J Exp Biol* 209.Pt 19, pp. 3887–3897.

MacKay, D. M. and McCulloch, W. S. (1952). The limiting information capacity of a neuronal link. *The bulletin of mathematical biophysics* 14.2, pp. 127–135.

Manger, P. R., Rosa, M. G., and Collins, R. (2001). Somatotopic organization and cortical projections of the ventrobasal complex of the flying fox: an "inverted" wing representation in the thalamus. *Somatosens Mot Res* 18.1, pp. 19–30.

Marshall, W. H., Woolsey, C. N., and Bard, P. (1937). Cortical Representation of Tactile Sensibility as Indicated by Cortical Potentials. *Science* 85.2207, pp. 388–390.

Martin, R. L. (1993). Representation of the body surface in the gracile, cuneate, and spinal trigeminal nuclei of the little red flying fox (*Pteropus scapulatus*). *Journal of Comparative Neurology* 335.3, pp. 334–342.

Martinez-Conde, S., Macknik, S. L., and Hubel, D. H. (2000). Microsaccadic eye movements and firing of single cells in the striate cortex of macaque monkeys. *Nat Neurosci* 3.3, pp. 251–258.

Maxim, H. (1912). The sixth sense of the bat. Sir Hiram's contention. The possible prevention of sea collisions. *Sci Am* 27, pp. 80–81.

May, R. M. (1988). How many species are there on Earth? *Science* 241.4872, pp. 1441–1449.

Mazurek, M. E. and Shadlen, M. N. (2002). Limits to the temporal fidelity of cortical spike rate signals. *Nat Neurosci* 5.5, pp. 463–471.

Meister, M. and Berry 2nd, M. (1999). The neural code of the retina. *Neuron* 22.3, pp. 435–450.

Moore, C. I. and Nelson, S. B. (1998). Spatio-temporal subthreshold receptive fields in the vibrissa representation of rat primary somatosensory cortex. *J Neurophysiol* 80.6, pp. 2882–2892.

Mountcastle, V. B. and Powell, T. P. (1959). Neural mechanisms subserving cutaneous sensibility, with special reference to the role of afferent inhibition in sensory perception and discrimination. *Bull Johns Hopkins Hosp* 105, pp. 201–232.

Muijres, F. T., Johansson, L. C., Barfield, R., Wolf, M., Spedding, G. R., and Hedenström, A. (2008). Leading-edge vortex improves lift in slow-flying bats. *Science* 319.5867, pp. 1250–1253.

Necker, R. D. (1985). Receptors in the skin of the wing of the pigeon and their possible role in flight control. *Biona Report 3, Bird Flight - Vogelflug*. Ed. by W. Nachtigall. Fischer, Stuttgart New York, pp. 433–444.

Necker, R. D. (2000). The Somatosensory System. *Sturkie's Avian Physiology*. Ed. by G. C. Whittow. 5th ed. Academic Press.

Nelson, R. J., Sur, M., Felleman, D. J., and Kaas, J. H. (1980). Representations of the body surface in postcentral parietal cortex of Macaca fascicularis. *J Comp Neurol* 192.4, pp. 611–643.

Niehaus, M. (1981). Flight and flight control by the antennae in the Small Tortoiseshell (Aglais urticae L., Lepidoptera). *Journal of comparative physiology* 145.2, pp. 257–264. ISSN: 0340-7594.

Niehaus, M. and Gewecke, M. (1978). The antennal movement apparatus in the small tortoiseshell (Aglais urticae L., Insecta, Lepidoptera). *Zoomorphologie* 91.1, pp. 19–36. ISSN: 0340-6725.

Norberg, U. M. (1976a). Aerodynamics, kinematics, and energetics of horizontal flapping flight in the long-eared bat Plecotus auritus. *J Exp Biol* 65.1, pp. 179–212.

Norberg, U. M. (1976b). Aerodynamics of hovering flight in the long-eared bat Plecotus auritus. *J Exp Biol* 65.2, pp. 459–470.

Norberg, U. M. (1985). Evolution of vertebrate flight: an aerodynamic model for the transition from gliding to active flight. *American Naturalist*, pp. 303–327.

Norberg, U. M. (1994). Ecological morphology: integrative organismal biology. Ed. by P. C. Wainwright and S. M. Reilly. University of Chicago Press. Chap. Wing design, flight performance, and habitat use in bats, pp. 205–239.

Norberg, U. M. and Rayner, J. M. V. (1987). Ecological morphology and flight in bats (Mammalia; Chiroptera): wing adaptations, flight performance, foraging strategy and echolocation. *Philosophical Transactions of the Royal Society of London. Series B, Biological Sciences*, pp. 335–427.

Nurse, C. A. and Diamond, J. (1984). A fluorescent microscopic study of the development of rat touch domes and their Merkel cells. *Neuroscience* 11.2, pp. 509–520.

Page, K. L. and Matheson, T. (2004). Wing hair sensilla underlying aimed hindleg scratching of the locust. *J Exp Biol* 207.Pt 15, pp. 2691–2703.

Panzeri, S., Petersen, R. S., Schultz, S. R., Lebedev, M., and Diamond, M. E. (2001). The role of spike timing in the coding of stimulus location in rat somatosensory cortex. *Neuron* 29.3, pp. 769–777.

Panzeri, S., Senatore, R., Montemurro, M. A., and Petersen, R. S. (2007). Correcting for the sampling bias problem in spike train information measures. *J Neurophysiol* 98.3, pp. 1064–1072.

Panzeri, S. and Treves, A. (1996). Analytical estimates of limited sampling biases in different information measures. *Network: Computation in Neural Systems* 7.1, pp. 87–107.

Pawlas, Z., Klebanov, L. B., Benes, V., Prokesová, M., Popelár, J., and Lánský, P. (2010). First-spike latency in the presence of spontaneous activity. *Neural Comput* 22.7, pp. 1675–1697.

Pennycuick, C. J. (2008). *Modelling the flying bird*. Vol. 5. Elsevier.

Petersen, C. C. H. (2007). The functional organization of the barrel cortex. *Neuron* 56.2, pp. 339–355.

Pouget, A., Deneve, S., Ducom, J. C., and Latham, P. E. (1999). Narrow versus wide tuning curves: What's best for a population code? *Neural Comput* 11.1, pp. 85–90.

Quay, W. B. (1970). Integument and derivatives. *Biology of bats (WA Wimsatt, ed.). Academic Press, New York* 2, pp. 1–477.

Reep, R. L., Marshall, C. D., and Stoll, M. L. (2002). Tactile hairs on the postcranial body in Florida manatees: a Mammalian lateral line? *Brain Behav Evol* 59.3, pp. 141–154.

Reichard, J. D., Fellows, S. R., Frank, A. J., and Kunz, T. H. (2010). Thermoregulation during flight: body temperature and sensible heat transfer in free-ranging Brazilian free-tailed bats (Tadarida brasiliensis). *Physiol Biochem Zool* 83.6, pp. 885–897.

Reinisch, C. M. and Tschachler, E. (2005). The touch dome in human skin is supplied by different types of nerve fibers. *Ann Neurol* 58.1, pp. 88–95.

Rieke, F., Warland, D., de Ruyter van Steveninck, R. R., and Bialek, W. (1997). *Spikes: Exploring the Neural Code*. 1st. Cambridge, MA: MIT Press.

Riskin, D. K., Bahlman, J. W., Hubel, T. Y., Ratcliffe, J. M., Kunz, T. H., and Swartz, S. M. (2009). Bats go head-under-heels: the biomechanics of landing on a ceiling. *J Exp Biol* 212.Pt 7, pp. 945–953.

Riskin, D. K., Iriarte-Díaz, J., Middleton, K. M., Breuer, K. S., and Swartz, S. M. (2010). The effect of body size on the wing movements of pteropodid bats, with insights into thrust and lift production. *J Exp Biol* 213.Pt 23, pp. 4110–4122.

Sabussow, N. (1910). Zur Innervation der Flughaut von Chiropteren. *Trans Soc Nat Univ Kasan, Bd* 43, pp. 1–67.

Sane, S. P. (2003). The aerodynamics of insect flight. *J Exp Biol* 206.Pt 23, pp. 4191–4208.

Sane, S. P., Dieudonné, A., Willis, M. A., and Daniel, T. L. (2007). Antennal mechanosensors mediate flight control in moths. *Science* 315.5813, pp. 863–866.

Schneider, D. (1964). Insect Antennae. *Annual Review of Entomology* 9.1, pp. 103–122.

Schöbl, J. (1871). Die flughaut der fledermause, namentliche die endigung ihrer nerven. *Archiv für Mikroskopische Anatomie und Entwicklungsmechanik* 7, pp. 1–31.

Sears, K. E. (2008). Molecular determinants of bat wing development. *Cells Tissues Organs* 187.1, pp. 6–12.

Sears, K. E., Behringer, R. R., Rasweiler, J. J., and Niswander, L. A. (2006). Development of bat flight: morphologic and molecular evolution of bat wing digits. *Proc Natl Acad Sci U S A* 103.17, pp. 6581–6586.

Severson, K. (2002). *Cynopterus brachyotis*.

Shadlen, M. N. and Newsome, W. T. (1998). The variable discharge of cortical neurons: implications for connectivity, computation, and information coding. *J Neurosci* 18.10, pp. 3870–3896.

Shadlen, M. N. and Newsome, W. T. (2001). Neural basis of a perceptual decision in the parietal cortex (area LIP) of the rhesus monkey. *J Neurophysiol* 86.4, pp. 1916–1936.

Shannon, C. E. (1948). A Mathematical Theory of Communication. *The Bell System Technical Journal* 27, pp. 379–423, 623–656.

Simons, D. J. and Carvell, G. E. (1989). Thalamocortical response transformation in the rat vibrissa/barrel system. *J Neurophysiol* 61.2, pp. 311–330.

Smola, U. (1970). Untersuchung zur Topographie, Mechanik und Strömungsmechanik der Sinneshaare auf dem Kopf der Wanderheuschrecke Locusta migratoria. *Zeitschrift für vergleichende Physiologie* 67.4, pp. 382–402.

Softky, W. R. and Koch, C. (1993). The highly irregular firing of cortical cells is inconsistent with temporal integration of random EPSPs. *J Neurosci* 13.1, pp. 334–350.

Spedding, G. R., Rayner, J. M. V., and Pennycuick, C. J. (1984). Momentum and energy in the wake of a pigeon (Columba livia) in slow flight. *Journal of Experimental Biology* 111.1, pp. 81–102.

Spedding, G. R., Rosén, M., and Hedenström, A. (2003). A family of vortex wakes generated by a thrush nightingale in free flight in a wind tunnel over its entire natural range of flight speeds. *J Exp Biol* 206.Pt 14, pp. 2313–2344.

Sterbing-D'Angelo, S. J., Chadha, M., Chiu, C., Falk, B., Xian, W., Barcelo, J., Zook, J. M., and Moss, C. F. (2011). Bat wing sensors support flight control. *Proc Natl Acad Sci U S A* 108.27, pp. 11291–11296.

Storchi, R., Bale, M. R., Biella, G. E. M., and Petersen, R. S. (2012). Comparison of latency and rate coding for the direction of whisker deflection in the subcortical somatosensory pathway. *J Neurophysiol* 108.7, pp. 1810–1821.

Strong, S. P., Koberle, R., de Ruyter van Steveninck, R. R., and Bialek, W. (1998). Entropy and Information in Neural Spike Trains. *Physical Review Letters* 80.1, pp. 197–200.

Studier, E. H. (1972). Some physical properties of the wing membranes of bats. *Journal of Mammalogy* 53.3, pp. 623–625.

Sur, M., Wall, J. T., and Kaas, J. H. (1984). Modular distribution of neurons with slowly adapting and rapidly adapting responses in area 3b of somatosensory cortex in monkeys. *J Neurophysiol* 51.4, pp. 724–744.

Sur, M., Weller, R. E., and Kaas, J. H. (1981). The organization of somatosensory area II in tree shrews. *J Comp Neurol* 201.1, pp. 121–133.

Swartz, S. M. (1997). Allometric patterning in the limb skeleton of bats: implications for the mechanics and energetics of powered flight. *Journal of Morphology* 234.3, pp. 277–294.

Swartz, S. M., Bishop, K., and Ismael-Aguirre, M. F. (2005). Dynamic complexity of wing form in bats: implications for flight performance. *Functional and evolutionary ecology of bats*. Ed. by A. Zubaid, G. F. McCraken, and T. H. Kunz. Oxford University Press, pp. 110–130.

Swartz, S. M., Groves, M. S., Kim, H. D., and Walsh, W. R. (1996). Mechancial properties of bat wing membrane skin: aerodynamic and mechanical functions. *Journal of Zoology* 239.2, pp. 357–378.

Swartz, S. M., Iriarte-Díaz, J., Riskin, D. K., Song, A. J., Tian, X., Willis, D., and Breuer, K. S. (2007). Wing structure and the aerodynamic basis of flight in bats. *AIAA J* 1.

Swartz, S. M. and Middleton, K. M. (2008). Biomechanics of the bat limb skeleton: scaling, material properties and mechanics. *Cells Tissues Organs* 187.1, pp. 59–84.

Taylor, G. K. and Krapp, H. G. (2007). Sensory Systems and Flight Stability: What do Insects Measure and Why? *Insect Mechanics and Control*. Ed. by C. J. and S. S. J. Vol. 34. Advances in Insect Physiology. Academic Press, pp. 231–316.

Teeling, E. C., Springer, M. S., Madsen, O., Bates, P., O'brien, S. J., and Murphy, W. J. (2005). A molecular phylogeny for bats illuminates biogeography and the fossil record. *Science* 307.5709, pp. 580–584.

Thewissen, J. G. M. and Babcock, S. K. (1992). The Origin of Flight in Bats. *BioScience* 42.5, pp. 340–345.

Thorpe, S., Delorme, A., and Van Rullen, R. (2001). Spike-based strategies for rapid processing. *Neural Netw* 14.6-7, pp. 715–725.

Tian, X., Iriarte-Díaz, J., Middleton, K., Galvao, R., Israeli, E., Roemer, A., Sullivan, A., Song, A. J., Swartz, S. M., and Breuer, K. S. (2006). Direct measurements of the kinematics and dynamics of bat flight. *Bioinspir Biomim* 1.4, S10–S18.

Tobalske, B. W., Warrick, D. R., Clark, C. J., Powers, D. R., Hedrick, T. L., Hyder, G. A., and Biewener, A. A. (2007). Three-dimensional kinematics of hummingbird flight. *J Exp Biol* 210.Pt 13, pp. 2368–2382.

Tolhurst, D. J., Movshon, J. A., and Dean, A. F. (1983). The statistical reliability of signals in single neurons in cat and monkey visual cortex. *Vision Res* 23.8, pp. 775–785.

Tucker, V. A. (1993). Gliding birds: reduction of induced drag by wing tip slots between the primary feathers. *Journal of experimental biology* 180.1, pp. 285–310.

Victor, J. D. (2006). Approaches to Information-Theoretic Analysis of Neural Activity. *Biol Theory* 1.3, pp. 302–316.

Videler, J. J., Stamhuis, E. J., and Povel, G. D. E. (2004). Leading-edge vortex lifts swifts. *Science* 306.5703, pp. 1960–1962.

Wang, Z. J. (2004). The role of drag in insect hovering. *J Exp Biol* 207.Pt 23, pp. 4147–4155.

Warrick, D. R., Tobalske, B. W., and Powers, D. R. (2005). Aerodynamics of the hovering hummingbird. *Nature* 435.7045, pp. 1094–1097.

Weatherbee, S. D., Behringer, R. R., Rasweiler, J. J., and Niswander, L. A. (2006). Interdigital webbing retention in bat wings illustrates genetic changes underlying amniote limb diversification. *Proc Natl Acad Sci U S A* 103.41, pp. 15103–15107.

Weaver, K. N., Alfano, S. E., Kronquist, A. R., and Reeder, D. M. (2009). Healing rates of wing punch wounds in free-ranging little brown Myotis (Myotis lucifugus). *Acta Chiropterologica* 11.1, pp. 220–223.

Weis-Fogh, T. (1949). An aerodynamic sense organ stimulating and regulating flight in locusts. *Nature* 164.4177, p. 873.

Wiegmann, B. M. and Yeates, D. K. (2007). *Brachycera*.

Willmott, A. P. and Ellington, C. P. (1997). The mechanics of flight in the hawkmoth Manduca sexta. I. Kinematics of hovering and forward flight. *J Exp Biol* 200.Pt 21, pp. 2705–2722.

Winter, Y. and von Helversen, O. (1998). The energy cost of flight: do small bats fly more cheaply than birds? *J Comp Physiol B* 168.2, pp. 105–111.

Wise, L. Z., Pettigrew, J. D., and Calford, M. B. (1986). Somatosensory cortical representation in the Australian ghost bat, Macroderma gigas. *J Comp Neurol* 248.2, pp. 257–262.

Wolf, M., Johansson, L. C., von Busse, R., Winter, Y., and Hedenström, A. (2010). Kinematics of flight and the relationship to the vortex wake of a Pallas' long tongued bat (Glossophaga soricina). *J Exp Biol* 213.Pt 12, pp. 2142–2153.

Woodbury, C. J., Ritter, A. M., and Koerber, H. R. (2001). Central anatomy of individual rapidly adapting low-threshold mechanoreceptors innervating the "hairy" skin of newborn mice: early maturation of hair follicle afferents. *J Comp Neurol* 436.3, pp. 304–323.

Woolsey, T. A. and Van der Loos, H. (1970). The structural organization of layer IV in the somatosensory region (SI) of mouse cerebral cortex. The description of a cortical field composed of discrete cytoarchitectonic units. *Brain Res* 17.2, pp. 205–242.

Yezierski, R. P. (1988). Spinomesencephalic tract: projections from the lumbosacral spinal cord of the rat, cat, and monkey. *J Comp Neurol* 267.1, pp. 131–146.

Zhang, K. and Sejnowski, T. J. (1999). Neuronal tuning: To sharpen or broaden? *Neural Comput* 11.1, pp. 75–84.

Zhu, J. J. and Connors, B. W. (1999). Intrinsic firing patterns and whisker-evoked synaptic responses of neurons in the rat barrel cortex. *J Neurophysiol* 81.3, pp. 1171–1183.

Zimmermann, K., Hein, A., Hager, U., Kaczmarek, J., Turnquist, B. P., Clapham, D. E., and Reeh, P. W. (2009). Phenotyping sensory nerve endings in vitro in the mouse. *Nat Protoc* 4.2, pp. 174–196.

Zook, J. M. (2005). The neuroethology of touch in bats: cutaneous receptors of the bat wing. *Neurosci Abstr*. Vol. 78, p. 21.

Zook, J. M. (2006). Somatosensory adaptations of flying mammals. *Evolution of Nervous System*. Ed. by J. H. Kaas. Vol. 3. Academic Press, Oxford, pp. 215–226.

Zook, J. M. and Fowler, B. C. (1986). A specialized mechanoreceptor array of the bat wing. *Myotis* 23.24, pp. 31–36.